Huntington's Disease

Transcriptional Dysregulation and Computational Models for Cell Death Caused by Protein Aggregation

DISSERTATION

zur Erlangung des akademischen Grades
doctor rerum naturalium
(dr. rer. nat.)
im Fach Biologie

eingereicht an der
Mathematisch-Naturwissenschaftlichen Fakultät I
Humboldt-Universität zu Berlin

von
Frau Dipl.-Biol. Branka Bernard
geboren am 30.04.1974 in Zagreb, Kroatien

Präsident der Humboldt-Universität zu Berlin:
Prof. Dr. Dr. h.c. Christoph Markschies

Dekan der Mathematisch-Naturwissenschaftlichen Fakultät I:
Prof. Dr. Christian Limberg

Gutachter:

1. Prof. Hanspeter Herzel
2. Prof. Thomas Hoefer
3. Prof. Marijana Krsnik-Rasol

eingereicht am:	27. Februar 2008
Tag der mündlichen Prüfung:	30. Juni 2008

Abstract

Huntington's disease (HD) is a fatal neurodegenerative disorder characterized by a progressive decline in cognitive, motor, and psychiatric functions. These symptoms are associated with the extensive neuronal loss in the striatum of HD patients. HD is caused by a CAG repeat expansion which translates into a polyglutamine (polyQ) stretch at the N-terminus of the huntingtin protein (htt). The polyQ stretch induces misfolding, cleavage and aggregation of htt. Insoluble protein aggregates are a hallmark of a number of neurodegenerative disease, which raised hope that understanding the process of aggregation and its potential as a therapeutic target in one of the diseases may have implications for the others.

It has been postulated that the sequestration of transcription-related proteins into the htt aggregates causes transcriptional changes observed in HD models. To test that hypothesis, I compiled lists of genes controlled by the transcription factors associated with HD. These genes were spotted on cDNA microarrays that were later hybridized with RNA extracted from cell lines expressing a mutant htt fragment. Upon induction of expression, htt fragments formed aggregates and the cells showed reduced viability. Transcriptional changes after the induction of htt fragment expression were monitored and their time series analysed. In this study, no systematic changes within the groups of genes regulated with the specific transcription factors were observed, which indicates that targeting a specific transcription factor might not be a feasible therapeutic strategy for treating HD.

It is well established that the formation and the accumulation of htt aggregates causes neurotoxicity in different HD model systems. However, there is an intense debate as to which protein structure, i.e. monomers, oligomers or aggregates of htt fragment, is responsible for neuronal dysfunction and loss. Understanding the dynamical properties of the htt aggregation process can help understanding the consequences of therapeutic strategies targeting aggregation. For this purpose, I derived several mathematical models describing htt aggregation and cell death. A core deterministic model of htt aggregation allowed monitoring changes in the concentration of different htt conformers in the course of the disease. Based on this core model, a stochastic model of htt aggregation was constructed and the assumption that the toxicity is proportional to the concentration of each htt conformer was included. The results showed that transient dynamics observed in the system and the non-monotonic response of cell survival to a change of parameter might lead to the non-intuitive outcome of a treatment that targets htt aggregation. Moreover, the numerical simulations of the stochastic model show that if aggregates are the toxic species, the onset of aggregation, marked by the overshoot in the concentration of aggregates, is the event most likely to kill the cell. Therefore. if the cell survives the onset of aggregation, it might have a higher life expectancy than a cell without aggregates despite the presence of toxic aggregates. This phenomenon was termed a one-shot model. The one-shot model could explain how aggregates could be toxic and neuroprotective at the same time.

HD is a late onset disorder whose symptoms usually appear between 30 to 50 years of age. It is possible to measure the functional decline of the affected brain regions in

HD patients, but what dictates the dynamics of that decline is not known. To address the open question of the late-onset of HD, I built an enlarged deterministic model of htt aggregation. The model showed that a nucleation process and a positive feedback loop acting on the htt fragment release describe well the late onset of aggregation through an intrinsic mechanism.

The principal cause of the variability of the age at onset (AO) is the length of the CAG repeat. Still, there is a great variance in the AO even for the same CAG repeat length. This notion prompted a search for additional genetic factors that could modify the AO of HD. At the same time, neuronal decline in a group of neurodegenerative diseases including HD fits well a one-hit model, in which a rare random event triggers cell death. To study the variability of the AO, I developed a stochastic model for neuronal death in the HD striatum based the one-hit model. In this model, it is assumed that neurons do not die independently, but in clusters due to cross-talk between the cells, excitotoxicity or inflammation. The model was used to explore the variability introduced in the development of the disease by the random times of cluster deaths. The stochastic model of neuronal death showed that a significant part of the unexplained variance can be attributed to the intrinsic stochastic dynamics of neurodegeneration.

Keywords: Huntington's disease, protein aggregation, transcriptional dysregulation, mathematical model

Zusammenfassung

Die Huntington'sche Krankheit (Huntington's disease, HD) ist eine tödliche neurodegenerative Erkrankung, die durch den progressiven Verlust kognitiver, motorischer und psychiatrischer Funktionen gekennzeichnet ist. Diese Symptome gehen bei HD-Patienten mit einem extensiven Verlust von Neuronen im Striatum einher. Die Ursache für HD ist eine genetische Mutation, bei der eine CAG-Wiederholungssequenz verlängert wird. Im resultierenden Protein, das Huntingtin (htt) genannt wurde, wird diese CAG-Sequenz in eine Polyglutamin (PolyQ)-Sequenz im N-Terminus translatiert. Die PolyQ-Sequenz führt zur Missfaltung von htt, woraufhin es gespalten wird. Die entstehenden Fragmente von htt bilden unlösliche Aggregate. Die Entstehung von unlöslichen Proteinaggregaten ist ein gemeinsames Merkmal von etlichen neurodegenerativen Erkrankungen, was Anlass zur Hoffnung gab, dass Erkenntnisse über den Aggregationsprozess und sein Potential als therapeutischen Ansatzpunkt bei einer der Krankheiten auch Anwendungsmöglichkeiten für die anderen Krankheiten eröffnen würden.

In Modellen für HD wurden Veränderungen der Transkription beobachtet, und es wurde postuliert, dass diese durch die Rekrutierung von transkriptions-assoziierten Proteinen in htt-Aggregate verursacht werden könnten. Um diese Hypothese zu testen, habe ich untersucht ob die Bildung von htt-Aggregaten die Transkription von Genen, von denen bekannt ist, dass sie von HD-assoziierten Transkriptionsfaktoren kontrolliert werden, verändert. In den für diese Versuche verwendeten Zelllinien führte die Induktion der Expression eines mutierten htt-Fragments zur Bildung von htt-Aggregaten, und die Zellen wiesen eine verminderte Vitalität auf. Zur Untersuchung der Transkription wurden die zu untersuchenden Gene auf cDNA-Mikroarrays aufgebracht und mit RNA, welche aus den Zellen zu unterschiedlichen Zeiten nach der Induktion der Expression des mutierten htt-Fragments gewonnen wurde, hybridisiert. So konnte auch die Zeitabhängigkeit der Transkription gemessen werden. Es wurden keine systematischen Veränderungen innerhalb der durch spezifische Transkriptionsfaktoren regulierten Gengruppen gefunden, was darauf hindeutet, dass die Fokussierung auf einen spezifischen Transkriptionsfaktor eher nicht als sinnvolle therapeutische Strategie für die Behandlung von HD angesehen werden kann.

Es ist bekannt, dass die Ausbildung und Ansammlung von htt-Aggregaten in verschiedenen HD-Modellsystemen zum Absterben von Nervenzellen im Striatum führt. Es herrscht jedoch rege Diskussion darüber, welche Proteinstruktur, d.h. Monomere, Oligomere oder Aggregate des htt-Fragments, die neuronalen Dysfunktionen und letztendlich den Zelltod verursacht. Ein besseres Verständnis der Dynamik des htt-Aggregationsprozesses könnte zur Abschätzung der Auswirkungen von therapeutischen Strategien, die die Proteinaggregation beeinflussen, beitragen. Zu diesem Zweck habe ich mehrere mathematische Modelle erstellt, welche die htt-Aggregation und den Zelltod beschreiben. In einem deterministischen Kernmodell der htt-Aggregation konnten Veränderungen der Konzentrationen verschiedener htt-Konformere im Krankheitsverlauf beobachtet werden. Aufbauend auf dem Kernmodell wurde als nächstes ein stochastisches Modell der htt-Aggregation erstellt, bei dem angenommen wurde, dass die Toxizität proportional zur

Konzentration eines jeden htt-Konformers ist. Die Ergebnisse zeigten, dass eine transiente Dynamik im System und die nicht-monotone Reaktion auf Parameteränderungen zu den nicht-intuitiven Ergebnissen bei Behandlungsansätzen, welche die htt-Aggregation beeinflussen, führen könnten. Für den Fall, dass Aggregate die toxische Form von htt sind, zeigten die numerischen Simulationen mit dem stochastischen Modell, dass das Einsetzen der Aggregation, welches durch ein Überschießen der Aggregatkonzentration gekennzeichnet ist, am ehesten zum Zelltod führt. Deshalb kann eine Zelle, die das Einsetzen der Aggregation überlebt hat, trotz des Vorhandenseins von toxischen Aggregaten eine höhere Lebenserwartung haben als eine Zelle ohne Aggregate. Dieses Phänomen wurde "one-shot"-Modell genannt, und es könnte die paradoxen Befunde erklären, nach denen Aggregate zugleich toxisch und neuroprotektiv sein können.

Die Symptome von HD manifestieren sich bei den Betroffenen üblicherweise erst im Alter von 30 bis 50 Jahren. Es ist möglich, den Funktionsverlust der betroffenen Gehirnregionen bei HD-Patienten zu messen, aber wodurch die Dynamik dieses Verlusts verursacht wird ist nicht bekannt. Um zur Klärung dieser Frage beizutragen habe ich ein erweitertes deterministisches Modell der htt-Aggregation erstellt. Das Modell zeigte, dass zur Erklärung des späten Einsetzens der Aggregation ein intrisischer Mechanismus ausreichend ist. Dieser Mechanismus beinhaltet einen Nukleationsprozess und eine positive Feedback-Schleife, die die Freisetzung des htt-Fragments bewirkt.

Die Hauptursache für die Variabilität des Alters bei Krankheitsausbruch (age of onset, AO) bei HD-Patienten ist die Länge der CAG-Wiederholungssequenz. Jedoch gibt es auch bei Patienten mit gleicher Länge der CAG-Wiederholungssequenz eine große Varianz des AO . Diese Tatsache führte zur Suche nach zusätzlichen genetischen Faktoren, die das AO bei HD beeinflussen könnten. Gleichzeitig passt der neuronale Abbau bei einer Gruppe neurodegenerativer Erkrankungen inklusive HD gut zu einem one-hit-Modell, bei dem ein Zufallsereignis den Zelltod verursacht. Um die Variabilität des AO zu studieren, habe ich ein stochastisches Modell für den neuronalen Zelltod im Striatum entwickelt, welches auf dem one-hit-Modell basiert. In diesem Modell wird angenommen, dass Neurone nicht einzeln und unabhängig voneinander sterben, sondern in Gruppen aufgrund von Kommunikation zwischen den Zellen, Exzitotoxizität oder entzündlichen Prozessen. Das Modell wurde dazu verwendet, die Variabilität, die in die Krankheitsentwicklung durch gruppierten Zelltod an zufälligen Zeitpunkten eingeführt wird, zu untersuchen. Das stochastische Modell neuronalen Zelltods zeigte, dass ein signifikanter Anteil der nicht erklärbaren Varianz des AO der intrinsischen stochastischen Dynamik der Neurodegeneration zugeschrieben werden kann.

Schlagwörter: Huntington'sche Krankheit, Proteinaggregation, Veränderungen der Transkription, mathematisches Modell

Contents

Foreword

In 1872, George Huntington, whose vivid and accurate description of hereditary chorea led to the eponymous designation of this fatal disorder as Huntington's disease (HD), accounts: "The treatment of chorea now most generally adopted is by purgatives, tonics, counter-irritants, and anti-spasmodics. Bleeding used to be employed, and it is said with good results, but it is rarely used at present, except in cases when there is much pain in the head, or along the spine, when it may be taken moderately by cups or leeches." A hundred and forty years and 8000 papers later, a treatment of HD still focuses on relieving the symptoms and preventing complications.

HD is caused by a mutation in a single gene coding for a protein that has thus been called huntingtin (htt). The mutation is a pathological extension of a CAG repeat that is translated in the polyglutamine stretch at the N-terminus of the htt, causing htt misfolding and cleavage. Cleaved htt fragments aggregate to form large and dense protein inclusions. A number of transcription factors co-localize with the protein inclusions in HD models. It has been postulated that sequestration of those proteins leads to transcriptional dysregulation, neuronal cell dysfunction and ultimately cell death. Protein inclusions are a hallmark of a number of neurodegenerative diseases, which raised hope that a common therapeutic agent could be found. However, the pathogenicity of the protein inclusions has been controversial. The question whether aggregates are harmful or beneficial, and consequently whether one should fight them or promote them, polarizes HD research community. During my PhD studies I have also entered this buzzing field of research. The experimental part of my PhD thesis deals with the transcriptional dysregulation in HD as a consequence of htt aggregation, and theoretical part focuses on mathematical models of htt aggregation and neuronal cell death.

Chapter 1

Introduction

1.1 Living with HD

Huntingon's disease (HD) is a progressive neurodegenerative disorder "hardly ever manifesting itself until adult or middle life, and then coming on gradually but surely, increasing by degrees, and often occupying years in its development, until the hapless sufferer is but a quivering wreck of his former self" (75).

The symptoms usually appear in an individual between 30 to 50 years of age and progress over a period of 10 to 15 years (108). The prevalence of HD in Western Europe and Northern America is 5 to 10 per 100,000 persons (109). Initial symptoms of HD may include personality changes, such as increased irritability, suspiciousness, impulsiveness, and lack of self-control. In the beginning it might be difficult to attribute those changes to such a devastating disease as HD. However, as HD progresses, additional symptoms develop like inability to absorb and understand new information, diminished memory retrieval, progressively impaired judgment and impulse control, diminished language skills with slurred speech, difficulty swallowing, and increasingly impaired ability to plan, initiate, or perform certain purposeful movements. Many HD patients have a distinctive manner of walking that may be unsteady, disjointed, or staggering. A dramatic weight loss may occur due to energy expenditure from choreic movements. HD patients often suffer from anxiety, depression, mania, obsessive-compulsive behaviors, and sleep disturbances. Suicide rate is high among HD patients (52).

Because of severe dementia and progressive motor dysfunction, patients with advanced HD may become unable to walk, have poor dietary intake, eventually cease to talk, and become unable to care for themselves. Pneumonia and heart failure are the two most frequent primary causes of death in HD patients (154).

There are a number of interventions available today that can improve the quality of life for HD sufferers. In the early and middle stages of the disease, medications can be given in small doses to HD patients to help suppress the involuntary movements (29). Depression and other psychiatric conditions in people with HD can be quite effectively treated (151). Proper nutrition, exercise and precautions at home can help minimize many of the potential consequences of HD (104). However, there is still no way to postpone or slow down the progress of this fatal disorder.

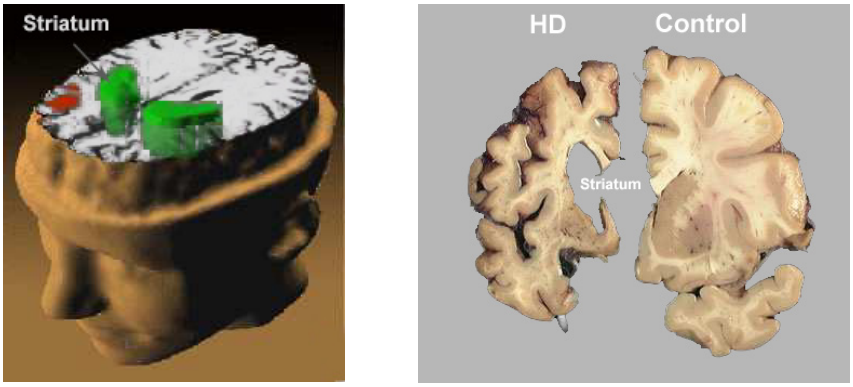

Figure 1.1: Striatal degeneration. (*Left*) Location of the striatum in the brain. (*Right*) Comparison of a brain from a HD patient and from a control showing atrophy of the striatum in the HD patient. (From: http://hdroster.iu.edu/AboutHD/brainAndHD.asp)

1.2 Neuropathology of HD

Inability of HD patients to control movements or plan an action is a consequence of premature, gradual dying of medium-sized "spiny" neurons, the most abundant type of neurons in the striatum (53). As striatal degeneration progresses, degenerative changes occur to other brain regions connected to the striatum, in particular the globus pallidus, the subthalamus, and the cerebral cortex. In the final stage of the disease, HD brains weigh approx. 10–20% less than age-matched controls (66) (Figure 1.1, right panel).

Striatal medium-sized neurons are highly specialized cells that secrete gamma-aminobutyric acid (GABA), the primary inhibitory neurotransmitter in the brain. Their selective loss results in decreased inhibition of the thalamus and continuous glutamate excitation causing random and frequent motions (Figure 1.2). Glutamate is the principal excitatory neurotransmitter in the mammalian central nervous system. It binds to a variety of excitatory amino acid receptors, which are ligand-gated ion channels. In normal synaptic functioning, activation of excitatory amino acid receptors is transient. However, if receptor activation becomes excessive or prolonged, the target neurons become damaged and eventually die. This process of neuronal death is called excitotoxicity and appears to involve sustained elevations of intracellular calcium levels (48).

The striatum receives large glutamatergic input from the cerebral cortex, and it is thus at risk of glutamate-mediated excitotoxic injury. Indeed, intrastriatal injections of glutamate agonists (e.g. quinolinic acid) lead to neuronal depletion and a neurologic phenotype that is similar to HD (20). Moreover, subsets of glutamate receptors, specifically the metabotropic glutamate receptor mGluR2, are significantly decreased in a transgenic mouse model of HD (37). mGluR2 receptors down-regulate glutamate release at corticostriatal presynaptic terminals, and depletion of these receptors could lead to overstimulation of postsynaptic striatal neurons.

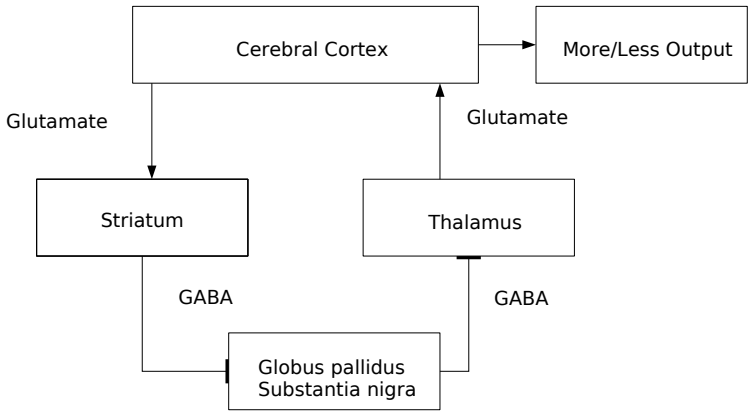

Figure 1.2: Striatal circuitry: The striatum receives direct input from most regions of the cerebral cortex, and indirect input from sensorimotor and motivational regions of the brain stem via relays in the thalamus. Dysfunction of striatal-thalamo-cortical circuits underlies the pattern of motor, behavioral and cognitive symptoms in HD.

1.3 Protein inclusions: a common theme in polyglutamine disorders

Nine neurodegenerative disorders are caused by expanded CAG repeats coding for polyglutamine (polyQ). They include Spinal and Bulbar Muscular Atrophy (SBMA), the first one discovered; Huntington's disease (HD), the most actively studied; DentatoRubral and PallidoLuysian Atrophy (DRPLA), which is similar to HD; and several forms of Spino-Cerebellar Ataxia (SCA). Each of the disorders is characterized by selective and progressive neuronal cell death in specific regions of the brain. While the exact areas affected in each disease differ, there is considerable overlap, including basal ganglia, brainstem nuclei, cerebellum, and spinal motor nuclei (131).

Although the proteins causing these diseases share no homology aside from the polyQ stretch itself, the diseases themselves share many. This led to the conclusion that the polyQ stretch confers toxicity on the disease protein and opened the possibility that polyQ diseases share a pathogenic mechanism. Ideally, a therapeutic approach befitting several neurodegenerative diseases could thus be found.

All of the mutant proteins appear to undergo a conformational change and aggregate in cells, forming characteristic inclusion bodies. Aggregation in these proteins is facilitated by proteolytic cleavage and covalent modifications of the disease proteins or protein fragments. In HD, phosphorylation alters cleavage and toxicity (143) of HD-causing protein huntingtin (htt), palmitoylation is necessary for the normal function of htt (183), and SUMOylation decreases its aggregation, increases its nuclear localization and increases neurodegeneration in a HD fly model (158).

Therefore, boosting the refolding, preventing the proteolytic cleavage, interfering with covalent modifications, and enhancing mutant protein clearance represent common therapeutic concepts for all polyQ diseases.

1.3.1 Identification of toxic polyglutamine species

The aggregation process generates protein complexes of different multimerization grades and three-dimensional structures which probably differ in the level of toxicity they confer. Low temporal and spatial resolution have limited the interpretation of past experiments that correlated aggregate formation with neurodegeneration. Resolution of this issue is necessary because many current studies aim to interfere with aggregate formation as a potential treatment for HD and the other neurodegenerative disorders characterized by protein aggregates (132).

Recently, an automated microscopic system was developed that allows to simultaneously follow aggregate formation, the presence of diffuse htt and cell survival in the same neuron over a period of days. The study showed that the formation of the final forms of aggregated htt (i.e. the inclusion bodies) prolonged survival and protected neurons, seemingly by reducing the amount of a toxic, diffusely distributed form of mutant htt (9). However, this does not rule out the possibility that the major toxic species are the microaggregates, early precursors to inclusion bodies.

Identifying therapeutics to arrest the creation of the toxic species is an important research goal in the HD field. Both aggregation inhibitors and aggregation promotors have been shown to have beneficial effects in experimental HD models (86, 171, 27, 51). These conflicting findings are probably due to the fact that it is very hard to specifically interfere with the aggregation by affecting only one conformer.

1.4 A curious protein called huntingtin

In 1993, a multicentre consortium, organized by the Hereditary Disease Foundation, discovered the HD-causing gene and the variable and prolonged sequence of nucleotides (CAG)n that codes for the stretch of glutamine amino acids (polyQ) at the N-terminus of htt (166). People with more than 40 glutamines in that stretch will develop HD; those with fewer than 36 will be unaffected. Larger polyQ expansions in htt are associated with earlier onset and increased severity of the disease (50, 153, 3). The sharp threshold of the pathogenic polyQ length suggests that a transition to a new, stable and toxic conformation of mutant htt triggers the disease (120).

The primary amino acid sequence of htt reveals little, as it contains only a few known sequence motifs and no structural domains with defined functions (35). Known sequence motifs include HEAT repeats, tandemly arranged structures that appear to serve as flexible scaffolding on which other components can assemble, and which are found in a number of proteins involved in intracellular transport and chromosomal segregation (164). The other obviously important portion of htt is the polyQ region itself, which is present in many transcription factors and aberrantly expanded in at least eight other disease-causing proteins (126). Unlike many other proteins of a similar size (328 kDa), htt is completely soluble. Its widespread expression and intracellular localization have not eased the definition of its function. Here is what we know so far.

Htt is ubiquitously expressed in moderate amounts in and outside the nervous system (169). It is essential for embryogenesis: homozygous htt knockout mice die before embryonic day 8.5 (111), and it is neuroprotective in brain cells exposed to various apoptotic stimuli, such as serum deprivation, mitochondrial toxins or transfection of death genes

(125). It stimulates brain-derived neurotrophic factor (BDNF) gene transcription through inhibition of a silencer element (Repressor element 1, also known as neuron-restrictive silencer element, NRSE) located in the promoter of the BDNF gene (186). Through a similar mechanism, htt controls the transcription of many other neuronal genes that carry a repressor silencer 1 transcription repressor factor, REST/NRSE, repeat in their promoters (187). It also regulates fast axonal trafficking (65), vesicle transport (57), and synaptic transmission (152).

The search for normal htt function is far from over. Recently, 234 high-confidence htt-associated proteins have been identified (79). It will be a challenging task to determine which of the identified interactions contribute to HD pathology and to use that knowledge to alleviate the symptoms of HD.

One study showed that different conformations of full-length htt, distinguished by epitope accessibility, were localized to different sets of nuclear and perinuclear organelles (168). Together with the remarkable potential of htt to bind a variety of proteins, this study suggest that htt has a flexible or multifunctional structure capable of assuming specific conformations and activities depending on its subcellular location (101).

1.5 When htt becomes toxic: cellular pathogenesis

The pathogenic process begins with the synthesis of a htt protein with an expanded polyQ tract (>36 repeats). The expanded polyQ tract alters the native conformation of htt (120). A fraction of the abnormally folded protein is subjected to lysosomal-dependent proteolysis, or degraded by the proteasome (82). The rest is cleaved by caspases or calpains, producing a short N-terminal fragment that favours the aggregation process (179, 55). The mutant proteins shifts, in part, from a monomeric random coil or β-sheet into oligomeric β-sheets and eventually into insoluble aggregates (amyloid fibrils) (121).

The development of transgenic mouse, fly, and worm models has led to the discovery of multiple pathways induced by the mutant htt (figure 1.3). Aggregation intermediates inhibit proteasomal processing (146). The monomers or oligomers directly activate caspases or disrupt mitochondrial function, leading to indirect activation of caspases (41). Proto-aggregates translocate into the nucleus and recruit specific nuclear factors, co-activators and co-repressors, inhibiting their normal activities and resulting in altered gene transcription (126). The presence of mutant htt fragments in the nucleus is a signal for caspase-1 up-regulation (94). As the disease progresses, caspase-3, -8, and -9 are activated, and there is release of cytochrome c, which serves as an apoptotic trigger (136). Also, disruption of the binding between htt and HIP-1 (htt interacting protein 1) sets HIP-1 free to bind its partner hippi (HIP-1 protein interactor). Thus formed HIP-1/hippi heterodimer can then recruit procaspase-8 and launch apoptosis (59).

The conformational change of mutant htt and subsequent aggregation lead to the loss of multiple physiological functions preformed by wild-type htt. The htt mutation reduces BDNF production, represses transcription of a number of neuronal genes, reduces transport of mitochondria and BDNF, and alters synaptic transmission (34). A few pathways leading to neuronal dysfunction and cell death are explained in more detail below.

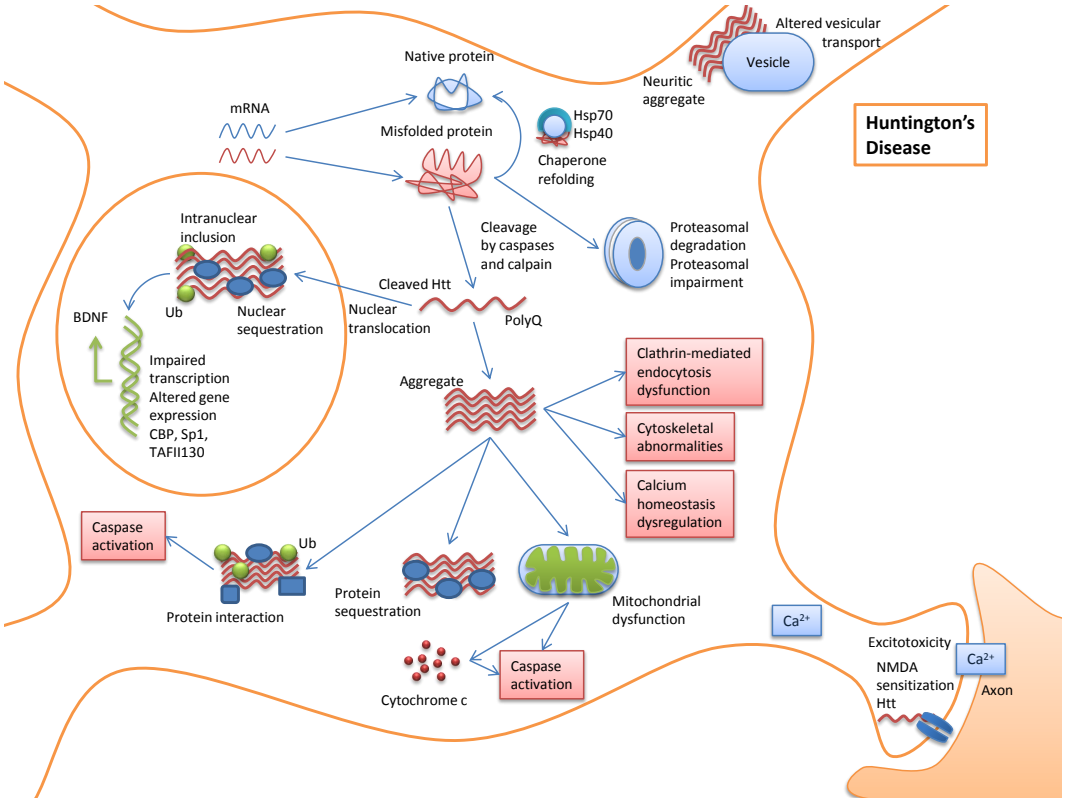

Figure 1.3: The pathogenic mechanisms induced by mutant htt include: Impaired transcription, altered vesicular transport, proteasomal impairment, clathrin-mediated endocytosis dysfunction, cytoskeletal abnormalities, calcium homeostasis dysregulation, mitochondrial dysfunction, protein sequestration and caspase activation.

1.5.1 Transcriptional dysregulation

Some of the most consistently observed actions of htt involve interference with gene transcription. It has been shown that transcription factors such as p53, CREB-binding protein (CBP), specificity protein 1 (Sp1), TAFII130, and TATA-binding protein can be recruited to intranuclear aggregates (156, 49, 173). Many transcription factors contain a polyQ-rich domain which has been found to enhance their activity (58). Therefore, it was expected that the interaction between CBP, for instance, and mutant htt would be through that polyQ domain. Surprisingly, it was shown that mutant htt interacts with the acetyltransferase domain in CBP and thus causes reduced histone acetylation in HD cells (157). This led to the finding that inhibition of histone deacetylase (HDAC) or promotion of histone acetylation relieves neurodegeneration in cellular and fly models and motor deficits in a mouse model of HD (157, 72).

Although the nucleus is thought to be a primary site for mutant htt to elicit its effect on gene transcription, mutant htt has a decreased affinity to the cytoplasmic pool of the nuclear receptor REST/NRSF. In HD, this leads to a decreased expression of BDNF and other genes controlled by REST (187).

1.5.2 Mitochondrial dysfunction

Mitochondria play a central role in both apoptotic and necrotic cell death. Mitochondrial dysfunction leads to a number of deleterious events including impaired calcium buffering, generation of free radicals, activation of the mitochondrial permeability transition and secondary excitotoxicity (19).

The evidence for the dysfunction of mitochondria in HD patients is abundant. HD patients have increased lactate production in cerebral cortex and basal ganglia (77), decreased glucose metabolism (6), and impaired complex II-III activity and aconitase in the striatum (63). Systemic administration of mitochondrial toxins to primates leads to the selective degeneration of the striatum (32). Metabolic defects in skeletal muscles of HD patients might explain the observations that HD patients suffer progressive weight loss despite increased caloric intake (96).

Recently, it was shown that mutant htt binds to the outer mitochondrial membrane and directly increases susceptibility of mitochondria to the calcium-induced permeability transition and cytochrome c release (41). Mutant htt also binds to and upregulates p53 leading to mitochondrial membrane depolarization (14).

1.5.3 Disrupted balance in protein folding and protein clearance

The ubiquitin-proteasome and macroautophagy-lysosome pathways are major routes to cytosolic protein degradation. Normally, misfolded proteins are tagged with ubiquitine and then degraded by the proteasome. However, polyQ sequences are poor substrates for the proteasome, and highly ubiquitinated aggregates of htt are eventually targeted to the endosomal-lysosomal organelles to be removed by autophagy. In the presence of a chronic, aggregation-prone htt the protein folding and clearance process becomes overwhelmed. Proteins that are normally harmless are no longer correctly folded, leading to dysfunction in a diverse set of cellular pathways (21).

Helping the cells to degrade the protein aggregates is a promising therapeutic option. Toxicity induced by disruption of global balance of protein folding quality control can be attenuated by increasing the autophagy with histone deacetylase 6, a microtubule-associated deacetylase that interacts with polyubiquitinated proteins (116). Moreover, treatment with rapamycin, which stimulates autophagy, reduces htt accumulation and neurodegeneration in cell, fly and mouse models of HD (180).

1.6 The pursuit of HD cure

The central nervous system tissue has very limited regenerative capacity so it is crucial to limit the damage caused by neuronal death. It is likely that there are many dysfunctional neurons present at any given time in the course of HD. All the processes that are affected by HD mutation present a potential therapeutic target. Recent studies in HD transgenic mice have demonstrated significant neuroprotective effects of several substances, namely: remacemide (glutamate antagonists), coenzyme Q10 and creatine (enhancers of mitochondrial function), minocyclin (antiapoptotic antibiotic), suberoylanilide hydroxamic acid (SAHA) and sodium butyrate (transcriptional modulators), and cystamine (transglutaminase inhibitor) (93).

Different approaches like DNA vaccination and neuronal tissue transplantation have shown the first promising results. DNA vaccination was used to present the mutant intracellular htt to the immune system which ameliorated the diabetic phenotype of HD mice (106). Transplanted fetal neural tissue improves HD symptoms temporarily (up to 4 years) (13).

Trials of neuroprotective treatments for HD require large numbers of patients and long trial durations. Given the growing pipeline of potential neuroprotective agents attractive for testing in clinical trials it is vital to develop reliable and reproducible markers of HD onset and HD progression. The morphological brain changes that occur during the course of HD are observable with *in vivo* brain imaging techniques. Many studies have used volumetric analysis of computed tomography (CT) scans and magnetic resonance images (MRIs) to demonstrate progressive bilateral atrophy of the striatum which may occur gradually even years before motor symptoms appear (16, 11).

Functional brain imaging is based on the premise that focal neuronal activity is related to either regional cerebral blood flow (rCBF), the local degree of glucose metabolism or regional changes in receptor binding. These tests can be done repeatedly and can assess temporal changes in the neuronal degeneration both before and after the development of clinical symptoms. The application of several imaging techniques in parallel may give us the opportunity to gather even more revealing information about the metabolic, functional and neuroanatomical alterations that take place during the various stages of the disease. Most importantly, morphometric markers may provide a sensitive and reliable method to determine whether a drug is effective in symptomatic patients.

1.7 Thesis at a glance

HD has been a real challenge for cell biologists. A multitude of cellular processes are afflicted in HD, which seems to be the consequence of both loss of function of wild type

htt, and toxic gain of function of mutant htt. Moreover, results obtained using different disease models often disagree, presumably because the models represent different stages of HD. For example, some publications reported a large number of differentially transcribed genes in HD model (100), whereas the others reported just a few (148). Some publications report a correlation between the appearance of htt aggregates and cell death (184), others report that no such correlation exists (139). Neuronal cell death underlies the appearance of symptoms in HD patients, but a number of animal models display symptoms of HD without any neuronal loss (118).

The HD field still abounds with open questions, and in my PhD thesis I have tried to answer several of them. To test the hypothesis that transcriptional dysregulation in HD stems from the sequestration of certain transcription factors into htt aggregates, I compiled lists of genes under regulation of those factors and those genes where then spotted on cDNA microarrays. The cDNA microarrays were hybridized with the RNA extracted from cell lines expressing a mutant htt fragment prone to aggregation. These experiment and the results are described in chapter 2.

Htt is expressed throughout life, but most of the HD patients do not display the disease symptoms before 30 or even 50 years of age. In chapter 3, I introduce a deterministic model of htt aggregation that allows us to monitor what is happening with different htt conformations as the cellular environment changes in the course of the disease, and use this model to explain the delayed onset of HD by an intrinsic mechanism.

The greatest controversy in the HD field revolves around the toxicity of different htt conformations that arise in the process of aggregation. Both inhibitors and promoters of aggregation have been shown to have beneficial effects in HD models (51, 27). In chapter 4, I present a stochastic model of htt aggregation and cell death in HD. The models allows us to assign different toxicities to htt conformations. Using this model, I tested how the outcome of the therapeutic strategies targeting aggregation in HD depends on the kinetic constants of the aggregation and the toxicity of different htt conformers.

The age at onset of HD patients is mainly predicted by the polyQ repeat length. However, for a given polyQ repeat length a wide range of ages at onset is observed. In chapter 5, I propose that the observed variance is a consequence of an intrinsic stochastic property of the pattern of neuronal death in the striata of HD patients.

Chapter 2

Transcriptional Dysregulation in Huntington's Disease: Testing Hypotheses with Customized Chips

2.1 Summary of the chapter

Mutant huntingtin (htt) triggers multiple pathways of neurodegeneration, including dysregulation of transcription. Understanding the molecular basis of transcriptional dysregulation in HD is necessary for selecting an appropriate therapeutic strategy aiming at reversing htt-induced expression changes. Mutant htt readily aggregates with itself and other proteins and forms insoluble protein inclusions. A number of transcription related proteins interact with mutant htt and co-localize with htt inclusion (112, 156, 49). It has been postulated that sequestration of these proteins by htt aggregates underlies transcriptional dysregulation observed in many HD models (36). To test this hypothesis, I compiled lists of genes controlled by the transcription factors that were shown to interact with htt, together with lists of genes belonging to the several pathways which are impaired in HD. cDNA microarrays spotted with the selected genes were hybridized with the RNA extracted from the human cell line that has been stably transfected with a vector carrying htt fragment coding sequence with a CAG triplet expansion in the pathological range (83 CAGs). Upon induction of htt fragment expression, these cells form aggresome-like inclusions and show reduced viability (176). Transcriptional changes after the induction of htt fragment expression were monitored and their time series analyzed. In this study, no systematic changes within the groups of genes regulated by the same transcription factor were observed, which indicates that targeting a specific transcription factor might not be a feasible therapeutic strategy for treating HD.

2.2 Introduction

Precise spatial and temporal patterns of gene expression are crucial for normal development and functioning of the cell. Coordinated transcription requires the synchronization of a number of mechanisms that depend on the trafficking and interaction of diverse proteins, e.g. DNA-binding transcription factors, non-DNA-binding coregulators, and

components of the basal RNA-polymerase apparatus. It is believed that dysregulation of these mechanism presents an early even in HD pathogenesis. However, the precise causes of transcriptional alterations in HD and how they relate to the observed phenotype remain elusive.

2.2.1 Transcriptional dysregulation in HD

The first notion that alterations in nuclear function underlie HD pathogenesis came from a study demonstrating that for the polyQ htt fragment to be toxic, it had to enter the nucleus (139). Later, a number of studies have shown that mutant htt co-aggregates with various transcription factors, like CREB-binding protein CBP, TATA-binding protein TBP, p53, Sp1, as well as with the members of basal transcriptional machinery, like TAFII130, TFIID and TFIIF (112, 156, 73, 49, 185). Moreover, soluble mutant htt inhibits Sp1 binding to DNA in postmortem brain tissues of HD patients, and coexpression of Sp1 and TAFII130 in cultured striatal cells from HD mice reverses the transcriptional inhibition of the dopamine D2 receptor gene induced by mutant htt (49). These observations gave a push to the sequestration theory of HD pathogenesis that stated that transcription factors, precipitated in the form of insoluble aggregates, get depleted from the cellular pool, which causes transcriptional dysregulation and subsequent death of HD cells (36).

Many transcription factors, like Sp1 and CBP, contain polyQ rich regions that can act as activation domains that enable transcription factors to interact with one another and thus regulate gene expression (165, 78). It is through the polyQ regions that mutant htt interacts with Sp1 and TAFII130, a coactivator involved in transcriptional activation dependent on the cAMP-responsive element (CRE)-binding protein (CREB) (95, 156). Moreover, the expanded htt fragments suppress CREB-dependent transcriptional activation and deplete CBP from nuclear locations (112). However, it came as a surprise that htt binds to the acetyltransferase domain of CBP, not its polyQ tract. This interaction leads to a decrease in the level of histone acetylation in the cells, and consequently to a decrease in gene transcription. These observations pointed the histone deacetylase (HDAC) inhibitors as potential therapeutics for HD. Indeed, administration of HDAC inhibitors has been shown to rescue lethality and photoreceptor neurodegeneration in a *Drosophila* model of HD (157). Furthermore, suberoylanilide hydroxamic acid (SAHA), a potent HDAC inhibitor, had remarkable effects in a HD mouse model (72).

2.2.2 Microarray data from different HD models

The most comprehensive analysis of transcription changes in different HD models has been reported in a series of published articles (99, 100, 38, 148). In these studies, the groups standardized experimental methods using a single microarray platform and consistent sample preparation methods. Nevertheless, detected changes in RNA levels were specific for each HD model used and the overlap of common altered transcripts was small. The first paper by Luthi-Carter et al. showed that in R6/2 mice expressing only a truncated htt fragment, a considerable number of genes have an altered pattern of expression and that this pattern shows little sign of regional specificity (99). The second paper from the Luthi-Carter group compared gene expression changes between mouse models of

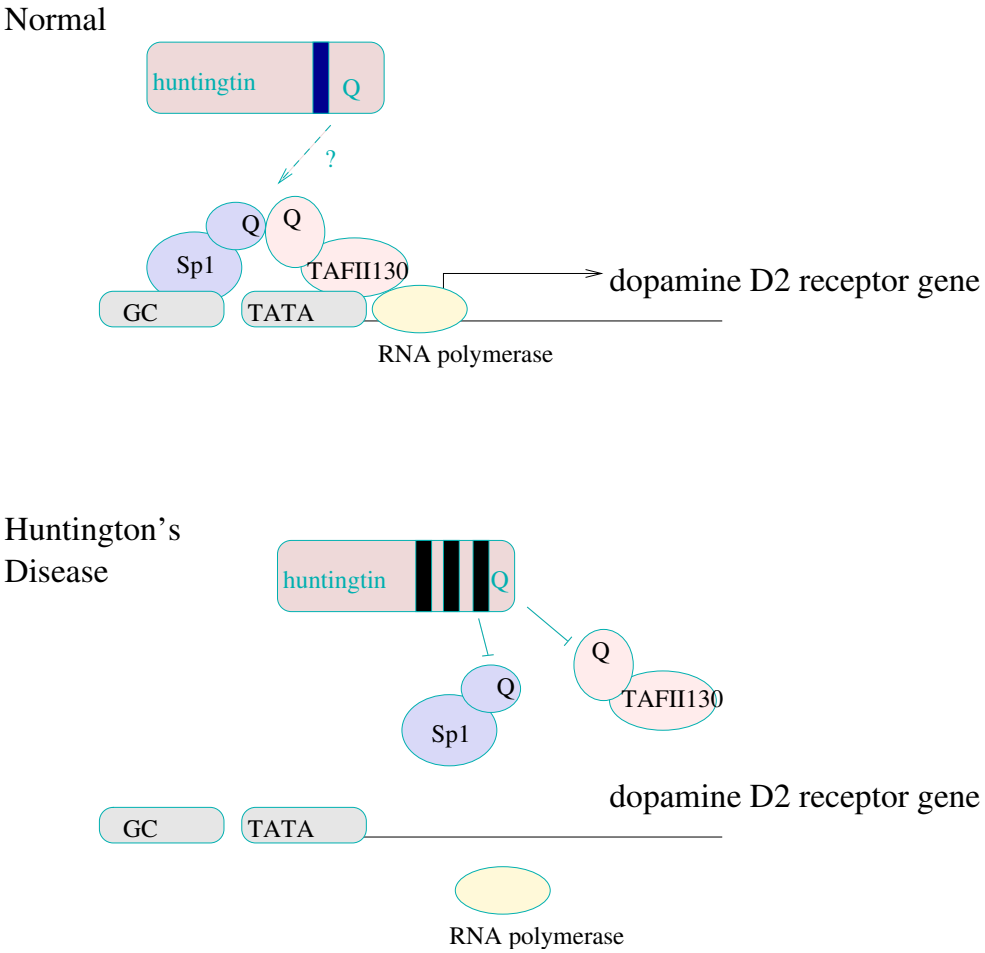

Figure 2.1: Normal: Htt is predominantly located in the cytoplasm. Sp1 binds to DNA elements called GC boxes in cellular promoters. An interaction between the polyQ regions in Sp1 and the TAFII130 is required for recruitment of the general transcriptional machinery that properly positions RNA polymerase II that transcribes mRNA. In HD, htt sequesters Sp1 and TAFII130 through the interactions of the polyQ regions. RNA polymerase II cannot bind properly and the transcription of the dopamine receptor gene is impaired (drawn according to the image from www.bio.davidson.edu).

HD chip: Gene Groups	
AP1-regulated genes	AP2-regulated genes
AR-regulated genes	Akt-regulated genes
c-myc-regulated genes	C/EBP regulated genes
CREB-regulated genes	E2F-regulated genes
Elk-1 regulated genes	RUNX-regulated genes
Fatty acid metabolism genes	Sp1-regulated genes
FOXO3 (FKHRL1)-regulated genes	Sp3-regulated genes
Genes coding heat shock proteins	Stat1-regulated genes
IRF1-regulated genes	TFEB-regulated genes
Genes coding for vesicular transport proteins	LEF1-regulated genes
Luthi-Carter data 2000 and 2002 overlap	Proteasome coding genes
NFAT-regulated genes	NFκB-regulated genes
p53-regulated genes	

Table 2.1: cDNA array gene groups. The list comprises the transcription factors and several cellular pathways that have been implicated in HD. A full list of genes regulated by those transcription factors and the genes belonging to those cellular pathways can be found in the appendix A.

HD and dentatorubral-pallidoluysian atrophy, another polyQ disease. They showed that in the cerebella of these mice, there was a considerable overlap in the genes showing altered gene expression (100). Thus, there might be polyQ-induced changes in gene expression that are independent of the polyQ protein context. The paper by Chan et al. reports that mice expressing a truncated mutant htt had many more genes with altered expression than mice expressing a full-length mutant protein. However, none of the three HD mice strains used in that study exhibited altered mRNA levels similar to those observed previously in R6/2 mice, or in other HD models. The overall number of differentially expressed genes in these study was small (38). And last, Sipione et al. used clonal HD striatal cells and reported downregulated genes belonging to the fatty acid metabolism pathway, vesicular trafficking and synaptic vesicle formation. Unlike in the R6/2 mice, the expression changes in striatal cells can be seen very early after the induction of the htt fragment (148).

In follow-up studies, age and progression-dependent changes in transcript levels during disease progression in HD patients were characterized. Transcriptional alterations were detectable in the blood of pre-symptomatic subjects and pronounced in the symptomatic subjects (31). It still needs to be evaluated if those alterations could be used as biomarkers reflecting HD progression and response to therapies.

2.3 Results

2.3.1 Selection of cDNA probes

Through literature search a list of transcription factors that might be implicated in HD has been assembled. Transcription factors Sp1, p53 and CBP, have been shown to co-localize with htt aggregates (49, 156). Dopaminergic and glutamatergic stimuli in stria-

tum, that are dysregulated in HD, influence the induction of AP-1 proteins (c-Fos and c-Jun). In striatal neurons, glutamate induces the phosphorylation of AP-1, CREB and Elk-1, a transcription factor with pro-apoptotic function in neuronal cells, which increases their transcriptional activity (144, 174). Elevated levels of the CREB-regulated gene product, C/EBP β were found in HD mice (113). A key regulatory regions in htt promoter are two Sp1 sites in a tandem repeat acting synergistically and an AP-2 site (44). Expansions to over 40 CAG repeats in the first exon of the human androgen receptor (AR) lead to spinal bulbar muscular atrophy (SBMA), another late onset neurodegenerative disease. It has been shown that excitotoxic aberrant Ca^{2+} influx activates Akt pro-survival signaling pathway in HD patients (74). Akt is a serine/threonine protein kinase that blocks neuronal death by regulating the expression of genes involved in cell death and survival (60). Increased expression of inducible nitric oxide syntheses seen in striatal cells from HD patients and HD mice, is a response to inflammatory stimuli, such as interferon regulatory factor-1 (IRF-1) and nuclear factor κB (NF-κB) (64). It has been shown that C-terminal fragments of htt interact with members NF-κB protein family involved in neuronal survival and death (164). NF-κB may promote an apoptotic response in striatal medium-sized neurons to excitotoxic insult through upregulation of c-Myc and p53 (122). By an *in vitro* binding assay it has been shown that htt interacts with PIASy (61), a nuclear-matrix associated SUMO ligase, which is a negative regulator of transcription factors Stat1, NFκB and LEF1 (163, 135). Stat1 interacts with Runx2, a transcription factor with polyQ tract, and inhibits its nuclear localization and transcriptional activity (84). Mutant htt inhibits transcription of PGC-1α, a transcriptional repressor of FoxO3 (138, 46). Sp1 and Sp3 are oxidative stress-induced transcription factors in cortical neurons that positively regulate neuronal survival in HD models and patients (134). Htt mutation leads to the aberrant interaction with calmodulin (17). The activity of NFAT proteins is tightly regulated by the calcium/calmodulin-dependent phosphatase calcineurin (123). Histone deacethylase inhibitors, proteins that repress the pro-apoptotic E2F transcription factor pathway, show beneficial effects in HD models (85). TFEB is another polyQ stretch containing transcription factor (25).

Once the list of transcription factors that might be implicated in HD was made (Table 2.1), we started to collect the genes regulated by those transcription factors. Genes were collected through literature search and the information from TRANSFAC, a database on transcription factors, their genomic binding sites and DNA-binding profiles (181). The full list of the selected genes can be found in the appendix A. Literature search resulted in lists of genes with various identifiers. To handle those lists HomGL, a web-based tool for comparing and unifying lists of genes with GenBank, RefSeq, UniGene, or other identifiers was developed (Fig. 2.2) (24). Once we had a complete list of genes, the clones corresponding to the selected genes were obtained from German Resource Center for Genome Research (RZPD), now called ImaGenes (www.imagenes-bio.de). When possible, clones from Human Unigene Set, a sequence-verified non-redundant cDNA collection for the human genome, were obtained. The genes that were not contained in Human Unigene Set were obtained from the human IMAGE libraries of cDNA clones, that are often not sequence-verified.

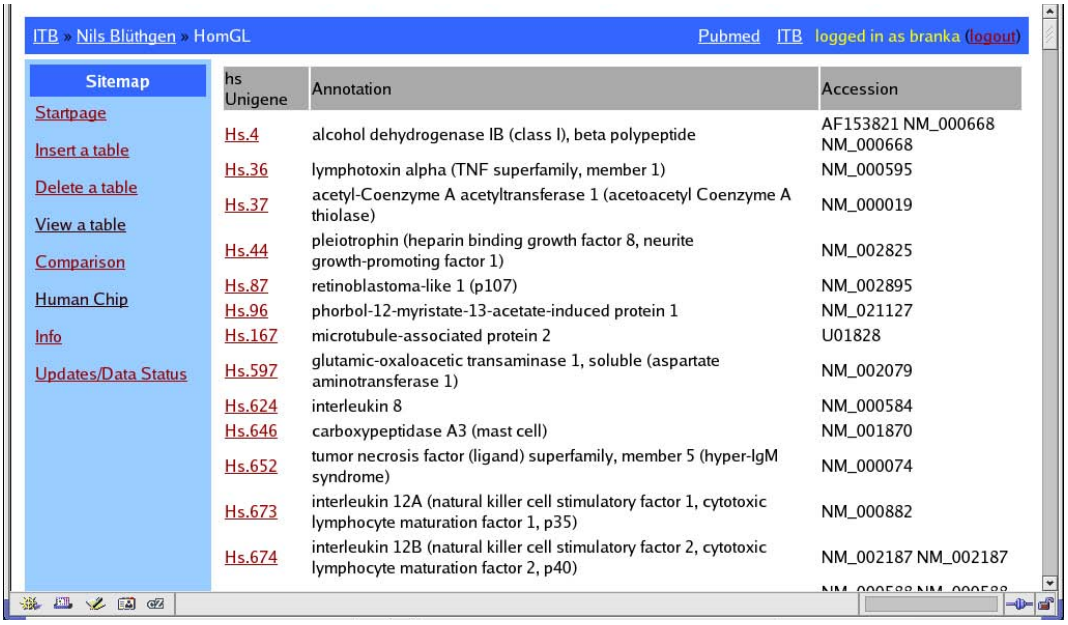

Figure 2.2: Homology Gene List (HomGL). HomGL is a web-based tool for comparing gene lists with different accession numbers and identifiers and between different organisms. The user interaction is realized through a web-interface for submitting, editing and viewing lists of gene accession numbers. A user provides a list of genes with any of the supported identifiers and retrieves a table with corresponding UniGene identifiers (24).

2.3.2 Experimental protocol

Details of the experimental protocol are given in the chapter Materials and Methods. Here, I briefly name the experimental steps. The experimental model I used was 293 Tet-off cell line (developed from human embryonic kidney cells) that is stably transfected with N-terminal htt fragments with the 83 glutamines long polyQ stretch (176). Accumulation of insoluble htt aggregates in those cells reduces the cell viability and results in the redistribution of several stress proteins and components of the proteasome system to the inclusion bodies (176). In this tetracycline (tet)-regulated system, when cells are grown in the presence of doxycycline then there is no transcription of htt fragment. Htt expression was induced by thoroughly washing the cells and adding fresh medium lacking doxycycline. Upon induction of htt fragment, these cells form perinuclear htt aggregates. I isolated RNA from the cells that had transcription of htt fragment induced for 0, 2 and 4 days. The quality of RNA was controlled by optical density measurements. Presence of htt aggregates in the cultured cells was verified by Western blot analysis (Fig. 2.3). HD microarrays containing the selected clones were spotted in the laboratory of Dr. Ulrike Nuber in Max Planck Institute for Molecular Genetics, Berlin. Also, RNA labelling and hybridisation, and the scanning of the hybridized HD microarrays was done in Dr. Nuber's lab. The analysis of microarray data was performed by Dr. Matthias Futschik from Institute of Theoretical Biology, Humboldt University, Berlin.

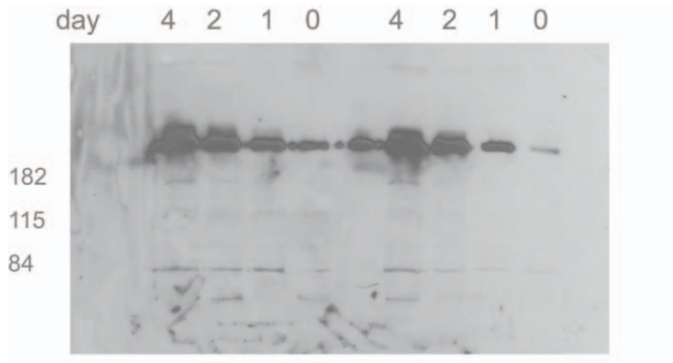

Figure 2.3: Immunoblot analysis of insoluble (pellet) protein fractions prepared from induced and uninduced 293 Tet-Off cells. For induction of htt fragment expression, cells were grown for 1, 2 and 4 days in the absence of doxycycline. Proteins were resolved by SDS-PAGE, blotted onto nitrocellulose membranes, and probed with the anti-htt antibody HD1. The htt aggregates stay at the origin of electrophoresis (left is the protein size marker in kDa). The longer the expression of htt fragment is induced, the more aggregates are present.

2.3.3 Expression changes within the gene groups

The main motivation for the studies with customized HD microarrays was to test whether systematic transcriptional changes specific for the transcription factors implicated in HD could be observed.

cDNA microarray measurements are carried out as differential hybridizations to minimize errors originating from cDNA spotting variability. cDNA from two different conditions (here, repressed and induced transcription of htt fragment) is labelled with two different fluorescent dyes and the two samples are co-hybridized to an array. After washing, the array is scanned at two different wavelengths to detect the relative abundance for each condition derived from competitive hybridization. The reference sample in all hybridisation was RNA isolated from the same cell line but grown in the presence of the inhibitor of htt transcription. The reference sample was pooled (different RNA isolations mixed together and labelled) so that all the microarrays were hybridised with the same reference sample. Two conditions that were tested were 2 and 4 days of htt fragment induction. For each condition three biological replicate samples were prepared and hybridized. Dye-swap repeats were performed for each of the six co-hybridizations. Thus, 12 arrays were used in total.

Comparing two different samples hybridized to the same array involves making adjustments for systematic errors introduced by differences in procedures and dye intensity effects. Here, first replicate spots were averaged and then dye-swaps were averaged. Dye normalization was achieved by local regression. Subsequently, significance testing was performed.

All groups of genes present on the HD microarray were analyzed in the same way as represented in the Fig. 2.4. The MA plots in Fig. 2.4 are measurements of relative expression of a gene (M) versus its average intensity (A). The MA plots show the usual intensity-dependent variability in the relative expression (noise in the obtained signals is much greater at the lower signal intensities). In all the gene groups the median and

mean difference of the $\log_2$ intensities between the samples (2 and 4 days of htt fragment induction) and the reference (0 days of htt fragment induction) did not significantly differ from 0.

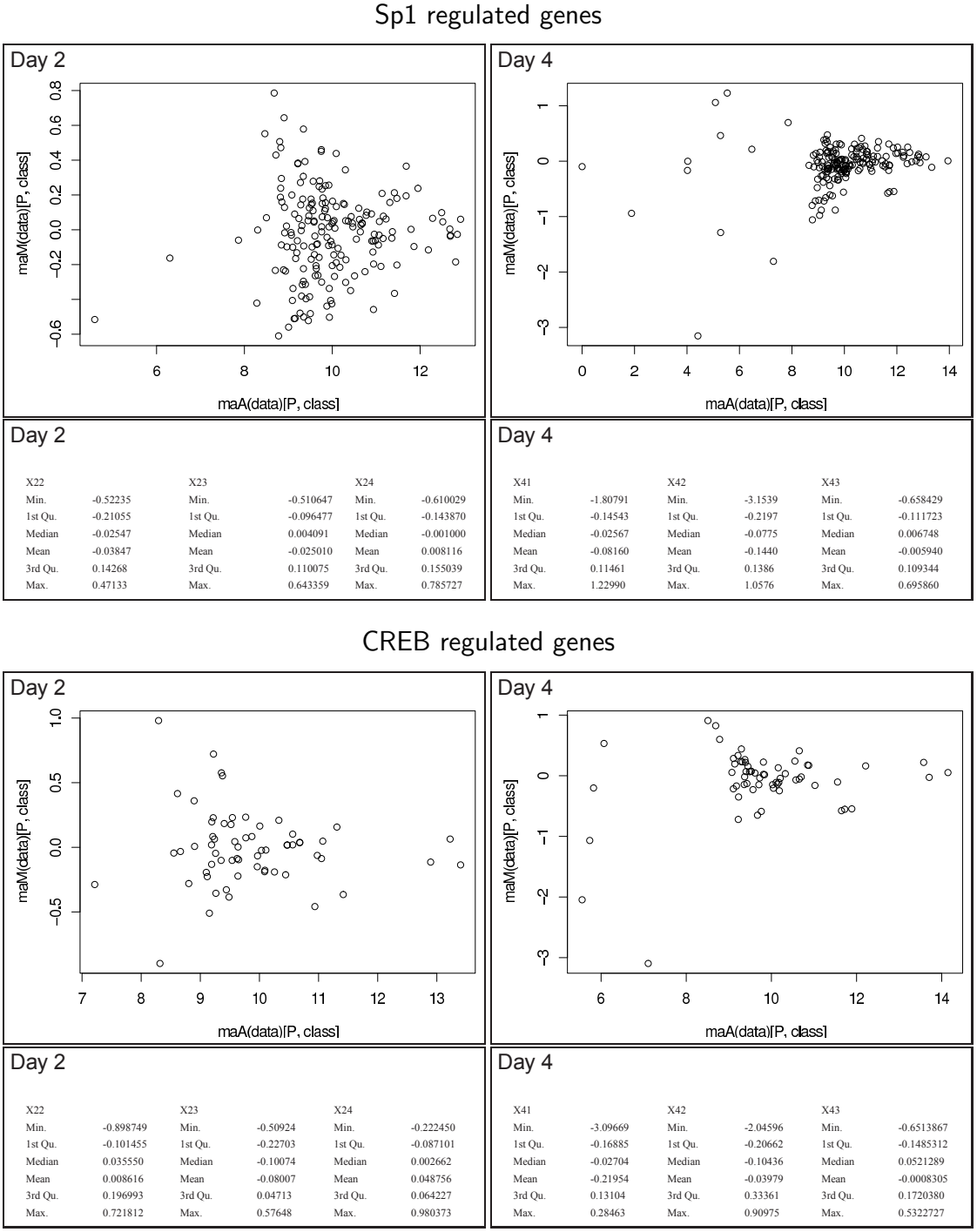

Figure 2.4: Sp1 and CREB regulated genes, 2 and 4 days after the induction of htt expression. MA plots show the mean difference of $\log_2$ intensity of the sample relative to the control versus the mean $\log_2$ intensity of Sp1 regulated genes (upper panel) and CREB regulated genes (lower panel) at day 2 (left panels) and day 4 (right panels). For each panel, the statistical analysis of 3 biological replicas are shown. For all samples, median and mean difference of $\log_2$ intensities relative to the control is not significantly different from 0.

2.3.4 Differentially expressed genes

In microarray data analysis, ratio calculations of significant changes in gene expression derived from globally normalized data are performed by computing the ratio of the average of all the measurements from one condition to the reference. The z-score is calculated by substracting the overall mean intensity from the intensity of a given gene, and dividing the results by the standard deviation of all measured intensities. The z-scores only loosely correspond to fold-changes as the change of variance is large along the intensity axis (40). The t-test is based on normalizing the expression level change with the variance of the mean expression levels (of the tested condition and the reference samples). If the expression level change in comparison with the variance of the mean expression values, one can assume there is a real difference in gene concentration.

Although no systematic changes in gene expression specific to a transcriptional factor were observed, a number of genes showed differential expression in tested conditions (2 and 4 days of htt expression). These genes are listed in Figure 2.5 and Figure 2.6. In differential gene expression comparisons of any given gene, there is a greater variance in the fold-change calculation at lower signal intensities (107). To avoid false positive results for a differential expression of genes in our samples, only genes with an average $\log_2$ signal intensity larger than 7 (the low signal intensity cut-off is often set to 100), and a z-score larger than 2 were considered to have significantly different expression. Within these boundaries we observed relatively small number of differentially expressed genes. Next, I discuss possible connections between the observed changes and HD.

Profilin, an actin-binding protein involved in dynamic turnover and restucturing of the actin cytoskeleton, and kinesin, a protein belonging to the class of motor proteins that move along microtubules and thus support mitosis, meiosis and axonal transport, were shown to be down-regulated upon the induction of htt fragment. Indeed, the disruption of axonal transport by pathogenic polyQ proteins is considered to contribute to the early neuropathology in HD (65).

Platelet-derived growth factor A (PDGF-A), one of the proteins that regulate cell growth and division, was shown to be down-regulated both at day 2 and at day 4 after the htt induction. Wild-type htt is involved in transcription of brain-derived neurotrophic factor (BDNF), and the mutation in htt leads to the loss of BDNF transcription which is detrimental to striatal neurons (186). PDGF proteins also exert trophic effect on developing striatal neurons and are a normal response to striatal injury. Thus, there is hope that they might be used to counteract striatal degeneration in HD (150, 110). Learning more about the PDGF transcriptional regulation in the presence of mutant htt would help those attempts.

Huntingtin gene seems to be down-regulated at day 4, but the IMAGE clone spotted on the array has no verified sequence. If correct, the sequence would correspond to the C-terminal end of htt, and so the htt fragment induced in the experiment would not be detected by this clone.

Comparisons between the list of differentially expressed genes from this study and the list of differentially expressed genes from seven other microarray studies (38, 98, 100, 182, 148, 89, 7), as well as the comparisons between the seven microarray studies showed very little overlap (Dr. Nils Bluethgen, personal communication).

Gene.Title	Clone.ID	A	z.Mav	z.z	z.p	t.t	t.p	M.22	M.23	M.24
ribosomal protein L31	IMAGp956B0241	11.470	0.747	8.655	+0.00E+00	1.316	0.319	0.408	-0.022	1.856
plasminogen activator inhibitor, type I	IMAGp956C1759	10.244	0.814	6.977	+1.51E-12	1.021	0.415	2.409	-0.032	0.066
ribosomal protein L27a	IMAGp956P23126	9.749	0.547	3.427	+3.05E-04	1.726	0.227	0.369	0.109	1.164
NADH dehydrogenase (ubiquinone	IMAGp956E1778	9.253	0.598	2.765	+2.84E-03	1.209	0.350	0.147	0.060	1.585
protective protein for beta-galactosidase (galactosialidosis	IMAGp956O0959	8.900	0.723	2.697	+3.49E-03	3.099	0.090	1.106	0.301	0.763
G protein pathway suppressor 1	IMAGp956E0225	9.879	0.378	2.573	+5.04E-03	2.283	0.150	0.677	0.355	0.104
Mediator of receptor-induced toxicity	HU3 p972D07273	10.048	0.312	2.365	+9.01E-03	5.902	0.028	0.229	0.298	0.410
Human interferon-gamma (HuIFN-gamma) mRNA, complete cds	HU3 p972B08319	9.820	-0.343	-2.243	+1.24E-02	-2.768	0.109	-0.426	-0.503	-0.099
Kinesin family member 13A	HU3 p972E09309	10.075	-0.339	-2.614	+4.47E-03	-2.553	0.125	-0.525	-0.411	-0.082
Profilin 1	IMAGp956M05195	8.795	-0.826	-2.891	+1.92E-03	-1.101	0.386	-2.325	-0.109	-0.043
Brain-specific angiogenesis inhibitor 1	HU3 p972F08324	9.347	-0.611	-2.992	+1.39E-03	-6.029	0.026	-0.780	-0.621	-0.430
ESTs, Moderately similar to T47135	IMAGp998A225997	9.374	-0.617	-3.071	+1.07E-03	-1.021	0.415	-1.824	0.009	-0.035
Platelet-derived growth factor PDGF-A	HU3 p972B09311	9.700	-0.510	-3.102	+9.60E-04	-2.596	0.122	-0.680	-0.733	-0.118
Sema domain, immunoglobulin domain (Ig	IMAGp956G1970	9.929	-0.508	-3.569	+1.79E-04	-2.231	0.155	-0.406	-0.944	-0.175
Tissue inhibitor of metalloproteinase 2	IMAGp956E01196	10.772	-0.353	-3.686	+1.14E-04	-0.776	0.519	0.315	-0.151	-1.221
Endothelial differentiation, G-protein-coupled receptor 6	IMAGp956C0853	10.500	-0.399	-3.925	+4.33E-05	-2.278	0.150	-0.105	-0.382	-0.710
ATP synthase, H+ transporting, mitochondrial F0 complex, subunit F6	IMAGp956K1353	9.724	-0.814	-5.019	+2.60E-07	-1.026	0.413	-0.164	0.115	-2.393

Figure 2.5: Differentially expressed genes 2 days after htt fragment induction. The column labels have the following meaning: Clone.ID is Imagenes identifier, A is average (mean) $\log_2$ intensity, z.Mav is average (mean) difference of $\log_2$ intensity of samples relative to the control samples, z.z is intensity related z-score, z.p is p-value based on intensity related z-score, t.t is t-score of comparison, t.p is p-value based on t-score, M22, M23 and M24 are difference of $\log_2$ intensity of individual samples relative to the control sample. Positive values of z.Mav correspond to up-regulated genes, and negative values of z.Mav correspond to down-regulated genes.

Gene.Title	Clone.ID	A	z.Mav	z.z	z.p	t.t	t.p	M.41	M.42	M.43
Platelet-derived growth factor PDGF-A	HU3 p972B09311	10.239	-1.276	-7.890	+0.00E+00	-14.919	0.004	-1.107	-1.384	-1.336
Brain acid-soluble protein 1	IMAGp956H0970	8.341	-1.153	-3.027	+1.24E-03	-1.502	0.272	-0.525	-2.681	-0.253
Brain-specific angiogenesis inhibitor mRNA, complete cds 1	HU3 p972F08324	9.456	-1.112	-4.743	+1.05E-06	-6.257	0.025	-1.467	-0.923	-0.946
Dodecenoyl-Coenzyme A delta isomerase (3,2 trans-enoyl-Coenzyme A isomerase)	HU3 p972D07300	8.080	-1.047	-2.477	+6.63E-03	-11.776	0.007	-1.203	-1.041	-0.896
Huntingtin	IMAGp998D0552Q2	8.853	-1.011	-3.265	+5.48E-04	-1.624	0.246	-0.513	-2.247	-0.271
Tyrosine phosphatase (PAC-1)	HU3 p972A09305	9.390	-1.008	-4.175	+1.49E-05	-6.151	0.025	-0.893	-1.331	-0.800
EEN-B2-L3 mRNA, complete cds	HU3 p972G10131	8.593	-0.994	-2.870	+2.05E-03	-1.120	0.379	0.110	-0.341	-2.749
Olfactory receptor, family 2, subfamily L, member 2 (OR2L2)	IMAGp998A0913279Q3	9.155	-0.840	-3.135	+8.60E-04	-8.896	0.012	-0.884	-0.976	-0.658
Mdm2, transformed 3T3 cell double minute 2, p53 binding protein	IMAGp998F04223Q3	9.653	-0.806	-3.761	+8.48E-05	-1.111	0.382	-0.131	-2.257	-0.031
3-phosphoglycerate dehydrogenase	IMAGp956K2318	8.697	-0.789	-2.376	+8.74E-03	-1.245	0.339	-0.136	-0.175	-2.055
Antigen NY-CO-28 (NY-CO-28) mRNA, partial cds	HU3 p972D08292	8.848	-0.785	-2.532	+5.67E-03	-1.225	0.345	-0.190	-2.066	-0.100
Kinesin family member 13A	HU3 p972E09309	10.608	-0.748	-5.376	+3.80E-08	-8.943	0.012	-0.740	-0.608	-0.897
MHC class I polypeptide-related sequence A (MICA) gene	HU3 p972D03299	10.109	-0.728	-4.230	+1.17E-05	-24.765	0.002	-0.769	-0.671	-0.744
Axin (AXIN) mRNA, partial cds	HU3 p972C04322	9.749	-0.712	-3.467	+2.63E-04	-8.044	0.015	-0.543	-0.842	-0.751
Human interferon-gamma (HuIFN-gamma) mRNA, complete cds	HU3 p972B08319	9.549	-0.705	-3.136	+8.56E-04	-7.869	0.016	-0.884	-0.607	-0.624
Endothelial differentiation, G-protein-coupled receptor 6	IMAGp956C0853	11.368	-0.649	-5.904	+1.77E-09	-10.926	0.008	-0.764	-0.615	-0.567
Glial fibrillary acidic protein [human, glioma cell line U-251 MG, mRNA]	HU3 p972H0337	11.752	-0.558	-5.154	+1.28E-07	-62.466	0.000	-0.553	-0.576	-0.546
Heat shock 70kDa protein 1B	IMAGp998F1070Q3	13.890	-0.484	-4.026	+2.84E-05	-17.462	0.003	-0.458	-0.540	-0.455
Human glucose-6-phosphatase mRNA, complete cds	HU3 p972C0213	10.073	-0.454	-2.589	+4.81E-03	-1.370	0.304	0.033	-1.088	-0.308
Porc-Pl gene similar to yeast CDC45	HU3 p972C05319	10.795	-0.374	-2.867	+2.07E-03	-10.383	0.009	-0.438	-0.313	-0.370
Lactate dehydrogenase B gene exon 1 and 2 (EC 1.1.1.27) (and joined CDS)	HU3 p972E1251	12.923	-0.366	-3.022	+1.25E-03	-13.973	0.005	-0.329	-0.416	-0.351
Glyceraldehyde-3-phosphate dehydrogenase	IMAGp956H0677	11.076	-0.317	-2.685	+3.62E-03	-3.345	0.079	-0.355	-0.137	-0.458
Human prosomal protein P30-33K (pros-30) mRNA, complete cds	HU3 p972C0217	11.483	-0.307	-2.831	+2.32E-03	-1.432	0.288	-0.045	-0.732	-0.145
Human c-myc-P64 mRNA, initiating from promoter P0, (HLmyc3.1) partial cds	HU3 p972B12122	11.618	0.300	2.776	+2.75E-03	8.914	0.012	0.353	0.309	0.237
DnaJ (Hsp40) homolog, subfamily B, member 11	HU3 p972H0998	11.02	0.324	2.626	+4.32E-03	10.085	0.010	0.388	0.294	0.290
Human tra1 mRNA for human homologue of murine tumor rejection antigen gp96	HU3 p972E1293	12.966	0.683	5.657	+7.70E-09	7.041	0.020	0.845	0.510	0.695
Epithelial membrane protein 2 (EMP2)	IMAGp956C2058	8.280	1.047	2.684	+3.63E-03	1.539	0.264	2.173	-0.178	1.147
SHC (Src homology 2 domain-containing) transforming protein	IMAGp956C1252	8.154	1.414	3.446	+2.84E-04	1.775	0.218	2.765	1.471	0.007

Figure 2.6: Differentially expressed genes 4 days after htt fragment induction. The column labels have the following meaning: Clone.ID is Imagenes identifier, A is average (mean) $\log_2$ intensity, z.Mav is average (mean) difference of $\log_2$ intensity of samples relative to the control samples, z.z is intensity related z-score, z.p is p-value based on intensity related z-score, t.t is t-score of comparison, t.p is p-value based on t-score, M41, M42 and M43 are difference of $\log_2$ intensity of individual samples relative to the control sample.Positive values of z.Mav correspond to upregulated genes, and negative values of z.Mav correspond to downregulated genes.

2.4 Discussion

Many transcriptional alterations have been reported early in HD progression (161). Understanding these early molecular mechanisms could provide an opportunity to interfere with the effects of mutant htt before the development of disease symptoms. However, the relevance of the transcriptional pathways implicated in HD to disease pathogenesis remains uncertain. Different methods such as yeast two-hybrid, co-localization and immunoprecipitation show the interactions between the mutant htt and a number of nuclear proteins, but the functional consequences of many of them have not been determined *in vivo*. For a disease that takes decades to develop, it is clear that the pathogenic and coping mechanisms advance in parallel. The levels of hundreds of RNA transcripts are altered in different HD models, but it is uncertain which are the most pathogenic. Moreover, even though DNA microarray studies demonstrate a measure of selectivity in which genes are affected, the overlap of common altered transcripts is small.

Transcriptionally active therapies would attempt to normalize the abberant transcription profiles found in HD models. So far, no single transcriptional regulator has emerged as a primary actor in HD. The basis of transcriptional dysregulation appears to be in aberrant protein-protein interactions between mutant htt and a variety of transcription factors. However, these protein-protein interactions do not constitute conventional and easy targets for drug molecules (81). So far, administration of histone deacetylase (HDAC) inhibitors, that increase the overall levels of gene expression in the cells, has been the only successful therapeutic strategy targeting transcription dysregulation in HD (72).

It has been suggested that the depletion of transcription factors by sequestration into htt aggregates underlies the transcriptional changes in HD models and that restoring normal transcriptional activity of these factors would reverse early pathological processes in HD (36). A surprising number of diverse clinical phenotypes are due to mutations in genes encoding transcription factors. The mechanism by which such transcription factor defects cause disease is often haploinsufficiency, or a reduction by half in the protein levels of the encoded transcription factor (reviewed in ref. (145)). For HD models, there are no quantitative data about the fraction of transcription factors trapped in the htt aggregates.

The study presented here aimed at getting the first information about the global, transcription factor specific changes in the gene expression induced by mutant htt. I used customized cDNA chips containing groups of genes regulated by 20 trancription factors and 4 additional groups of genes belonging to the pathways that are affected in HD to test whether systematic changes in expression of these groups of genes can be observed. However, in none of the gene groups systematic trancriptional changes were observed.

The change in gene expression induced by a small changes in the concentration of regulatory proteins controlling a specific the gene, termed sensitivity. However, knowledge about the sensitivity of human promoters is scarce (22, 23). To elicit their effects on gene expression, transcriptional activators require the cooperation of a diverse family of coregulator proteins (114). The complexity and diversity of the gene regulation is likely to cause different sensitivity of individual promoters to the concentration of the transcription factors involved in their regulation. This means that even if the changes in the levels of

certain transcription factors are induced by the mutant htt, these changes might be too small to affect a large subset of genes under the control of those transcription factors.

Mutant htt triggers multiple pathways of neurodegeneration, including dysregulation of transcription but it is uncertain which, if any, might have a primary position in a cascade. Transcriptional changes do occur in HD, but the cause and the consequences of these changes remain to be elucidated. The non-intuitive format and the vast amounts of the transcriptomics data makes it difficult to generate hypothesis based on this kind of experimental observation. On the other hand, mathematical modelling of biological processes requires a clear question and aim of what the model should accomplish, and is conceptually similar to generating a hypothesis (87). I had hoped that the time-resolved detection of changes in gene expression profiles in relation to htt aggregate formation would provide the supporting data for building a mathematical model. However, the transcriptional changes detected in this study do not support the tested hypothesis and could thus not be used for mathematical modelling. Moreover, the huge differences in the trancriptional output of different experimental HD models pose a serious question about the validity of extrapolating the results from HD models to the pathological changes in HD patients. Therefore, the question of transcriptional dysregulation in HD was not further pursued. Instead, in the next chapter I formulate a simple mathematical model of htt aggregation that forms the foundation on which I build more complex models as a framework for evaluating the existing experimental data and conclusions about htt aggregation.

Chapter 3

Deterministic Models of Huntingtin Aggregation

3.1 Summary of the chapter

Huntington's disease (HD) is a late onset, progressive disorder. In the course of HD, the patients slowly lose their physical and mental abilities. It is possible to measure the functional decline of the affected brain regions in HD patients but what dictates the dynamics of that decline is not known. Mutation in the polyglutamine (polyQ) stretch hinders proper folding of huntingtin (htt). Misfolded htt undergoes a proteolytic cleavage releasing a short-htt fragment with a propensity to form aggregates. Misfolding, aggregation and accumulation of specific proteins underly the pathology of HD and a number of other neurodegenerative diseases. Understanding the dynamics of the aggregation process in HD and related disorders, might help us formulate successful therapeutic strategies. In this chapter, I present and analyze a simple mathematical model of htt aggregation. It is a deterministic model that consists of a set of ordinary differential equations describing htt aggregation as a nucleation process. This model allows us to monitor how the variables of the model: full-length htt, and monomers, oligomers and aggregates of htt fragment change in time, what steady state such a system acquires, and how the change in parameters affects the system. In the model, I use htt fragment release rate, A, as a sensor of environmental changes and a bifurcation parameter. First, I analyze a core model of htt aggregation in which A has a constant value. I determined the steady states of the system and their stability depending on the value of A. As the value of A changes, the system goes through two bifurcation points, corresponding to the two nucleation events: the onset of oligomerization and the onset of aggregation. Second, I extend the core model of htt aggregation and include the dependence of A on the concentrations of enzymes involved in htt cleavage in striatal cells. Caspase-mediated htt cleavage process involves regulation via positive feedback loop. I conclude that a nucleation process and a positive feedback loop acting on the htt fragment release rate describe well the late onset of aggregation through an intrinsic mechanism.

3.2 Introduction

The most striking feature of mutant htt is its tendency to form insoluble protein aggregates with a fibrilar morphology (47, 140). The formation of protein aggregates is a hallmark of a number of neurodegenerative diseases: Alzheimer's disease with β-amyloid in plaques, Parkinson's disease with α-synuclein in Lewy bodies, and frontotemporal dementia with mutant tau. These diseases share multiple pathogenic mechanisms: loss of physiological activity of the misfolded protein, neurotoxicity of the aggregation species, and chronic brain inflammation triggered by the accumulation of protein deposits (132).

Small molecules are being developed that inhibit aggregation of β-amyloid (28), α-synuclein (92), and htt (51). A great hope is that the development of a therapy for one of the diseases may have implications for the others. Understanding the mechanisms of aggregation of the disease proteins might be a step toward fulfilling that hope.

3.2.1 Mechanism of htt aggregation

The late onset of HD was first explained by the cumulative damage hypothesis, according to which affected neurons die when a critical amount of damage is reached. As a consequence, the probability of the neurons to die would increase with age. Surprisingly, in a number of neurodegenerative disease, including HD, it was shown that the probability of the neurons to die was constant in time (43). This result, which implies that cell death is caused by a random, rare event, together with the finding that the time before the onset of aggregation is inversely proportional to the length of the polyQ repeat (141), led to now established hypothesis that the aggregation of htt is a nucleation-dependent process (119).

Nucleation is a sudden phase-transition phenomenon where the first steps are energetically less favoured than continuation of growth. Nuclei of molecular aggregates are unstable when very small because of their large ratio of surface area to volume. Perutz et al. (119) proposed that initial nucleation of intracellular aggregates is the event that leads to cell death. The growth rate of the aggregate, once nucleated, is typically of the order of tens of micrometers per second (119). For any process that occurs on a timescale of years, the controlling step will thus be nucleation, not growth.

3.2.2 Toxic fragment hypothesis

Htt was the first neuronal protein shown to be a caspase substrate (62), with defined sites for caspase-3, caspase-2, and caspase-6 (177). Calpains, from the family of cystein proteases, further cleave htt fragments (55). Toxicity of caspase-resistant mutant htt is markedly reduced in transfected cells (178). Proteolytic cleavage of the mutant htt that generates aggregation-prone N-terminal fragments denotes a key event in HD pathogenesis (103). Caspase-mediated cleavage of full-length mutant htt precedes the neuronal dysfunction and selective neurodegeneration in HD (179), and the toxicity of caspase-resistant mutant htt is markedly reduced in transfected cells (178). Unlike the full length mutant htt, a short N-terminal htt fragment released by cleavage faces no steric hindrance to form the new aggregation-prone secondary structure. Perutz was the first to propose that the sharp threshold in the pathogenic polyQ length stems from the struc-

tural transition of the mutant htt fragment to a β-sheet structure prone to aggregation (120, 121).

In HD patients, the cleavage of a full-length htt and a release of a htt fragment is a complex process. Proteases acting on mutant htt generate cleaved products that differentially build up cytoplasmic and nuclear inclusions. Smaller fragments appear solely responsible for amassing nuclear aggregates, while cytoplasmic inclusions contain fragments of various lengths (97).

3.2.3 Selective vulnerability: role of caspase-2

Mutant htt is expressed in all cell types tested so far (147). However, only specific areas of the brain are affected by this mutation. In HD, selective neural death leads to the choreic movements and dementia. The most vulnerable cells are medium spiny neurons in the striatum, which are the first to die. What renders these cells more susceptible to toxic effects of the mutation has not yet been fully understood. However, it has been recently shown that wild-type htt upregulates the transcription of brain-derived neurotrophic factor (BDNF), a pro-survival factor produced by cortical neurons. This beneficial activity of htt is lost when the protein becomes mutated (186). Decreased levels of BDNF in the striatum and cortex of HD transgenic mice upregulate caspase-2 (71), a default executioner as well as initiator caspase in neuronal cells deprived of nerve growth factor (170). Activated caspase-2 causes the mitochondrial pores to open and cytochrome c to be released (127, 117). These findings suggest that caspase-2 is involved in the selective neuronal cell death in the striatum and cortex of HD patients.

3.2.4 Mathematical analysis of dynamical systems

When life scientists talk about models they usually refer to experimental systems that show a characteristic behaviour and therefore are useful to study the underlying mechanisms. Similarly, systems biology models are analytical tools whose purpose is to give insight into mechanisms and reveal what determines a particular behaviour with the aim to eventually predict that behaviour (87).

Various biological systems have been modelled, with the aim of better articulating how the underlying dynamics contribute to observed cellular behaviour. Modelling can be carried out at various levels of details. The choice depends on the nature of questions to be addressed.

The process of htt aggregation can be described as a dynamical system, but the exact kinetics are unknown. We are thus interested in the qualitative behaviour of the system as the parameters change rather than quantitative changes. The first step in studying the qualitative behaviour of the system is to find its steady states, i.e. the states at which the variables have a rate of change equals to zero. Once the steady states are identified, it is necessary to determine their stability. A steady state is locally stable if solutions with any initial conditions sufficiently close to the steady state converge toward that steady state. The steady state is unstable if there exists a solution with arbitrarily close initial conditions that does not converge to the steady state. A formal way to analyze the stability of a nonlinear system is to linearize it around the fixed point, and study

the behavior of the linear system. In the vicinity of the steady state, both nonlinear and linear systems will behave in the same way.

Parameters are quantities in the system that do not change dynamically in time, unlike dynamical variables, but may be changed by a drug or other external factors. A qualitative change in the dynamics of a system in dependence upon the value of a parameter is called a bifurcation. The parameter is thus called bifurcation parameter, and the threshold value where the bifurcation occurs is called bifurcation point. A nucleation process is well described by a transcritical bifurcation. A transcritical bifurcation is characterised by an exchange in stability between two steady-states. Below the bifurcation point, one steady-state (e.g. htt monomers) is stable, and the other one (e.g. htt aggregates) unstable. At the bifurcation point, the two steady states merge, and exchange stability: the unstable steady-state becomes stable and the stable steady state becomes unstable (80). Transcritical bifurcations are relevant for switch-like phenomena (162, 1). In the model for aggregation presented here, there are two transcritical bifurcations that correspond to the nucleation of oligomers and aggregates.

3.3 Mathematical Models

To express aggregation kinetics in terms of ordinary differential equation (ODE), we assume that molecular concentrations are continuous (it ignores the discrete nature of molecules), that reactions occur in a homogeneous, well-stirred volume and that these reactions occur in a deterministic manner. This is a common form of biological model and can represent both the transient dynamics and the long-term steady-state behavior of a system if the above approximations hold (4).

I use two levels of description of the htt aggregation: a core model, and an extended model. The core model consist of a set of four ODEs describing the change in the concentration of: the full-length mutant htt, and the monomers, the oligomers and the aggregates of the cleaved htt fragment. This simple system can be analytically solved. The bifurcation parameter was the htt fragment release rate, A, and thus the steady state analysis defines the values of A for which the oligomers and the aggregates are stable (Figure 3.1).

In the extended model, the release rate A is caspase-activity dependent, and the caspase activity is modeled explicitly. Thus the model consists of a set of 6 ODEs, with the full-length htt, the monomers, the oligomers and the aggregates of the cleaved htt fragment, a procaspase-2, and a caspase-2 as variables. The evolution of this system over time shows that the delay in the onset of aggregation can be explained by an intrinsic mechanism.

3.3.1 Core model for htt aggregation

The core model for htt aggregation consists of 4 variables: the concentrations of full length mutant htt Htt, N-terminal htt fragment M_{htt}, htt fragment oligomer O_{htt}, and htt fragment aggregate A_{htt} (Figure 3.1). Misfolded htt is a substrate for a proteolytic cleavage reaction in which short, N-terminal fragments that are prone to aggregation are released. Htt misfolding and aggregation follows a reversible nucleation mechanism

Table 3.1: List of parameters for the core model

Parameter	Value	Description
k_h	1.0	Htt synthesis rate
k_{dh}	0.5	Htt proteasomal degradation rate
k_{de}	0.2	Htt fragment proteasomal degradation rate
k_n	0.4	Rate of formation of oligomers
k_n^{-1}	0.01	Rate of release of monomers from oligomers
k_{dn}	0.1	Proteasomal degradation of oligomers
k_a	0.4	Rate of aggregation of oligomers
k_a^{-1}	0.01	Rate of release of oligomer from aggregates
k_{da}	0.02	Removal rate of aggregates by autophagy

modulated by environmental factors. A number of transgenic HD cell and mouse models express only N-terminal htt fragment at a constant rate. In the core model, this is equivalent to considering that the release of a htt fragment, A, has a constant value. Monomeric fragments start to aggregate through a number of intermediate oligomeric structures O_{htt}. Both monomeric and oligomeric structures are substrates for proteasomal degradation. As the oligomeric structures get bigger they become more resistant to proteasomal degradation, thus the corresponding rates decrease (Table 3.1). The proteasomal machinery cannot digest big aggregates, so the cell removes them by autophagy.

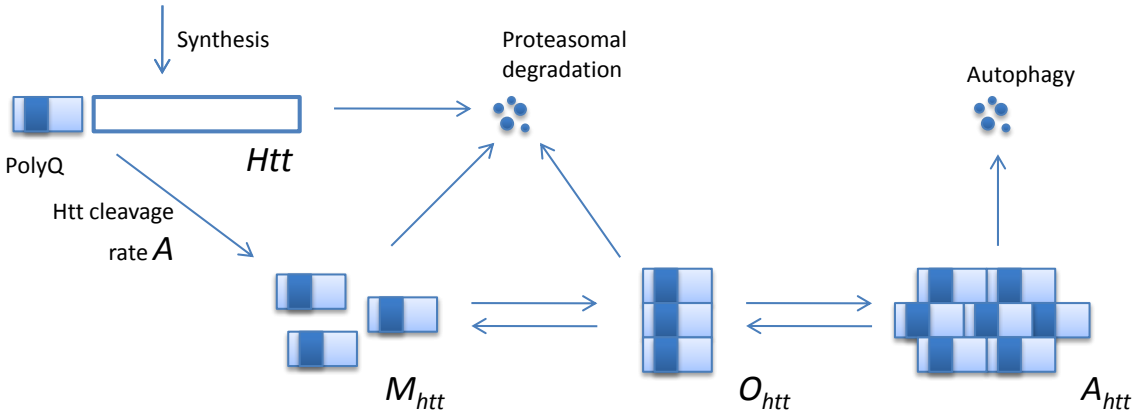

Figure 3.1: Core model for htt aggregation. Mutant full-length htt, Htt, is cleaved and a short N-terminal htt fragment, M_{htt}, is released with a constant rate A. Htt fragments aggregate and form htt oligomers, O_{htt}, which further aggregate and form htt aggregates, A_{htt}. Full-length htt, monomers and oligomers of htt fragments are degraded by the proteasome, and aggregates are removed by autophagy.

Table 3.2: Steady states of the core model.

	STST1	STST2	STST3
Htt	$\frac{k_h}{A+k_{dh}}$	$\frac{k_h}{A+k_{dh}}$	$\frac{k_h}{A+k_{dh}}$
M^i_{htt}	$\frac{AHtt}{k_{de}}$	$\frac{k_{dn}+k_n^{-1}}{k_n}$	$\frac{AHtt+k_n^{-1}O^3_{htt}}{k_nO^3_{htt}+k_{de}}$
O^i_{htt}	0	$\frac{AHtt-k_{de}M^2_{htt}}{k_{dn}}$	$\frac{k_a^{-1}+k_{da}}{k_a}$
A^i_{htt}	0	0	$\frac{O^3_{htt}}{k_{da}}\left[k_nM^3_{htt}-(k_{dn}+k_n^{-1})\right]$

Now the differential equations for the 4 variables considered can be written down.

$$\frac{\mathrm{d}Htt}{\mathrm{d}t} = k_h - AHtt - k_{dh}Htt, \tag{3.1}$$

$$\frac{\mathrm{d}M_{htt}}{\mathrm{d}t} = AHtt - k_nM_{htt}O_{htt} + k_n^{-1}O_{htt} - k_{de}M_{htt}, \tag{3.2}$$

$$\frac{\mathrm{d}O_{htt}}{\mathrm{d}t} = k_nM_{htt}O_{htt} - k_aO_{htt}A_{htt} + k_a^{-1}A_{htt} - [k_n^{-1}+k_{dn}]O_{htt}, \tag{3.3}$$

$$\frac{\mathrm{d}A_{htt}}{\mathrm{d}t} = k_aO_{htt}A_{htt} - [k_a^{-1}+k_{da}]A_{htt}. \tag{3.4}$$

3.3.2 Steady states of the core model

First, the steady states of the system are determined, i.e. the states at which the variables have a rate of change equal to zero, by setting the right hand sides of the equations to zero.

From Equation 3.4, two steady states are visible, $A^*_{htt} = 0$ (I) or $A^*_{htt} \neq 0$ (II). Two paths can be followed.

Case (I) $\mathbf{A^*_{htt} = 0}$. The steady state oligomer concentration satisfies

$$k_nM_{htt}O_{htt} - [k_n^{-1}+k_{dn}]O_{htt} = 0.$$

Two steady states are possible for O_{htt}.

Subcase (Ia) $O^*_{htt} = 0$. In this case, $M^*_{htt} = \frac{A\cdot Htt^*}{k_{de}}$.

Subcase (Ib) $O^*_{htt} \neq 0$. The second steady state for O_{htt} gives $M^*_{htt} = \frac{k_n^{-1}+k_{dn}}{k_n}$. It this case $O^*_{htt} = \frac{A\cdot Htt - k_{de}M_{htt}}{k_{dn}}$.

Case (II) $\mathbf{A^*_{htt} \neq 0}$. Here, Equation 3.4 gives $O^*_{htt} = \frac{k_a^{-1}+k_{da}}{k_a}$. Equation 3.3 can be solved for A_{htt}

$$A^*_{htt} = \frac{O_{htt}}{k_{da}}\left(k_nM_{htt} - \left(k_n^{-1}+k_{dn}\right)\right).$$

The steady state of Htt is independent of the the other variables, $Htt^* = \frac{k_h}{A+k_{dh}}$ for all cases. The three steady states (Ia), (Ib) and (II), are denoted as STST1, STST2 and STST3, and listed in Table 3.2. The superscripts i in M^i_{htt}, O^i_{htt} and A^i_{htt} refer to the ith steady state (STSTi, $i = 1...3$).

Table 3.3: Stability analysis of the core model.

	STST1	STST2	STST3
$A < A_1$	$\lambda < 0$	$\Re(\lambda_{2,2+3}) > 0$	$\lambda > 0$
$A_1 < A < A_2$	$\lambda_{1,3} > 0$	$\Re(\lambda) < 0$	$\lambda > 0$
$A > A_2$	$\lambda_{1,3} > 0$	$\lambda_{2,4} > 0$	$\Re(\lambda) < 0$

For any set parameter values, one steady state is stable, and two are unstable. Stability changes from STST1 to STST2 through a transcritical bifurcation when $A = A_1$, where

$$A_1 = \frac{k_{dh} a}{k_n k_h - a}, \quad \text{with } a = k_{de}(k_{dn} + k_n^{-1}). \tag{3.5}$$

Similarly, stability changes from STST2 to STST3 when $A = A_2$, where,

$$A_2 = \frac{k_{dh}(a+b)}{k_n k_h - (a+b)}, \quad a = k_{de}(k_{dn} + k_n^{-1}), \quad b = k_{dn} k_n \frac{k_a^{-1} + k_{da}}{k_a}. \tag{3.6}$$

The detailed stability and bifurcation analysis is in Appendix A.

When the rate A of htt release is low, htt monomers are present in a concentration too small for oligomeric structures to be stable, and STST1 is stable. As A increases, the system goes to STST2, where oligomers become stable but aggregates are still unstable. A further increase in A brings the system to STST3 where all three entities, monomers, oligomers, and aggregates, are present. Two threshold levels of caspase activity A_1 and A_2 (Equations 3.5–3.6) define transcritical bifurcation points, where an exchange in stability from one steady state to another occurs. The transition from one steady state to the other must be continuous, and only changes from STST1 to STST2 and STST2 to STST3 are possible. This requirement excludes bistable behaviour of the system.

3.3.3 Extended model for htt aggregation

The extended model is introduced to model the caspase-induced change in the release rate of htt fragment A. This change could bring the core model through the successive transcritical bifurcations by an intrinsic mechanism. In the core model, A was a bifurcation parameter that was changed without explicitly formulation where this change comes from.

Downstream of the first exon of htt there are several consensus sequences recognized by caspase-3, caspase-2, and caspase-6 (177). In different cell and animal models benefits

of inhibiting each of these proteases have been shown (178, 56). In the extended model of htt aggregation, caspase-2 is assigned as a representative cleavage enzyme, because of its involvement in the selective neuronal death in the striatum (71). However, the formulation of the model is not specific to caspase-2.

Several groups have shown that procaspases are not just inactive isoforms of caspases, but that they also have a catalytic activity, though at a much lower level than the caspases (159). Mutant full-length htt may provide a suitable substrate for a basal activity of procaspase-2, since it binds to procaspase-2 (71). Although procaspase-2 does not require cleavage for the initial acquisition of activity, dimerization and intersubunit cleavage is required to generate levels of activity that could induce cell death (15).

Caspase-dependent release of toxic htt fragment initiates a number of processes damaging to the cell. This leads to the activation of caspases in HD cells. Activated caspases have an even higher rate of mutant htt cleavage. It is very likely that such a positive feedback loop exists in HD cells, but its importance is not known. In the extended model I analyzed the effect of a representative positive feedback loop on the time of the onset of aggregation.

Biochemical reactions

Caspase-dependent release of toxic htt fragment and caspase activation are described by the following reactions. The variables are: Htt full length htt, P pro-caspase, C caspase, M_{htt} htt fragment (Figure 3.2).

$$Htt + P \overset{\theta_1}{\rightleftharpoons} HttP \qquad [Htt][P] = \theta_1[HttP], \quad (3.7)$$

$$HttP + P \overset{\theta_2}{\rightleftharpoons} PHttP \qquad [HttP][P] = \theta_2[PHttP], \quad (3.8)$$

$$PHttP \overset{k_1}{\rightarrow} M_{htt} + C + C, \quad (3.9)$$

$$Htt + C \overset{\theta_3}{\rightleftharpoons} HttC \qquad [Htt][C] = \theta_3[HttC], \quad (3.10)$$

$$HttC \overset{k_3}{\rightarrow} M_{htt}M_{htt} + C, \quad (3.11)$$

The reactions 3.7, 3.8, 3.10 occur on a very fast time scale compared to the changes in the concentration of the variables in our model (Htt, M_{htt}, P and C). We can therefore assume that intermediate complexes are approximately at their equilibrium. The rates of production of active caspase C and htt fragment M_{htt} can thus be written as functions of concentration in Equations 3.7, 3.8, and 3.10. Namely,

$$\frac{\mathrm{d}[C]}{\mathrm{d}t} = 2k_1[PHttP] \qquad \text{and} \qquad \frac{\mathrm{d}[M_{htt}]}{\mathrm{d}t} = k_1[PHttP] + k_3[HttC],$$

We can substitute intermediate complexes using the equilibrium equations for the reactions 3.7, 3.8, 3.10.

$$\frac{\mathrm{d}[C]}{\mathrm{d}t} = 2k_1\frac{[Htt][P]^2}{\theta_1\theta_2} \qquad \text{and} \qquad \frac{\mathrm{d}[M_{htt}]}{\mathrm{d}t} = k_1\frac{[Htt][P]^2}{\theta_1\theta_2} + k_3\frac{[Htt][C]}{\theta_3},$$

In the above equations $[Htt]$ represents the concentration of the free htt, i.e. htt that is not part of any intermediate complex. The conservation law states that the total htt concentration is

$$Htt_T = [Htt] + [HttP] + [PHttP] + [HttC],$$

$$Htt_T = [Htt] + \frac{[Htt][P]}{\theta_1} + \frac{[Htt][P]^2}{\theta_1\theta_2} + \frac{[Htt][C]}{\theta_3},$$

and solving for $[Htt]$ yields

$$[Htt] = \frac{Htt_T}{1 + [P]/\theta_1 + [C]/\theta_3 + [P]^2/\theta_1\theta_2}.$$

We assume that procaspase-2 is synthesised and degraded at constant rates. In the model, active caspase-2 is released by two processes: a complex reaction between htt and procaspase-2 at the rate r_{pe}, and the activation of procaspase-2 due to i.e. trophic factor deprivation in the striatum at the rate r_{pr}. The equations are as follows

$$r_{pe} = k_{pe}\frac{HttP^2}{1 + K_1P + K_2C + K_3^2P^2}, \tag{3.12}$$

$$r_{pr} = k_{pr}P^2, \tag{3.13}$$

Htt is cleaved by caspase-2 at a rate

$$r_{ce} = k_{ce}\frac{HttC}{1 + K_1P + K_2C + K_3^2P^2}. \tag{3.14}$$

In the core model presented earlier, A is constant, which allows an analytical treatment of that system. In the extended model this can be done by setting P and C to constant values. Assuming constant caspase activity, the nonlinear rates r_{ce} and r_{pe} as $r_{ce} + r_{pe} = Htt \cdot A$ are re-expressed as, with A as the caspase-mediated Htt cleavage rate,

$$A = \frac{k_{ce}C + k_{pe}P^2}{1 + K_1P + K_2C + K_3^2P^2}. \tag{3.15}$$

System of equations

The extended model for htt aggregation is composed of 6 variables: full length mutant htt Htt, N-terminal htt fragment M_{htt}, htt oligomers O_{htt}, htt aggregates A_{htt}, procaspase-2 P, and caspase-2 C (Figure 3.2). Procaspase- and caspase-2 cleave mutant htt and release htt fragment. Htt fragments form oligomers through a nucleation process (rate proportional to the concentration of oligomers), and are degraded at a constant rate. Oligomers are formed by binding of htt fragments, they form aggregates at a rate proportional to the aggregate concentration, and are degraded at a constant rate. Aggregates are formed by binding of oligomers, and are degraded by autophagy at a constant rate. For the

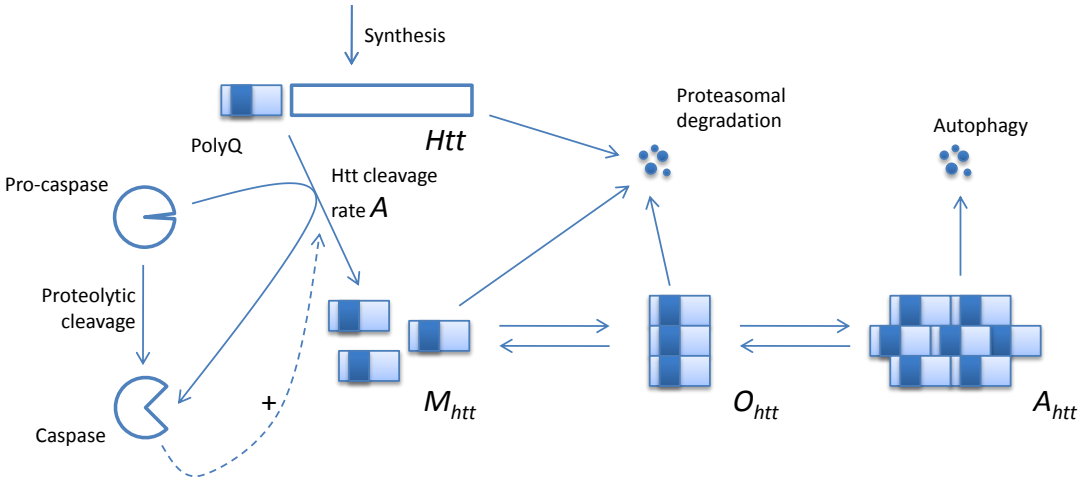

Figure 3.2: Model for caspase-2 mediated htt aggregation. A mutation in htt results a loss of function which leads to the activation of caspase-2. Mutant htt is cleaved by both procaspase-2 and caspase-2, and htt fragment is released. Interactions of procaspase-2 and htt release htt fragment and initiate autocatalysis of procaspase-2 into caspase-2. Htt fragments aggregate through a succession of oligomeric structures. Full-lenght htt, monomers and oligomers of htt fragments are degraded by the proteasome, and aggregates are removed by autophagy.

Table 3.4: List of additional parameters for the extended model

Parameter	Value	Description
k_p	0.005	Procaspase-2 synthesis rate
k_{dp}	0.005	Procaspase-2 degradation rate
k_{dc}	0.02	Caspase-2 degradation rate
k_{ce}	2.0	Maximal caspase-2 mediated cleavage rate
k_{pe}	0.01	Maximal procaspase-2 mediated cleavage rate
k_{pr}	0.01	Proteolytic cleavage rate of procaspase-2
K_i	1.0	Saturation constants of cleavage rates ($i = 1, ..., 3$)

parameters that are present in the core model same values were used as listed in the Table 3.1. The additional parameters of extended model are listed in the Table 3.4

Now the differential equations for the 6 variables considered can be written down.

$$\frac{\mathrm{d}Htt}{\mathrm{d}t} = k_h - r_{ce} - r_{pe} - k_{dh}Htt, \tag{3.16}$$

$$\frac{\mathrm{d}M_{htt}}{\mathrm{d}t} = r_{ce} + r_{pe} - k_n M_{htt} O_{htt} + k_n^{-1} O_{htt} - k_{de} M_{htt}, \tag{3.17}$$

$$\frac{\mathrm{d}O_{htt}}{\mathrm{d}t} = k_n M_{htt} O_{htt} - k_a O_{htt} A_{htt} + k_a^{-1} A_{htt} - [k_n^{-1} + k_{dn}] O_{htt}, \tag{3.18}$$

$$\frac{\mathrm{d}A_{htt}}{\mathrm{d}t} = k_a O_{htt} A_{htt} - [k_a^{-1} + k_{da}] A_{htt}, \tag{3.19}$$

$$\frac{\mathrm{d}P}{\mathrm{d}t} = k_p - 2(r_{pe} + r_{pr}) - k_{dp} P, \tag{3.20}$$

$$\frac{\mathrm{d}C}{\mathrm{d}t} = 2(r_{pe} + r_{pr}) - k_{dc} C, \tag{3.21}$$

where the nonlinear rates r are given by Equations 3.12, 3.13 and 3.14. Since quantitative estimations of concentrations and time scales vary greatly depending on the experimental setting, arbitrary time and concentration units were assigned to the parameters. The parameter values were chosen according to qualitative estimates of aggregation kinetics. The results shown here are representative of a wide range of parameter values as long as htt synthesis rate k_h is sufficiently large. Nonlinearities in the Equations 3.20 and 3.21, make the steady state analysis of the extended model cumbersome to do. However, as long as P and C change slowly, the steady states for Equations 3.17–3.19 will be the same as in the core model.

3.4 Results

3.4.1 Behaviour of the core model for htt aggregation

The simple model allows studying the equilibrium concentration of different htt conformers as the kinetic parameters vary. Parameter A, the release rate of aggregation-prone htt fragment, is the main bifurcation parameter in our analysis. It is an important therapeutic target on which various caspase inhibitors and chaperons that modulate refolding of the htt fragment act upon. With the increase in the release rate of htt fragment A, the system goes through two transcritical bifurcations, corresponding to the onset of oligomerization and the onset of aggregation. For each value of A, there is only one stable steady state for each of the variables, namely: full-length htt, monomers, oligomers, and aggregates of htt fragments (Figure 3.3, left panel). This is consistent with other models for protein aggragetion (115).

For high cleavage rates ($A > A_2$), the formation of aggregates is responsible for most of the change in the total concentration; the concentration of monomers increases slowly and the concentration of oligomers stays constant. Aggregates act as a buffer to limit the increase in concentration of htt oligomers. Moreover, the steady state value of oligomers (O_{htt}^3) depends only on the rates related to the formation of large aggregates k_a, k_a^{-1} and k_{da}, and not on particular levels of monomers M_{htt} or aggregates A_{htt}.

In the core model, aggregates are either quickly formed ($A > A_2$) or absent ($A < A_2$). To simulate slow evolution of aggregation in a cell, the release rate A was assumed

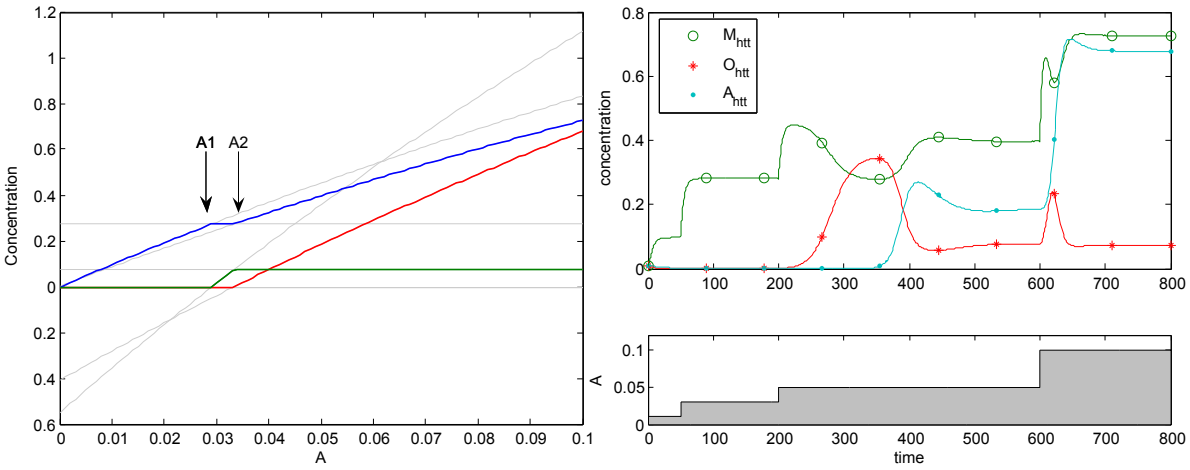

Figure 3.3: Behavior of the core model. (*Left*) Bifurcation diagram of aggregation. The steady states for M_{htt} (blue), O_{htt} (green) and A_{htt} (red) are plotted as a function of the htt release rate A. The bifurcation analysis shows that as A varies, the system successively goes through three steady states. For low values of A, the system is in STST1 (only monomers are present in the system). When A is larger than the threshold A_1, the system is in STST2 (monomers and oligomers are present in the system). For the values of A larger than the second threshold A_2, the system is in STST3 (monomers, oligomers and aggregates are present in the system). The two threshold levels A_1 and A_2 define transcritical bifurcation points, where an unstable steady state (*gray lines*) exchanges stability with a stable steady state (*bold lines*). (*Right*) Time courses of M_{htt} ($\circ$), O_{htt} ($+$), and A_{htt} ($\cdot$) (*upper panel*) and caspase-2 activity (*lower panel*). Increase in the release rate of htt fragments is simulated and indicated by the gray shading (*lower panel*, A=0.01, 0.03, 0.05, and 0.1).

to slowly increase in time (Figure 3.3, right panel). The concentration of aggregates increases abruptly, when A is larger than the threshold A_2 (Figure 3.3, right panel, $t \sim 400$). Further increase of A is immediately followed by an increase in the aggregate concentration.

3.4.2 Behaviour of the extended model for htt aggregation

The simulation of the model consisting of Equations 3.16–3.21 shows that, as in the core model for htt aggregation, an increase in caspase activity mainly affects the aggregate and monomer concentrations (Figure 3.4, left panel). After a transient peak, monomer and oligomer concentrations reach a steady state as aggregates start to form. With a higher htt cleavage rate, the aggregate and monomer concentrations increase, but the steady state concentration of oligomers remains constant. Thus, the evolution of htt conformations in time in the extended model is well represented by the core model.

In the extended model, I introduced a representative positive feedback loop influencing the htt release rate. This positive feedback loop could explain the delayed increase in the htt release rate, A, in the early stage of HD. This could be and intrinsic mechanism by which the system triggers aggregation. The proteolytic cleavage rate of procaspase-2,

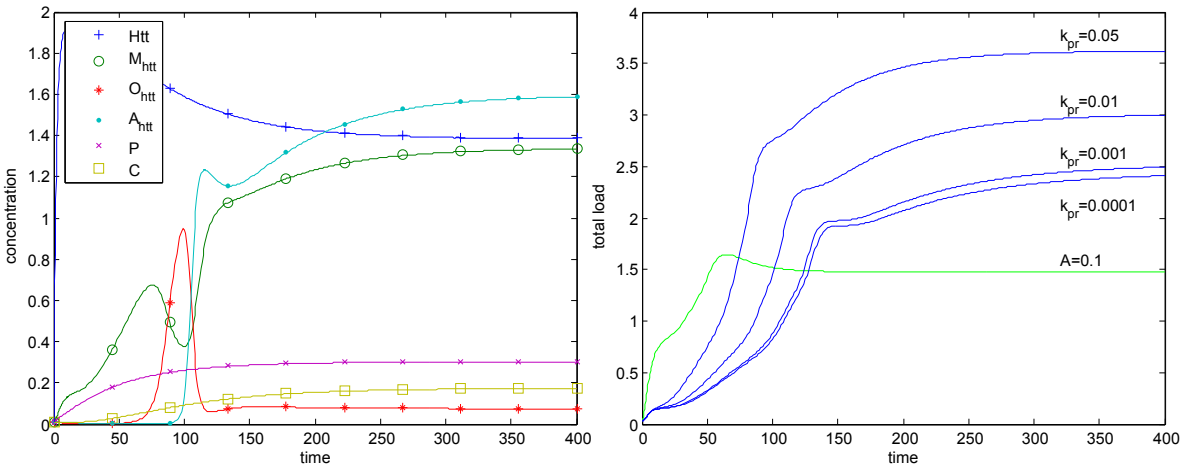

Figure 3.4: Behavior of the extended model. (*Left*) Time courses of M_{htt} ($\circ$), O_{htt} ($+$), A_{htt} ($\cdot$), P ($\times$), and C ($\square$). Parameters are listed in Table 3.1 and Table 3.4. (*Right*) Delay in the onset of aggregation. In the core model, for $A > A_2$ aggregation occurs rapidly (here $A = 0.1$). In the extended model the delay in the onset of aggregation introduced by the positive feedback loop in the release of htt fragments is pronounced for the small values of k_{pr}. For the larger values of k_{pr} it has little influence.

k_{pr}, is assumed to be a sensor of the toxicity in HD cell and its surrounding (i.e. toxicity of htt conformers or trophic factor deprivation can trigger the caspase activation). For all values of k_{pr}, the onset of aggregation occurs later than in the core model, which has a constant value of A. For low values of k_{pr}, the delay can be extended up to a certain point, but not indefinitely. For high values of k_{pr}, corresponding to the increased stress experienced by HD cell, the delay becomes very small and so does the influence of a positive feedback loop (Figure 3.4, right panel).

In the core model, depending on the value of A, there is either no aggregation at all ($A < A_2$), or a rapid aggregation ($A > A_2$). The variation in the value of A is due to the external change experienced by the cell, and this will determine the delay in the aggregation. In the extended model, a positive feedback loop slowly leads to the onset of aggregation even without the externally induced increase in the release rate of htt fragment. Thus, the positive feedback loop is sufficient to explain the delay in the onset of aggregation.

3.5 Discussion

A wide range of pathological changes in HD affecting: gene transcription, protein trafficking, protein degradation, glutamatergic synaptic transmission, neurotrophic modulation of synaptic function, mitochondrial function and oxidative metabolism, stem from the aberrant protein-protein interactions with different htt conformations arising from the aggregation process (67). Mathematical models presented in this chapter were the first molecular models of htt aggregation. These models allow us to monitor the evolution of the concentration of each htt conformer over time.

First, I analyzed the behaviour of a simple model for htt aggregation that I called the

core model. The core model describes htt aggregation kinetics as a nucleation process. It is a deterministic model that consists of a set of ordinary differential equations which define the time evolution of various htt conformers, namely: full-length htt, monomers, oligomers and aggregates of htt fragments. As the conditions in the environment worsen, the rate of release of htt fragment, A, increases, and the system goes through two bifurcation points corresponding to the two nucleation events: onset of oligomerization and onset of aggregation. Nucleation is a sudden phase-transition phenomenon where the first steps are energetically less favoured than continuation of growth. One thermodynamical study showed that the critical step for the onset of aggregation is a conformational change of a polyQ monomer (160). In the mathematical model, the concentration of htt monomer needs to be high enough for the probability of undergoing the structural transition to be significant. At this threshold concentration, a transcritical bifurcation occurs, i.e. the system goes into another stable steady state. Threshold behaviours like switches are present in many biochemical systems and are well understood (54).

Second, I enlarged the core model to address the question: how does the system go through the bifurcation point. The enlarged model consists of six differential equations with the mutant htt, htt monomers, oligomers, aggregates, procaspase-2 and caspase-2 as variables. A positive feedback loop that controls the release of htt fragment could be an intrinsic mechanism to cross the threshold in the release rate. It can also explain the delay in the onset of aggregation as a dynamic property of the system independent of the external influences. Indeed, mouse lines that contain a truncated form of HD gene show abnormal symptoms before lines containing full-length htt (105).

Both the core and the enlarged model predict that environmental changes and toxic effects of mutant htt, or the positive feedback loop, which all promote the release of htt fragments, lead to the increase in the level of monomers and aggregates. Once the aggregates are formed, i.e. the system is in Steady State 3, the concentration of the oligomers is constant. If the oligomers were the most toxic htt conformer, this would agree with the one-hit model of the cell death in different neurodegenerative diseases, according to which a probability that disease affected neurons die is constant. The influence of different htt conformers on cell death is the topic of the next chapter.

Few other studies have addressed the problem of aggregation in HD. Rieger et al (124) have considered a model in which protein refolding and de-aggregation rates are mediated by chaperones. They showed that the threshold phenomena in aggregation can be explained by a bistable process, and that chaperones are necessary for bistability. Bistability can explain the sudden transition to high aggregate concentration and differ from the nucleation mechanism in two ways: (1) aggregate concentration can take either low or high values but no intermediate, and (2) for a given set of kinetic parameters, aggregates can be stable either at high or low concentration. In practice, however, it would be difficult to discriminate between bistability and nucleation because of the presence of noise, and the possible narrow range of parameter values for which the threshold transition occurs. The nucleation model presented here does not include chaperone activity. Adding it might also produce a bistability transition, in addition to the trancritical bifurcations. Pallito et al. (115) considered an extensive model for β-Amyloid fibril growth associated with Alzheimer's disease to identify the toxic Aβ species. Their model and the one presented here are consistent in predicting a narrow range over which oligomers exist in the absence of large aggregates.

Many cell and mouse models for HD show early formation of aggregates, probably due to the strong expression and the length of polyQ stretches present in the cells. It is natural to represent the states of these experimental models by Steady State 3, marked by the presence of aggregates. In patients diagnosed with HD, however, a relevant question is to determine in which state vulnerable neurons are. In the context of mathematical modelling, therapy could allow the transition from one steady state to another, e.g. by inhibiting or promoting aggregation. However, since the relative toxicities of individual conformers are not yet known, it is difficult to predict the effect of such a transition. This problem will further be studied in the next chapter.

Much effort has been involved in finding substances that interfere with aggregation, either by direct inhibition with htt as a target, or by indirect inhibition by, for instance, caspase inhibitors. In various cell and mouse models, caspase inhibitors have been shown to reduce toxicity and aggregate formation (178). Interference with the later steps, i.e. with oligomerisation and aggregation, has been shown to be beneficial for the cell as well (137, 51). In the next chapter, I consider different assumptions concerning the toxicity of the soluble htt fragments and aggregates and I investigate the influence of intervention with various steps in the process of aggregation on the overall toxicity.

Chapter 4

Stochastic Model of Huntingtin Aggregation and Neuronal Death

4.1 Summary of the chapter

Although it is well established that the formation and the accumulation of insoluble proteins causes neurotoxicity in different disease model systems, there is an intense debate as to which protein structure is responsible for neuronal dysfunction and loss. While the mature aggregates have long been considered the toxic agent, more recent studies conclude that it is the soluble oligomers that are highly cytotoxic (9). However, the question whether mature fibrillar structures or smaller aggregation intermediates are primarily responsible for neuronal damage in patient brains has not been solved conclusively (18). In this chapter, I present a stochastic model for htt aggregation based on the core model introduced in the previous chapter. In the model, I assume that the toxicity is proportional to the concentration of each htt conformer. Three toxicity premises were considered: (a) htt monomers and oligomers are the toxic species, while aggregates are non toxic, (b) all three species are equally toxic, and (c) aggregates are the only source of toxicity. An executioner caspase serves as a toxicity sensor and functions like a switch: toxicity high enough can provoke sudden caspase activation, leading the cell into apoptosis. I use this extended model to explore the possible outcomes of therapies targeting different steps in the aggregation process depending on alternative toxicity premises. The results show that transient dynamics and non-monotonic response of the cell survival to a change of parameter can have a great effect on the outcome of a treatment that targets htt aggregation. Moreover, the stochastic model might offer an explanation of the seemingly conflicting results used to assign either toxic or neuroprotective role to htt aggregates.

4.2 Introduction

4.2.1 Aggregates: a friend or a foe

Since the discovery of polyQ aggregates, the aggregation process has been proposed to be central to the pathogenesis of the disease, to be a benign epiphenomenon, or even to be neuroprotective. A striking correlation between the threshold for aggregation *in vitro*

and the threshold for disease in humans (length of polyQ > 36) supported the idea that aggregation is a pathogenic event (47, 141). However, neurons with htt inclusions do not correspond exactly to the neurons that degenerate. For instance, inclusions are more enriched in populations of large striatal interneurons, which survive, than in medium spiny neurons, which are lost (88).

The process of aggregation involves the formation of at least three protein conformations: htt fragment monomers, oligomers and aggregates. Aggregates are defined by poor solubility in aqueous or detergent solvents, aberrant cellular localisation and non-native secondary structure. Attempts to correlate the presence of aggregates with the onset of phenotype have been complicated by the difficulties in detecting and quantifying small aggregated forms of polyQ, and because all possible structural conformers of the protein are present in the system under analysis (18). Yang et al. (184) circumvented these problems by pre-forming different polyQ aggregation species, which were then used to transfect cells in order to examine their toxicity. They demonstrated that polyQ aggregates and not the htt monomers are highly toxic when directed to the nucleus, but not toxic if they are in the cytoplasm. On the other hand, Arrasate and coworkers performed a survival analysis of the individual cells expressing mutant htt, and showed that it is the amount of diffuse intracellular htt that predicted whether and when cell death would occur. They also concluded that aggregates protect neurons by decreasing levels of the toxic diffuse forms of mutant htt (9).

Deleterious biochemical changes observed in HD models include altered signalling pathways, perturbed calcium homeostasis, production of reactive oxygen species, triggering of inflammatory cascades and mitochondrial dysfunction. It will be a challenge to find out which of the htt conformations induces which of the mechanisms leading to neuronal dysfunction in HD. Moreover, many of our current concepts about the molecular mechanisms involved in htt-mediated neuronal injury have arisen from *in vitro* experiments and tissue-culture studies with htt aggregates at concentrations that exceed the physiological levels, and should therefore be considered with care until they are validated *in vivo*.

4.2.2 Targeting htt aggregation

There are no effective strategies to slow down or prevent the neurodegeneration resulting from the HD mutation. However, factors regulating the synthesis and clearance of aggregation-prone htt represent promising therapeutic targets. Many screens for potential new HD therapeutics have been conducted *in vitro* and *in vivo*, with varying outcomes as to whether inhibition of aggregation is beneficial or detrimental. Bodner et al. (26) identified compounds that increase inclusion formation while simultaneously reducing toxicity in a cellular HD model. Schiffer et al. (142) found aggregation inhibitors that do not ameliorate htt toxicity in a Zebrafish model, suggesting that aggregate formation is independent from the toxic effects of mutant htt. On the other hand, compounds such as Congo Red, EGCG or C2-8 have been shown to decrease both htt aggregation and the pathological phenotype in Drosophila or mouse models of HD in a dose-dependent manner (137, 51, 42). It is possible that the aggregation inhibitors identified in these studies interfere with different steps in the aggregation cascade, thus leading to the accumulation of different monomeric or oligomeric, native or misfolded htt structures. The experimental detection and quantification of the different conformers has proven difficult

due to their intrinsic instability and the dynamic equilibrium of the system that does not easily allow for purification of single components. Moreover, the mechanism behind the action of the compounds that alter htt aggregation is often not known, and it is therefore hard to distinguish between their effects on the aggregates themselves and the effects on some other cellular process that indirectly influence htt aggregation.

The proteasome and autophagy-lysosomal pathways are the major routes for clearance of mutant htt conformers. While the narrow proteasome barrel precludes entry of oligomers/aggregates of mutant htt (or other aggregation-prone intracellular proteins), such substrates can be degraded by autophagy. Indeed, the autophagy inducer rapamycin reduces the levels of soluble and aggregated htt, and attenuates its toxicity in cells, as well as in transgenic Drosophila and mouse models (180).

Aggregation is a characteristic of abnormally folded proteins. In the cell, the heat-shock proteins Hsp70 and Hsp40 are the two main classes of molecular chaperones that facilitate protein folding and maintaining the proteins in a soluble conformation. PolyQ htt fragments interact with members of Hsp40 and Hsp70 families of chaperones in a polyQ length-dependent manner (76). The sequestration of chaperones into aggregates decreases their available amount in the cell, and this presumably enhances abnormal protein folding (68). If the production of misfolded proteins exceeds the degradative capacity of the cell, these polypeptides can form insoluble intracellular aggregates (90). Increasing the potential of the cell to deal with misfolded proteins, as by overexpression or induction of the Hsp70 and Hsp40 chaperones, prevents neurodegeneration in a number of HD models (30, 149, 33).

4.3 Mathematical model

In the last chapter, I presented models of htt aggregation that were based on ordinary differential equations (ODEs). Models based on ODEs are approximate because they treat molecules with continuously variable concentrations, rather than the discrete entities that they actually are. In reality, reactions occur as a rapid succession of separate elementary events, the exact timing of which is effectively random because of the Brownian motion of the reactants (4). The source of stochasticity can be intrinsic, i.e. small number of molecules, or extrinsic, i.e. external fluctuations. Here, I use a Langevin approach to describe the release rate of the htt fragment that depends on the stochastic intracellular fluctuations of proteolytic enzymes, which is an extrinsic source of stochasticity. Thus, the process is described using a stochastic differential equation (SDE) (172).

The stochastic model for htt aggregation presented here is based on the core model introduced in the previous chapter. The model is composed of 6 variables: full-length mutant htt Htt, N-terminal htt fragments containing polyQ repeat M_{htt}, htt fragment oligomers O_{htt}, htt fragment aggregates A_{htt}, an executioner caspase X, and the htt fragment release rate A (Fig. 4.1). Full-length htt is cleaved and refolded at rate A, releasing an aggregation-prone htt fragment. Monomeric fragments M_{htt} bind to each other to form oligomeric structures O_{htt}, and subsequently larger, insoluble aggregates A_{htt}. Formation of both oligomers and aggregates is described by a nucleation process. The release of htt fragments is described as a stochastic process. The three structural conformations of htt contribute to the overall toxicity by activating executioner caspases

X. In the extended model presented in the previous chapter, caspases were directly involved in the aggregation process. Here, they are used only to relate the aggregation dynamics to cell death.

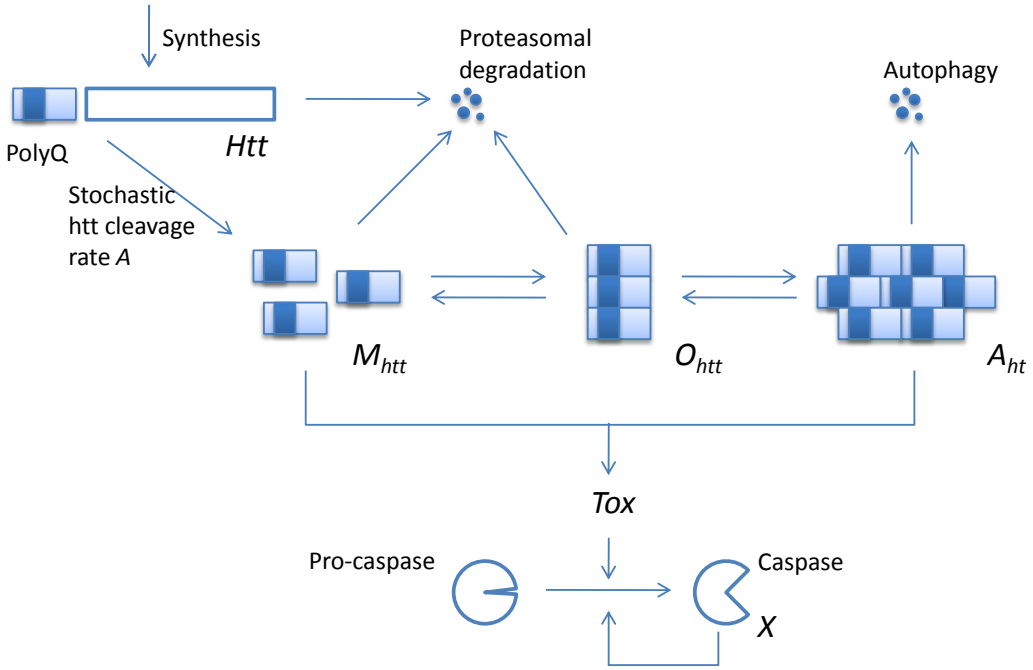

Figure 4.1: Stochastic model for htt aggregation. Mutant full-length htt, Htt, is cleaved and a short N-terminal htt fragment, M_{htt}, is released with a stochastic rate A. Htt fragments aggregate and form htt oligomers, O_{htt}, which further aggregate and form htt aggregates, A_{htt}. Full-length htt, monomers and oligomers of htt fragments are degraded by the proteasome, and aggregates are removed by autophagy. The three structural conformations of htt contribute to the overall toxicity by activating executioner caspases X.

Differential equations for the 5 variables considered are

$$\frac{dHtt}{dt} = k_h - AHtt - k_{dh}Htt, \tag{4.1}$$

$$\frac{dM_{htt}}{dt} = AHtt - k_n M_{htt}O_{htt} + k_n^{-1}O_{htt} - k_{de}M_{htt}, \tag{4.2}$$

$$\frac{dO_{htt}}{dt} = k_n M_{htt}O_{htt} - k_a O_{htt}A_{htt} + k_a^{-1}A_{htt} - (k_n^{-1} + k_{dn})O_{htt}, \tag{4.3}$$

$$\frac{dA_{htt}}{dt} = k_a O_{htt}A_{htt} - (k_a^{-1} + k_{da})A_{htt}, \tag{4.4}$$

$$\frac{dX}{dt} = C_0 + k_x Tox\frac{X^4}{1+X^4} - k_{dx}X, \tag{4.5}$$

$$Tox = u_1 M_{htt} + u_2 O_{htt} + (1 - u_1 - u_2)A_{htt}. \tag{4.6}$$

To quantify the effect of noise on aggregation kinetics, time-dependent noise was added to the htt fragment release rate A. The noise is described by a stationary Gaussian process

Table 4.1: List of parameters for the stochastic model

Parameter	Value	Description
k_h	1.0	Htt synthesis rate
k_{dh}	0.5	Htt proteasomal degradation rate
k_{de}	0.2	Htt fragment proteasomal degradation rate
k_n	0.4	Rate of formation of oligomers
k_n^{-1}	0.01	Rate of release of monomers from oligomers
k_{dn}	0.1	Proteasomal degradation of oligomers
k_a	0.4	Rate of formation of aggregates
k_a^{-1}	0.01	Rate of release of oligomers from aggregates
k_{da}	0.02	Removal rate of aggregates by autophagy
C_0	0.02	Basal activity of an executioner caspase
k_x	0.6	Proportionality constant for htt toxicity
k_{dx}	0.08	Degradation rate of an executioner caspase
a	0.1	Relaxation constant for the stochastic process
A_*	1	Average value of the htt fragment release rate
S	0.5	Standard deviation of the noise term
$u1$	0 - 0.5	Contribution of htt monomers to toxicity
$u2$	0 - 0.5	Contribution of htt oligomers to toxicity

(Ornstein-Uhlenbeck process) that satisfies the Langevin equation

$$\frac{dA}{dt} = a(A_* - A) + SL(t). \tag{4.7}$$

$L(t)$ is a Wiener process with average $\langle L(t)\rangle = 0$, and variance $\langle L(t)L(s)\rangle = \delta(t-s)$, and S is the standard deviation of the noise term. This process satisfies the equation $dB(t) = L(t)dt$, where $B(t)$ is a Brownian motion (172). The toxicity level Tox is a weighted average of the concentrations M_{htt}, O_{htt}, and A_{htt}. Three toxicity levels for the aggregates are assumed: non-toxic (Tox=0 or $u_1 = u_2 = 0.5$), equally toxic (Tox=1/3 or $u_1 = u_2 = 1/3$), and fully toxic (Tox=*1* or $u_1 = u_2 = 0$).

4.4 Results

4.4.1 Behaviour of the stochastic model of htt aggregation

Equations 4.1–4.7 were simulated using the first-order Forward Euler method for stochastic equations. Unless otherwise noted, the simulations were run for t between 0 and 480 (arbitrary units) or the time of cell death, whichever comes first. The time step, $\Delta t = 0.2$, was determined by reducing the time step until no significant differences were found between stochastic simulations. Parameter values are listed in the table 4.1. Figure 4.2 shows the evolution of the system over time for one cell. The sensor of toxicity is the activity of the executioner caspase X described by a bistable switch. When X reaches a threshold that lies midway between the lower and the upper steady state ($X_{thresh} = 4$), the cell dies (here at $t = 92$). The time scale is arbitrary but it is of the order of hours, to mimic the evolution of aggregation in cell lines.

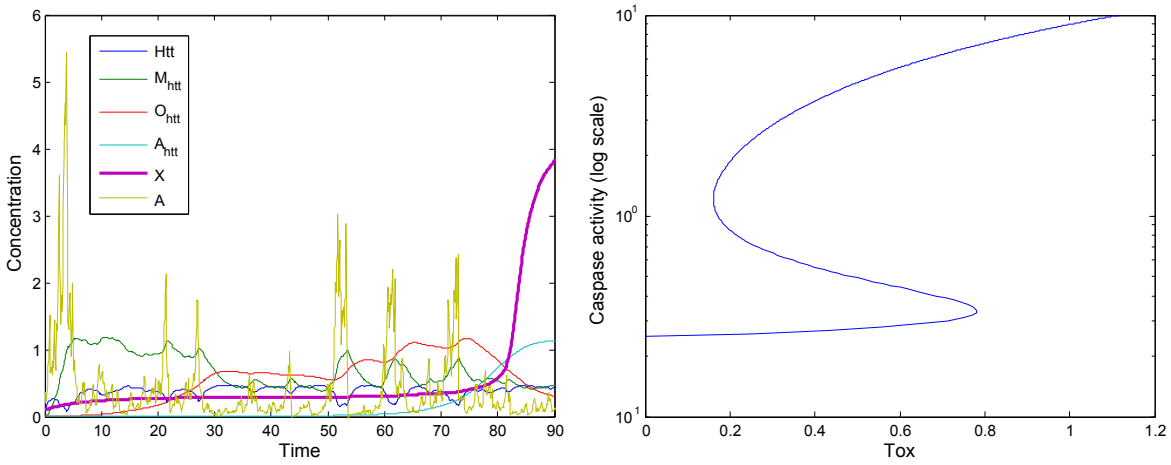

Figure 4.2: (Left panel) Time series of M_{htt}, O_{htt}, A_{htt}, X, and A for one cell. The cell dies when X reaches a predefined threshold $X_{thresh} = 4$, here at $t = 92$. The parameter values are listed in the table 4.1 (here, $u1 = 0.334$, $u2 = 0.334$). (Right panel) Bistability of caspase activity as a function of toxicity.

4.4.2 Cell survival analysis with respect to different treatment strategies

To study which factors influence cell survival, three parameters controlling htt aggregation and degradation, namely k_{de}, k_{da}, and the average value of k_a and k_n, $\text{avg}(k_a, k_n) = \frac{k_a+k_n}{2}$, were systematically varied. For each kinetic parameter, three toxicity assumptions of the aggregates were considered: non-toxic, equally toxic to the soluble protein (monomers and oligomers), and fully toxic. For each of the parameter/toxicity combinations, the time of cell death was monitored (25 stochastic runs over 40 equally spaced parameter values for each combination). Each simulation ran until cell death, as determined by the activation of X, or until $t = 480$. Cells staying alive until this time point were considered survivors. The results are shown in figures 4.3–4.5.

Removal rate of htt monomer k_{de}

Htt monomer removal includes degradation and refolding by chaperones (assuming irreversible reactions). When aggregates are non-toxic or as toxic as the soluble protein, increasing the monomer removal rate k_{de} improves cell survival (Fig. 4.3, middle left and middle center panels), since the concentrations of both soluble part and aggregates are decreasing (Fig. 4.3, upper panels). The same is true in when aggregates are fully toxic (Fig. 4.3, middle right panel). However, in this case two clusters of time of cell death are visible for higher values of k_{de} (early death, or survival). In the deterministic case, one would expect the time of death to follow the same pattern as for non-toxic aggregates and equally toxic aggregates because both aggregates and soluble part concentrations vary in a similar way (Fig. 4.3, upper panels). In the stochastic case, observed early death, even for the high values of k_{de}, may be due to a transient stochastic accumulation of aggregates briefly creating higher toxicity. After the onset of aggregation, the source of toxicity is

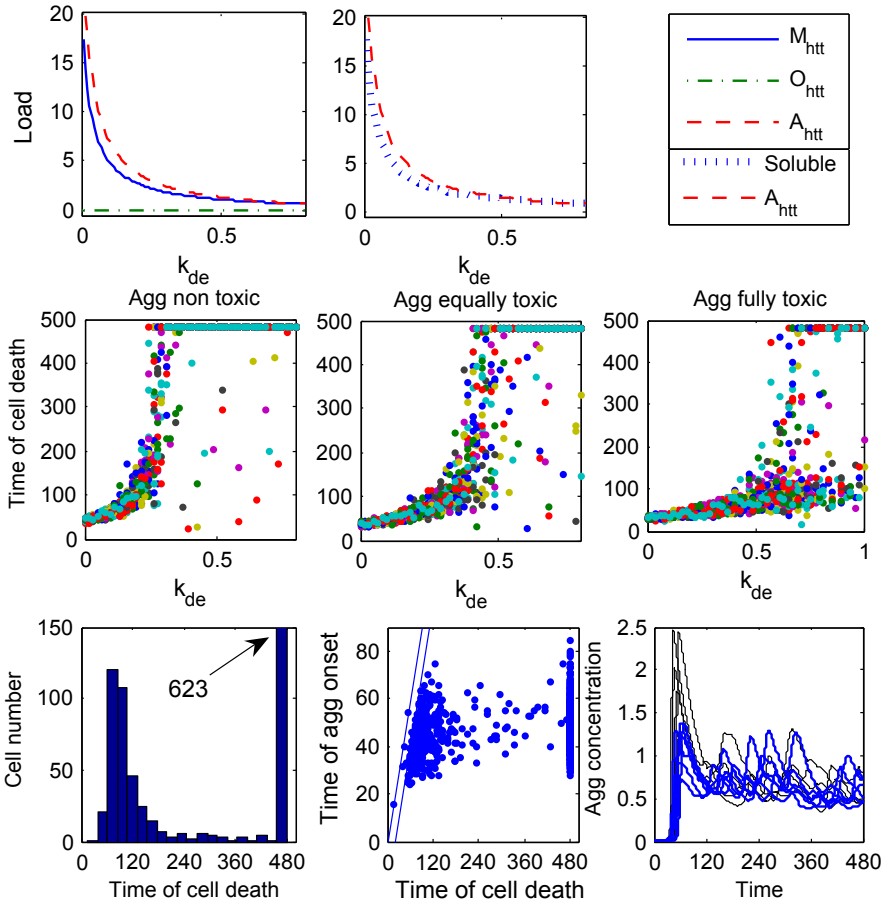

Figure 4.3: Cell survival with respect to the removal rate of htt monomers k_{de}. (Upper panels) Deterministic steady states for M_{htt}, O_{htt}, A_{htt}, and soluble protein ($M_{htt} + O_{htt}$). (Middle panels) Time of death of 25 cells for different values of k_{de} and different aggregate toxicity premises. (Lower panels) Detailed analysis of the case when aggregates are fully toxic (Lower left panel) Distribution of time of cell death for $k_{de} = 0.8$ for 1000 cells. (Lower middle panel) Time of onset of aggregation against time of cell death. The lines show that many cells start dying 20 time units after the onset of aggregation. (Lower right panel) The time course of the aggregate concentration for 4 early dying cells (thin gray lines) and 6 surviving cells (thick blue lines).

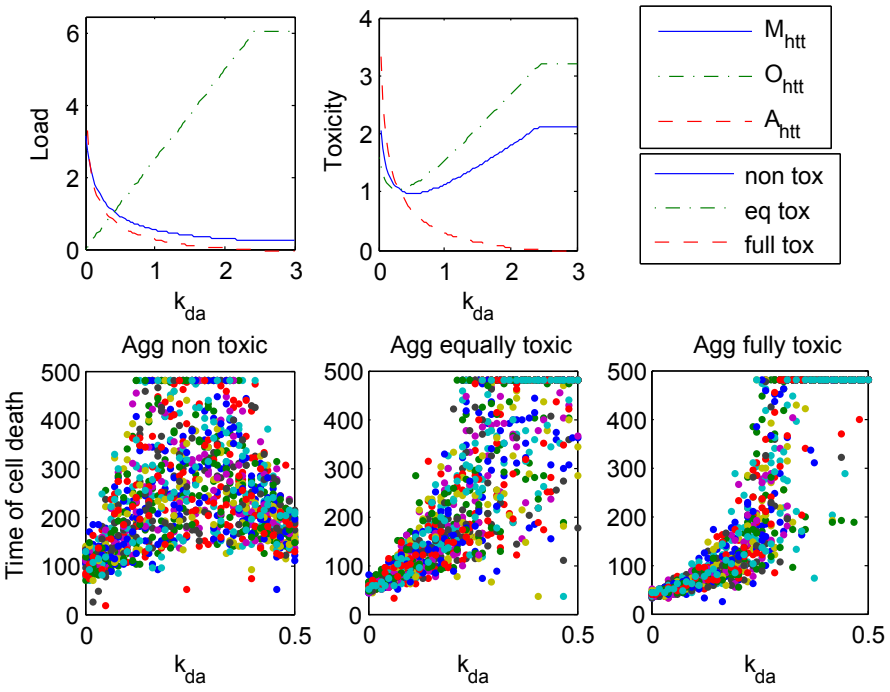

Figure 4.4: Cell survival with respect to the aggregate degradation rate k_{da}. (Upper panels) Deterministic steady states for M_{htt}, O_{htt} and A_{htt} (*left*) and toxicity levels for three combinations (*right*). (Lower panels) Time of death of 25 cells for different values of k_{da} and different toxicity levels of aggregates. When aggregates are non-toxic, the time of cell death depends on the value of k_{da} in a non-monotonic way (*left*). When aggregates are equally or fully toxic, increasing in k_{da} improves cell survival (*center* and *right*).

more stable and stochasticity plays a less important role. Thus, cells that are not killed at the onset of aggregation will survive longer.

To verify this, I looked at the time of death and time of aggregation onset of 1000 cells, for $k_{de} = 0.8$. The time of cell death shows a clear bimodal distribution; cells that just formed aggregates have a high risk of dying, whereas most cells that survived the onset of aggregation are still alive at $t = 480$ (Fig. 4.3, lower left and lower center panels). Simulations of the evolution of the aggregate concentrations in cells that die early (Fig. 4.3, lower right panel, thin lines) and cells that die late (Fig. 4.3, lower right panel, thick lines) show that cells that die early have a strong peak at the onset of aggregation, while cells that survive longer have a smooth onset of aggregation. After the onset of aggregation, all cells had a similar dynamics. For all toxicity assumptions removing htt monomers, by degradation or refolding, was beneficial to cell survival. However, in the case of fully toxic aggregates, transient dynamics of aggregation onset may affect the cell survival (Fig. 4.3, lower panels).

Degradation rate of htt aggregates $\mathbf{k_{da}}$

For non-toxic aggregates, increasing the aggregate removal rate by autophagy can lead to increased or decreased survival (Fig. 4.4, lower left). For low values of k_{da}, an increase in k_{da} is associated with a decrease in the concentration of the soluble protein; hence the improved survival. For high values of k_{da}, the concentration of the soluble part increases again, leading to a decreased survival. This result can be explained by the steady state value of the deterministic model. The steady state concentration of soluble protein is given by (STST3 in Table 3.2):

$$M_{htt} + O_{htt} = \frac{AHtt + k_n^{-1}\frac{k_a^{-1}+k_{da}}{k_a}}{k_n\frac{k_a^{-1}+k_{da}}{k_a} + k_{de}} + \frac{k_a^{-1} + k_{da}}{k_a}. \tag{4.8}$$

The first term decreases with k_{da} while the second term increases. The first term is dominant, but eventually reaches a plateau, allowing the increase of the second term to dominate at high values of k_{da}. This non-monotonic behaviour of the soluble protein explains the bell-shaped curve of the time of cell death. Although the change in concentration of the soluble protein is small, it has a dramatic effect on the time of cell death (Fig. 4.4, upper center and lower right panels). We could expect a similar behaviour in the case when all htt conformation are equally toxic, but for higher values of k_{da}. However, for the chosen parameter values, increasing k_{da} always has a beneficial effect (Fig. 4.4, lower center panel). As expected, if aggregates are fully toxic, increasing k_{da} is always beneficial (Fig. 4.4, lower right panel).

Htt fragment oligomerization and aggregation rate $\mathbf{avg(k_a, k_n)}$

The polyQ length determines the oligomerization and aggregation rates. Different HD models have a wide range of polyQ repeat lengths (i.e. 50–150), which might lead to several-fold differences in the oligomerization and aggregation rates. It is likely that compounds that cause either increase or decrease in the aggregation rates interfere with both the oligomerization and the aggregation step. In the following, I therefore, examine the influence of the average value of the oligomerization and aggregation rate on the cell survival.

In the model, for non-toxic aggregates, changing the oligomerization and the aggregation rates can have an opposite effect depending on the starting average value of those rates, i.e. depending on the polyQ length in a HD model (Fig. 4.5, lower left panel). The time until cell death is shortest around $\text{avg}(k_n, k_a) = 0.1$. Steady state analysis of the deterministic model shows two successive transcritical bifurcations just below $\text{avg}(k_n, k_a) = 0.05$. Around that value, the concentration of the soluble protein increase due to the accumulation of oligomers (Fig. 4.5, upper center panel). Although the decrease in cell survival is consistent with an increase of the concentration of the soluble protein, the parameter values do not match. Additional factors modulating the time of cell death, such as transient activity during onset of aggregation, may explain this discrepancy. If aggregates are equally or fully toxic, the time of cell death decreases in a rate-dependent manner, as expected (Fig. 4.5, lower center and right panels).

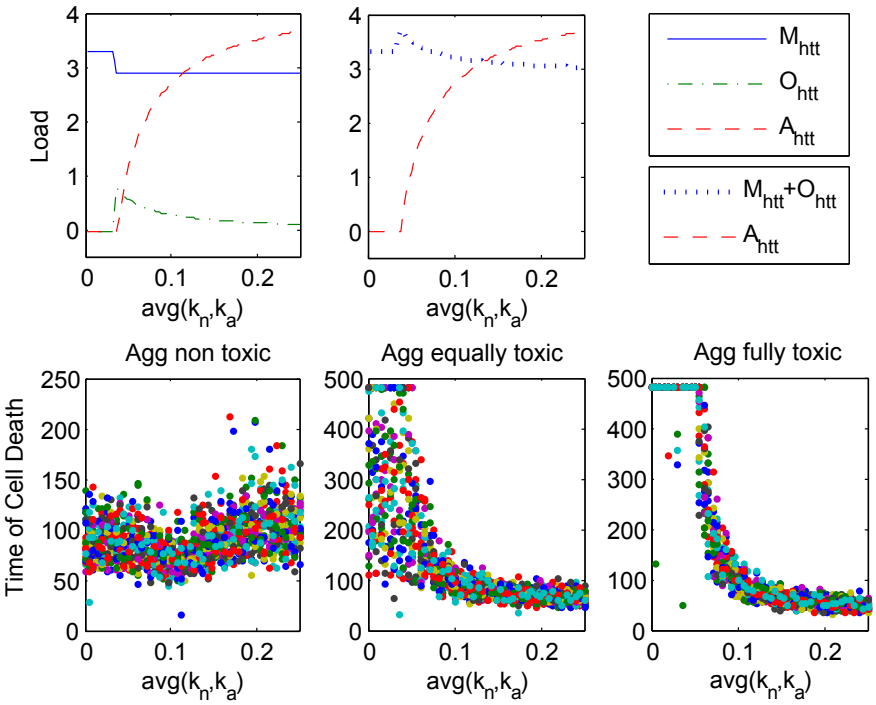

Figure 4.5: Cell survival with respect to average rate of oligomerization and aggregation avg(k_a, k_n). (Upper panels) Deterministic steady states for M_{htt}, O_{htt} and A_{htt} (*left*) and the total toxicity levels for different toxicity premises (*right*). (Lower panels) Time of death of 25 cells for different values of avg(k_a, k_n) and different toxicity levels of aggregates. For non-toxic aggregates, the time of cell death follows a v-shaped curve (*left*). For equally or fully toxic aggregates, the time of cell death decreases (*center* and *right*).

4.5 Discussion

Different therapeutic strategies targeting the aggregation process have been developed, e.g. inhibiting protein aggregation with peptides or small molecules identified via structure-based drug design or high-throughput screening, interfering with post-translational modifications that stimulate protein misfolding and aggregation, or upregulating molecular chaperones or aggregate-clearance mechanisms (128). The outcome of such treatments is often used as an argument to infer the toxic protein conformation. However, the analysis of the stochastic model for htt aggregation presented in this chapter reveals non-intuitive effects of different therapeutic strategies on cell survival. The results show that transient dynamics and non-monotonic changes in the concentrations of htt conformers might have a great effect on the outcome of a treatment that targets htt aggregation. Moreover, the stochastic model might help us explain the seemingly conflicting results used to assign either toxic or neuroprotective role to htt aggregates.

The stochastic model for htt aggregation is built on the deterministic core model introduced in the previous chapter. The extension of the core model is a stochastic equation for the release rate of the htt monomers and an equation for the activation of the executioner caspase. The core model allows monitoring of how the concentration of each htt conformer evolves in time for a given set of parameters. Here, I assigned different toxicity levels to htt conformers and can, therefore, monitor how the htt-induced toxicity evolves in time. An executioner caspase detects the toxicity, and when the toxicity exceeds a certain threshold, the caspase commits the cell to die.

Along the lines of dispute over the source of toxicity in HD cells, I considered three toxicity premises: only the soluble htt conformers are toxic, all three conformers are equally toxic, and only aggregates are toxic. For each case, I changed three parameters that have been common therapeutic targets in treating HD, namely: rate of htt monomer removal, degradation of htt aggregates, and htt oligomerization and aggregation rates, and monitored the influence of those changes on the time of cell death. Increasing the monomer removal rate has the expected effect of increasing cell survival, consistent with the deterministic steady state analysis. When aggregates are toxic, however, cells behave in two different ways, they either die early, or they survive. The early death, even for high values of k_{de}, may be due to a transient stochastic accumulation of aggregates causing short-term toxicity high enough to activate the executioner caspase. If the soluble protein is the only toxic species, increasing the degradation rate of htt aggregates can be harmful, since it leads to the accumulation of the toxic conformers in the cell. Moreover, if the soluble protein is the only toxic species, the effect of changing the oligomerization and aggregation rates will depend on the initial values of those rates.

Any non-monotonic response of the cell survival to a change of parameter has implications for the corresponding therapeutic strategies. Different HD models have a wide range of polyQ repeat lengths (50–150). The polyQ repeat length determines the rate of aggregation, i.e. the longer the repeat, the faster the aggregation. If htt monomers and oligomers are toxic, and aggregates are not, a system with a high oligomerization and aggregation rate would benefit from a further increase of the aggregation rate. A system with low aggregation rate, however, would be favored by a decrease in the rates, since the removal of htt oligomers would decrease overall toxicity (Fig. 4.5, lower left panel). This should be considered in the interpretations of results obtained from different experimental

HD models.

Transient behavior denotes how a dynamical system behaves while evolving toward, but still being far from a steady state. Transients can show complex behaviour that bears little resemblance to the long term equilibrium dynamics. Deterministic models introduced in the previous chapter also display transient dynamics that can be seen as an overshoot in the concentration of aggregates at the onset of aggregation. However, the overshoot is much weaker than in the stochastic model. Thus, introducing stochasticity into the model for htt aggregation had significant consequences by potentiating the strength of transient behaviour.

A one-hit model states that a rare, catastrophic event, rather than a prolonged elevated toxicity, causes cell death in a number of neurodegenerative diseases (43). Aggregation of misfolded proteins, as a nucleation process, is itself a sudden and rare event (119). In the stochastic model, the onset of aggregation is caused by a sudden elevated release of monomers (described by a stochastic process), which causes an overshoot in the aggregate concentration (Fig. 4.5, lower panels). This overshoot is transient and cannot be predicted by steady state analysis. If the aggregates are toxic, an overshoot that is high enough can kill the cell. After the overshoot, the concentration of aggregates decreases and fluctuates around an average value. If the cell survives the onset of aggregation, a decreased aggregate concentration may not be enough to kill the cell. In that case, a cell that is alive and contains aggregates might have a higher life expectancy than a cell without aggregates, because it has already survived the worst condition. This phenomenon could be termed a one-shot model. The one-shot model could explain how aggregates could be toxic and neuroprotective at the same time.

The stochastic nature of time of cell death has important implications for the onset and progression of the disease in patients. In the next chapter, I introduce and explore a model for neuronal degeneration in which cells die at random times and in clusters. For small number of clusters (strong dependences between the striatal cells) stochastic effects become visible and contribute significantly to the variability in age of onset of HD.

Chapter 5

Clustered Neuronal Death and the Variance of Age at Onset of Huntington's Disease

5.1 Summary of the chapter

Movement disturbances, psychological changes and dementia, usually appear in Huntington's disease (HD) patients between 30 to 50 years of age and progress over a period of 15 to 20 years. The principal cause of the variability of the age at onset (AO) is the length of the CAG repeat within the gene causing HD (3). Several additional genetic factors contribute to a lesser extent to the variance of the AO, but at least 35% of the variance remains unexplained. HD symptoms are a consequence of premature dying of medium-spiny neurons in the striatum. The extent of the striatal cell death provides a basis for grading the severity of HD (175). Once around 50% of the medium-spiny neurons are lost, motor symptoms associated with HD become noticeable, marking the onset of the disease. In a number of neurodegenerative diseases, the neuronal death rate can be described by an exponential kinetics (43). These observation were incorporated in a stochastic one-hit model of cell death that is presented in this chapter. The results of the model indicate that up to 20% of the observed variance in the AO of HD could be explained by a stochastic pattern of cell death in the striatum of HD patients.

5.2 Introduction

The discovery of the mutation underlying HD created the possibility of determining directly whether someone has inherited the gene for HD. In a healthy individual, the CAG repeat length ranges from 11 to 34 repeats, whereas 37 to more than 80 repeats have been found in HD patients (50, 3, 153). For patients at risk, predictive testing and being informed of having a CAG expansion in the pathological range, shifts the major unanswered question from "Will I get HD?" to "When will it manifest?". Unfortunately, even though the CAG repeat length is highly sensitive for predicting whether someone will develop HD, the ability to predict the age at onset (AO) of HD is only limited.

The longer the CAG repeat length, the earlier the symptoms occur and the more

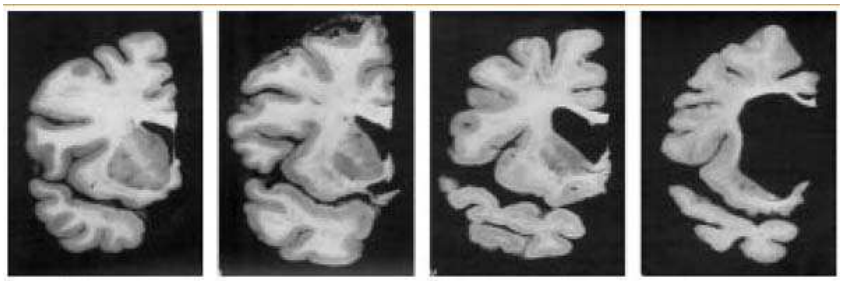

Figure 5.1: Neuropathology of HD in postmortem brains. A normal human brain is shown on the left for comparison, and the in the brain slices to the right, the severity of HD increases (taken from http://www.buckinstitute.org).

severe they are. However, for a given CAG repeat length, a wide range of the AO is observed, making predictions of the AO difficult to use in the counseling of presymptomatic individuals carrying a HD mutation. The CAG repeat length explains around 50% of the variance of the AO. Several additional genetic factors that can contribute to the variance of the AO have recently been identified. Namely, modifications in the genes encoding transcription factor p53 and human caspase activated DNase (39), glutamate receptor 6 subunit of kainate receptor (133) and N-Methyl-D-aspartate (NMDA) receptor subunit 2B (8) explain around 4% of variance each. Still, at least 35% of the variance of the AO remains unexplained.

Here, I put forward a novel answer to this question. I propose that the observed variance in the AO could be an intrinsic stochastic property of the pattern of progressive neuronal death in the striata of HD patients. The proposed mechanism is built upon the following characteristics:

(i) The onset of the disease is determined by the extent of neuronal loss. Premature, gradual dying of the medium spiny neurons in the striatum underlies the development of movement disturbances, psychological changes and dementia in HD patients. The extent of atrophy and cell loss correlates with the severity of the disease. Already 10 years before the onset of the clinical symptoms, a significant neuronal loss is observed. By the time the specific motor disorders appear (onset of the disease), at least 50% of the striatal neurons have been lost (12). Postmortem examinations of HD patients revealed up to 95% of neuronal loss in the striatum (175) (Figure 5.1).

(ii) The neuronal death rate is described by an exponential kinetics. The delay in the clinical onset of HD and other late-onset neurodegenerative diseases, has often been assumed to reflect the occurrence of age-dependent cumulative damage (45). A prediction of the cumulative damage hypothesis is that the probability of cell death will increase over time. However, Clarke et al. observed that the kinetics of the metabolic decline due to cell loss in HD patients are best described by a constant risk of cell death (43). This translates into an exponential neuronal death kinetics, where a single event triggers cell death and the time of death of any neuron is random. They named this kind of kinetics a 'one-hit' model of neuronal death. Perutz et al. proposed that initial nucleation of intracellular aggregates is the event that leads to such a cell death kinetics (119).

(iii) The death rate depends linearly on the CAG repeat length. A number

of studies supports this notion, namely: the striatal volume loss measured by MRI shows a linear correlation with the CAG repeat length (129); autoradiographic studies show that striatal dopamine receptor binding decreases in proportion to the degree of cell loss in early HD (10); and PET scans show a linear relationship between the CAG repeat length and the loss of dopamine receptor binding (5).

(iv) Neuronal death occurs in clusters. Using autopsy cases of early HD, Hedreen et al. found scattered islands of neuronal loss confined to the striosome compartment of the striatum (69). Thieben et al. reported unevenly distributed neuronal loss (167). Some earlier studies suggested that there was a dorsal to ventral gradient of neuronal loss with advancing disease (175). All those studies support the idea that neurons in the HD striatum die in clusters, corresponding to the striatal regions with similar conditions (e.g. level of the excitotoxicity, level of neurotrophic factors, inflammation etc.).

5.3 Stochastic one-hit model for striatal cell death in HD

Based on the characteristics of cell death in HD patients, I formulated a mathematical model relating the age at onset (AO) of the disease to the CAG repeat length. The neuronal death in HD follows an exponential kinetics, a process similar to radioactive decay. The average number of surviving striatal neurons at age t, $N(t)$, satisfies

$$\langle N(t)\rangle = N_0 \exp(-\gamma(CAG)t), \tag{5.1}$$

where N_0 is the initial number of neurons and CAG is the number of repeats. The neuronal loss rate

$$\gamma(CAG) = (\alpha + \beta(CAG - c_0)) \tag{5.2}$$

is a linear function of the CAG. The parameter α is a basal, CAG repeat-independent loss rate, i.e. loss due to aging and additional genetic factors. The parameter β represents the specific loss rate induced by every CAG repeat longer than $c_0 = 36$. Only CAG repeat lengths that are longer than 36 are evaluated with the model, since HD does not occur for the shorter repeat lengths. In the model, the age at onset is defined as the time at which the fraction of the initial number of neurons, N_0, remaining

$$\rho(t) = N(t)/N_0 \tag{5.3}$$

drops to the critical value $\rho_c = 0.5$ (Fig. 5.2A and C). A good predictor of the average AO is

$$\langle AO\rangle = \frac{\log(1/\rho_c)}{\gamma(CAG)}. \tag{5.4}$$

In the stochastic one-hit model, and any particular outcome of the AO will deviate from the average AO given by Eq. 5.4.

The number of striatal neurons in human is between 1.1×10^8 and 2.0×10^8 (70). If they die independently of each other, the variance of AO will be negligible (Figure 5.2, panels (A) and (B)). However, if we assume that striatal neurons die in clusters, then $N(t)$ does not represent the number of single neurons but the number of neuronal clusters experiencing similar external conditions. According to this hypothesis, N_0, the initial

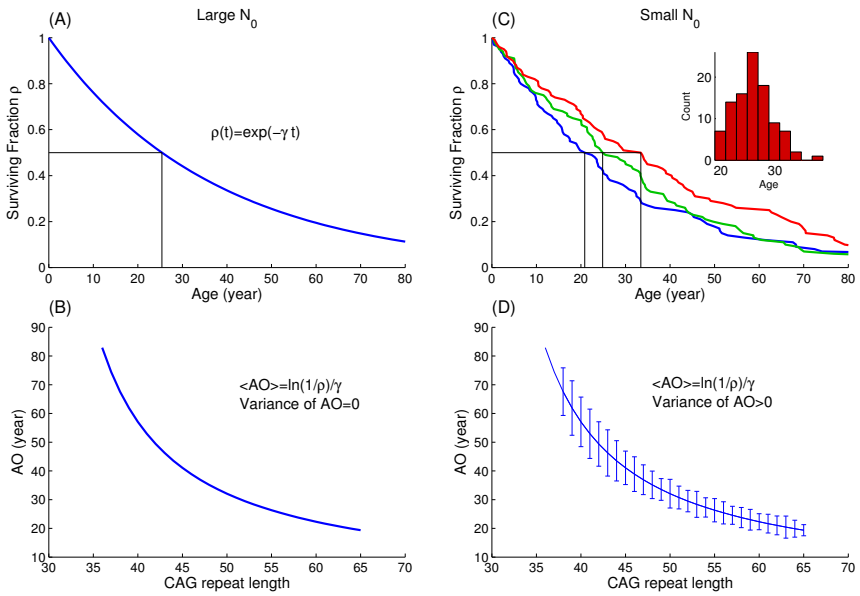

Figure 5.2: Stochastic model of neuronal death. For a large initial number of clusters ($N_0 \sim 10^8$) and a fixed CAG repeat length, the variance of the AO is negligible (panels (A) and (B)). (A) The fraction of surviving neurons $\rho(t)$ decays exponentially according to Eq. 5.1, and the threshold ρ_c uniquely defines the AO. (B) The AO is predicted by Eq. 5.4. For small initial number of clusters ($N_0 < 10^4$), the variance of AO is significant (panels (C) and (D)). (C) The fraction of surviving neurons decays randomly, and on average the decrease is exponential as described by Eq. 5.1. Individual simulations reach the threshold ρ_c at different times (three are shown, all with 56 CAG repeats). For a given repeat length, the AO follows a distribution exemplified in the insert of panel (C). (D) When simulations are performed, the average AO is predicted by Eq. 5.4, and the variance of the AO is greater than zero (the error bars indicate the standard deviation of 100 runs, for every CAG repeat length between 41 and 65).

number of clusters, will be small ($N_0 \leq 10^4$), and AO will have a significant variance (Figure 5.2, panels (C) and (D)).

5.4 Results

The results are organised as follows. First, the deterministic average AO (given by Eq. 5.4) of the one-hit model was fitted to six data sets comprising CAG repeat lengths and the corresponding AOs (3, 50, 83, 102, 153, 155). This fitting procedure yielded an estimate of the variance explained by the CAG repeat length in the one-hit model.

Second, the deterministic component of the one-hit model was compared to the widely used logarithmic model for predicting the AO, in which the log(AO) is a linear function of the CAG repeat length. The comparison showed that the deterministic part of the one-hit model and the logarithmic model explains the same fraction of variance in AO in the six data sets analyzed here.

Third, the contribution of the stochastic component of the one-hit model to the vari-

ance in the AO was assessed. The model showed that for a small number of cluster (N_0), the AO is spread around the predicted average. The variance of AO obtained by running stochastic simulation for the CAG repeat length of each patient was then compared to the observed variance of AO for the same repeat length. The ratio of the variance of the simulated AO to the observed variance in patient provides an estimate of the variance explained by the stochastic one-hit model.

5.4.1 Fitting the one-hit model for the AO

Equation 5.4 was fitted to six data sets (3, 50, 83, 102, 153, 155) using a nonlinear least-square regression from MATLAB's statistical package. The data sets and the variance of AO are represented in Fig. 5.3. In Eq. 5.4, the parameter α is a basal death rate of striatal neurons that is independent of the CAG repeat length, and parameter β describes by how much the death rate increases for each additional CAG repeat (> 36). The least-square regression finds the values of α and β that minimize the sum of squares of the errors, SSE,

$$SSE = \sum_{i=1}^{n} (y_i - \langle AO \rangle_i)^2 \tag{5.5}$$

where y_i is the i-th observed AO, $\langle AO \rangle_i$ is the predicted AO corresponding to CAG_i, and n is the number of points in a data set. The total variation of the data, SST, is given by a sum of squares of differences between the data and the mean,

$$SST = \sum_{i=1}^{n} (y_i - \bar{y})^2, \tag{5.6}$$

where y_i is the i-th observed AO and $\bar{y}$ the mean of all AOs. The coefficient of determination is the fraction of the total variance explained by the model, and is given by

$$R^2 = 1 - \frac{SSE}{SST}. \tag{5.7}$$

The fitted values of α and β, and the corresponding values of the coefficient of determination R^2 for each data set are given in Table 5.1. By averaging over the results for all 6 data sets, I obtain an average value of $\alpha = (10.7 \pm 1.2)^{-3}$ y^{-1} and for β the result is $\beta = (0.82 \pm 0.12) \times 10^{-3}$ y^{-1} per additional CAG repeat. For example, for 45 CAG repeats, this translates into an annual neuronal loss rate γ of 1.8%, and 3.4% for 65 CAG repeats.

5.4.2 Fitting the logarithmic model for the AO

In previous studies (133, 130, 39), a logarithmic model was used to fit the AO to the CAG repeat length. The model is

$$\log(AO) = a + b(CAG - c_0). \tag{5.8}$$

To be able to compare the one-hit model (defined by Eq. 5.4) to the logarithmic model, the latter was fitted using the same six data sets and the same algorithms from MATLAB's statistical package. The logarithm of AO ($\log(AO)$) was taken as the dependent variable,

Table 5.1: Results of the regression analysis. The parameters α and β of the regression of Eq. 5.4 are given in units of 10^{-3}/year. Values of R^2 are shown for the logarithmic model and Eq. 5.4. Numbers next to ΔR^2 are the initial numbers of cluster N_0.

Data	α	β	R^2 log	R^2 Eq. 5.4	ΔR^2 (5000)	ΔR^2 (500)	ΔR^2 (100)
Andrew 1993 (3)	9.3	0.85	0.41	0.43	0.0038	0.038	0.20
Duyao 1993 (50)	9.5	0.88	0.62	0.61	0.0032	0.032	0.17
Kieburtz 1994 (83)	12.1	0.66	0.45	0.43	0.0037	0.034	0.17
Margolis 2003 (102)	11.6	0.70	0.45	0.45	0.0035	0.035	0.18
Snell 1993 (153)	11.5	1.00	0.59	0.62	0.0054	0.057	0.30
Squitieri 2000 (155)	10.4	0.84	0.53	0.53	0.0034	0.035	0.19
Mean	10.7	0.82	0.51	0.51	0.0038	0.039	0.20
STD	1.2	0.12	0.09	0.09	0.001	0.01	0.05

the CAG repeat length as the independent variable, and a linear least-square regression was performed for the data sets. The coefficient of determination, R^2, was calculated using the procedure described above. The results of the regression analysis are summarised in Table 5.1. The logarithmic regressions gave an average of $R^2 = 0.51 \pm 0.09$, in agreement with previous studies (39, 133, 8) and identical to the R^2 calculated for the one-hit neuronal death model ($R^2 = 0.51 \pm 0.09$). This shows that both models fit the data equally well.

Earlier studies that used a logarithmic model have taken the residuals of the linear regression of $\log(AO)$ to calculate R^2. Here, R^2 was calculated using the residuals of AO and not $\log(AO)$, which was needed to compare the different models, therefore the discrepancy between the R^2 shown here and the values reported in other studies.

5.4.3 Estimating the variance of the AO using stochastic simulations

Stochastic neuronal death was simulated using the Gillespie algorithm with the fitted parameter values of Eq. 5.4, α and β. Stochastic simulations were used to assess the effect of different initial numbers of clusters N_0 (from 10^2 to 5×10^3) on the variance of the AO. The Gillespie algorithm computes the time intervals between the deaths of two neuronal clusters. The mean value and the variance of the time interval increases as the number of remaining clusters decreases. The AO is defined as the time at which the fraction of clusters $\rho_c = 0.5$ is left.

Simulated values of AO were obtained for each data point in each data set for each initial number of clusters (Fig. 5.3, $N_0 = 100$ and 500, STD shown). The simulated data sets thus obtained were analyzed as follows. The variability of the simulated AOs is given by the sum of squares of residuals of the simulated data sets, SSE_{STOCH}. This variability is compared to the total variability observed in the real data sets, SST by calculating the fraction of the total variance that comes from the stochastic process is

$$\Delta R^2 = SSE_{STOCH}/SST. \tag{5.9}$$

The values of ΔR^2 were averaged from 10 independent runs for each initial number of clusters (Table 5.1). The variability of ΔR^2 between each independent run was very small (results not shown). This ΔR^2 measures the variance that is specific to the stochastic one-hit kinetics of neuronal death.

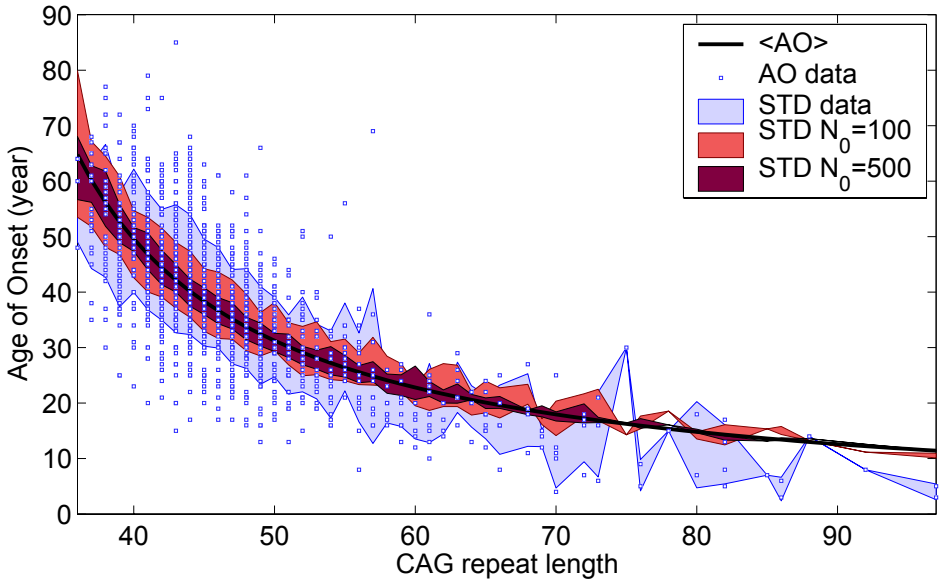

Figure 5.3: Simulation of the stochastic neuronal death model, and comparison with data from (3, 50, 83, 102, 153, 155) (all data points are shown in small blue squares, repeated points are overlaid). The predicted average of the AO was calculated using Eq. 5.4 (solid black line). The standard deviation (STD) of the AO for each CAG repeat (light blue shaded area) represents the unexplained variance of the AO. Simulations using the CAG repeat distribution from data (n=1147) were performed for $N_0 = 100$ and 500 (the corresponding STDs are shown by the shaded areas in salmon and dark red). The parameters are $\alpha = 10.7 \times 10^{-3}$/year, $\beta = 0.82 \times 10^{-3}$/year/CAG repeat and $N_0 = 100$ and 500.

For a given CAG repeat, the variance of AO is inversely related to the initial number of clusters N_0. Thus, when N_0 is small, intrinsic stochasticity due to clustered neuronal death can explain more variance, as shown in Table 5.1. For $N_0 = 500$, intrinsic stochasticity represents 4% of the total variance of the AO. If the number of clusters were smaller, the percentage of the explained variance could go up to 20% ($N_0 = 100$).

5.5 Discussion

Soon after the discovery of the gene and the underlying mutation in HD, a strong correlation between the CAG repeat length and the AO of HD was uncovered. However, due to the large variance of the AO for the same CAG repeat length, the time of onset remains difficult to predict. In the previous studies, logarithmic models have been used to fit the AO to the CAG repeat length (133, 39, 8). Moreover, using the largest cohort of HD patients analysed so far, Langbehn et al. developed a parametric survival model to predict the probability for HD gene carriers to develop the disease given their age and CAG repeat length (91). However, to increase the predictive power of those models, additional factors that modulate the AO would need to be included. To date, several such genetic modifiers of AO have been identified. Nevertheless, at least 35% of the variance of AO remains unexplained. In this chapter, I proposed that a part of the unexplained

variance can be explained by the intrinsic stochastic dynamics of neurodegeneration.

Since premature dying of striatal medium spiny neurons underlies the onset and progression of HD, I studied the effect of the kinetic properties of this process on the variance of AO. I developed a mathematical model for neuronal death in the striatum, assuming that the probability of a neuron to die is constant in time but depends on the CAG repeat length. The additional hypothesis in the model is that cell-cell interactions and the inhomogeneity of the striatum affect the probability of groups of neurons to die. That is, neurons do not die independently but rather in clusters. On these premises a predictor of the AO based on the fraction of surviving striatal neurons ρ (Fig. 5.2A–D) was formulated. Aylward et al. reported the values of ρ between 0.33 and 0.5 at the time of diagnosis (12). Here, a fixed value of $\rho_c = 0.5$ was used. Considering a distribution of the values of ρ at onset would result in an increased variance. In addition, there could be a correlation between the CAG repeat length and ρ_c, but this has yet to be established.

Based on six data sets where the AO and the CAG repeat length were known, neuronal death rates, the fraction of explained variance of the average AO (coefficient of determination R^2) and the additional explained variance (ΔR^2) due to clustered stochastic death were computed. The additional explained variance varied from 0.4% for $N_0 = 5000$ to 20% for $N_0 = 100$. The average annual cluster (and neuronal) loss rate ranged from 1.2% for the pathological threshold of 37 CAG repeats to 4.7% for 80 repeats. The estimates of α and β are consistent with the claim that neuronal half-life decreases by a factor 1.055 for every additional CAG repeat (119).

Genetic modifiers affect the variance of AO by modulating the neuronal death rate and can be viewed as extrinsic stochasticity: $\gamma = \gamma_{CAG} + \xi$, where random ξ represents the influence of additional factors. If we relate this to the one-hit model of neurodegeneration proposed by Clarke and coworkers (43), the CAG repeat length and additional factors will define the mutated steady-state in the vulnerable neurons, and thus determine the probability of the neurons to die. So, for the same CAG repeat length, there would be a distribution of the neuronal death rates and AOs caused by the difference in the genetic modifiers. In this chapter, I propose that even for the same neuronal death rate, the timespan needed for the critical fraction of striatal neurons to die is variable. This variability might be an intrinsic stochastic property of the clustered neuronal death. In principle, monozygotic twins with the HD gene living in the same conditions should display a difference in the AO due to intrinsic factors only. Recently, twins with 49 CAG repeats were reported to have AOs of 32 and 35 years (2). For 49 CAG repeats and $N_0 = 500$, our model predicts an age at onset of 32.5 ± 2.0 years.

Chapter 6

Conclusions and Outlook

6.1 Conclusion

In my work, I used experimental and mathematical models to investigate the dynamics of Huntington's disease (HD). In both cases, it has been difficult to tell how close these models replicate the disease in HD patients, which takes decades to manifest and progress. Nevertheless, the models allowed us to explore possible mechanisms behind the phenotypes and to gain better understanding of them. Complex dynamical properties of the biological systems can make causalities difficult to interpret. When faced with the intricate biological problems, we need synergy of different perspectives that can be attained only by combining experimental and theoretical methods.

Research dealing with a devastating disease such as HD primarily focuses on finding an appropriate treatment by identifying the robust principles that underly the observed pathology. Transcriptional dysregulation has been extensively reported in various HD models, which fueled the search for transcriptionally active therapeutics for HD. In chapter 2, I addressed the question whether htt aggregation, induced in a HD cell model, leads to systematic transcriptional changes in groups of genes regulated by transcription factors that have been implicated in HD. In this study, no systematic expression changes were observed, indicating that targeting a specific transcription factor might not be a feasible therapeutic strategy for treating HD.

Htt aggregation has been a common therapeutic target. However, since no conclusive answer as to which of the htt conformations arising from the aggregation process is the toxic one, an appropriate therapeutic strategy is far from obvious. In chapters 3 and 4, I introduced deterministic and stochastic mathematical models describing htt aggregation and cell death induced by different htt conformers. The steady state analysis and the numerical simulations of the models show that transient dynamics observed in the system and the non-monotonic response of cell survival to a change of parameter might lead to non-intuitive outcomes of a treatment targeting htt aggregation. For instance, numerical simulations of the stochastic model show that the outcome of a change in the htt aggregation rate in a specific HD model depends greatly on the starting value of that rate which is determined by the length of the polyglutamine (polyQ) tract. If htt monomers and oligomers are toxic, and aggregates are not, a system with a high oligomerization and aggregation rate would benefit from a furhter increase of the aggregation rate. A system with low aggregation rate, however, would be favoured by a decrease in the rates, since the

removal of htt oligomers would decrease the overall toxicity. This should be considered when interpreting results obtained from HD models with different polyQ lengths.

Furthermore, the analysis of the model pointed to the following observations. If aggregates are toxic, an overshoot in the aggregate concentration at the onset of aggregation might be strong enough to trigger cell death. However, if a cell survived the onset of aggregation, it might have a longer life expectancy than the cell without aggregates, although it contains toxic aggregates, because the worst is already behind it. I conclude that this one-shot model can explain how htt aggregates might be seen as toxic and neuroprotective at the same time.

In chapter 5, I propose that even for the same neuronal death rate (dependent on the polyQ repeat length), the timespan needed for the critical fraction of striatal neurons to die (corresponding to the age at onset) is variable. This means that the existence of additional genetic modifiers of the HD onset is not necessary to explain the variance in the age at onset of HD. The observed variance might be a consequence of an intrinsic stochastic nature of the clustered cell death in the striata of HD patients.

6.2 Outlook

In HD, mutation in a single gene induces complex pathological events. In the course of the disease a multitude of cellular pathways become affected, resulting in transcriptional dysregulation, mitochondrial dysfunction, proteasomal inhibition, disturbed vesicular transport, impaired synaptic plasticity, excitotoxicity, inflammation, oxidative damage, aberrant protein-protein interactions, and eventually cell death. Each of these pathways is a potential therapeutic target. Mathematical models of the pathways affected in HD could be a great help in evaluating the experimental results from compounds targeting those pathways. In that case, both experimental and mathematical models need to be developed in such a way as to be able to answer a specific question and the results obtained should be interpreted within these boundaries.

Since the rank of importance of an individual pathway on the progression of HD is not known, it is likely that treatment strategies will focus on administering cocktails of drugs affecting different pathways. However, cellular pathways are usually not independent, but rather form complex networks with behaviour that is difficult to predict without computational models. Computational models of cellular networks could help to determine the steps in those pathways that could elicit synergistic effects in a combinatorial treatment. Having in mind that any successful HD treatment would probably last for decades, identifying the combinations of compounds that are active in non-toxic concentrations will be an important issue in the future.

A major goal in preventing HD onset and progression is to slow down neuronal death. Widespread inflammation and excitotoxicity in the striatum of HD patients mediate coupled cell death in neighboring neurons. The stochastic one-hit model of cell death presented in the chapter 5 could be further analyzed to asses the influence of the compounds which reduce inflammation and thus improve the external conditions sensed by the striatal neurons. In mathematical terms, such compounds could uncouple the clusters of dying neurons which would decrease the neuronal death rate and delay the onset of the disease.

Neuroimaging techniques are becoming widely used to monitor neurodegeneration in HD patients. These techniques are becoming an essential tool in clinical trials, since they allow accurate measurement of the progression of the disease. However, to assess the efficacy of any HD treatments it will be necessary to take into account the stochastic nature of neuronal degeneration. Statistically significant results will be obtained when the progression of the disease lies outside the confidence interval predicted by the stochastic model for neurodegenation for a particular patient. Because of the dynamical nature of HD, such models should form the basis of the statistical protocols in clinical trials.

Appendix A

Materials and Methods

A.1 Experimental materials and methods

A.1.1 Cell line

HEK 293 Tet-Off cell line (Clontech) has been derived from HEK (human embryonic kidney) cell line as a single-stable Tet-Off cell line. Previously in Prof. Erich Wanker's lab, this cell line was transfected with the pTetCMV-Hyg-CAG83 vector (176). Stable transfected cell lines were selected using 150 μg/ml hygromycin. High-level transcription of the transfected gene is induced by growing the cells in a doxycyclin-free medium.

A.1.2 Culturing of cell line

Stable transfected 293 Tet-Off cells were grown in l-glutamine free MEM with Earle's Salts (Life Technologies, Gaithersburg, MD) and supplemented with 10% fetal bovine serum (FBS), 2 mM l-glutamine, 100 IU/ml penicillin plus 100 μg/ml streptomycin, 100 μg/ml G418, 150 μg/ml hygromycin B, and 10 ng/ml doxycycline in poly-l-lysine coated cell culture flasks. Expression was induced by thoroughly washing the cells with PBS buffer (8g NaCl, 0.2g KCl, 1.44g Na_2HPO_4, 0.24g KH_2PO_4, distilled water till 1l) and adding fresh medium lacking doxycycline. The medium was changed on the following day to remove the doxycycline completely. Expression was induced for 2 and 4 days.

A.1.3 Total RNA isolation

Total RNA was isolated from the stable transfected 293 Tet-Off cells using the RNeasy Midi Qiagen Kit, according to the manufacturer's instructions. RNeasy Midi Qiagen Kit includes the buffers used in this procedure.

Preparation

For all the steps RNase-free microtubes, Falcon tubes, pipettes, pipette tips and water was used. The working surfaces and centrifuge was cleaned with Rnase Zap solution from Ambion to remove RNase contamination. In the fume hood 10 μl 14.3 M β-mercaptoethanol per 1 ml RLT Lysis buffer was added. Before using for the first time, 4 volumes of ethanol (96–100%) were added to the RPE buffer to obtain a working solution. 20 μl of freshly

prepared RNase free DnaseI stock was added to 140 μl of RDD buffer. 70% RNase-free ethanol was prepared.

RNA isolation

T150 flask with 3/4 confluent stable transfected HEK 293 cells (more than 10^7 cells) were tripsinized for 5 min, taken in 7 ml medium, transfered to 50 ml Falcon tube, and centrifuged for 5 min, 1800 rpm at 4°C. The supernat was carefully aspirated, the pellet resuspended in 5 ml PBS, and centrifuged again for 5 min, 1800 rpm at 4°C. The supernatant was carefully aspirated and pellet thoroughly resuspended in 2 ml of RLT Lysis buffer by flicking the tube. Cell lysates were homogenized using Qiagen QIAshredder spin column: 700 μl were put on a column and centrifuged for 2 min, 14000 rpm, at room temperature (RT). Homogenized lysates were transfered to 15 ml Falcon tubes, and equal volume of 70% ethanol was added and mixed by vigorous shaking. The sample was immediately applied to a RNeasy Midi column, the tube gently closed and centrifuged for 5 min, 4000 rpm at RT. The flow-through was discarded. 2 ml of RW1 buffer was added to the column, the centrifuge tube gently closed and centrifuged for 5 min, 4000 rpm. The flow-through was discarded. 160μl of DNaseI in RDD buffer was applied directly to the column, and left for 15 min at RT. Then, 2 ml of RW1 buffer were added to the column and left for 5 min at RT. The column was then centrifuged for 5 min, 4000 rpm at RT. 2.5 ml of RPE buffer was added to the column, the column was centrifuged for 2 min, 4000 rpm at RT, and flow-through discarded. Another 2.5 ml of RPE buffer was added to the column, the column was centrifuged for 5 min, 4000 rpm at RT, and flow-through discarded. To elute, RNeasy column was transferred to a new 15 ml Falcon tube. 150 μl of the RNase-free water was pippeted directly onto the RNeasy silica-gel membrane, tube was gently closed, left for 1 min at RT, and then centrifuged for 3 min, 4000 rpm, at RT. To obtain higher RNA concentration, the obtained eluat was applied to the column again, and centrifuged for 3 min, 4000 rpm, at RT. Isolated RNA was kept on -80°C.

A.1.4 RNA quality control

The control of quality and quantity of RNA was performed using UV Photometer (Eppendorf). Several dilutions of the samples were prepared and optical density (OD) was measured at wavelengths 260 nm and 280 nm using a quartz cuvette. For exact measurement OD260 value of the RNA sample should lie between 0.05 and 0.5. An OD260=1 corresponds to an RNA concentration of 40 μg/ml. The quality was checked by calculating the ratio OD260/OD280. This ratio should be between 1.8 and 2. Quality was determined in 10 mM Tris-Puffer pH 7,4, and quantity was determined in water.

A.1.5 Preparation of supernatant and pellet protein fractions

Cells were washed and scraped in ice-cold PBS, and pelleted by centrifugation. Cell lysis was performed on ice for 30 min in 50 mM Tris-HCl (pH 8.8), 100 mM NaCl, 5 mM MgCl2, 0.5% NP-40, and protease inhibitors (2 mM PMSF, 10 g/ml leupeptin, 10 μg/ml pepstatin, 1 μg/ml aprotinin, and 50 μg/ml antipain). Insoluble material was pelleted

by centrifugation at 14000 rpm for 10 min at 4°C. The pellet was resuspended in 100 μl 20 mM Tris-HCl (pH 8.0)/15 mM MgCl2 containing 0.5 mg/ml DNAseI and incubated for 1 h at 37°C. Protein of the supernatant and pellet fraction was determined using the Bradford protein assay (Bio-Rad, Munich, Germany).

A.1.6 Immunodetection of htt aggregates

SDS-polyacrylamide gel electrophoresis (SDS-PAGE) was performed according to the standard procedure. The gels contained 12% polyacrylamide. As a marker, Benchmark pre-stained protein marker from Invitrogen was used.

The proteins separated on SDS-gels were blotted onto nitrocellulose membranes as follows: The gel was put onto a nitrocellulose membrane soaked in blotting buffer (25mM Tris-HCl pH 8.0, 192mM Glycine, 20% methanol), carefully avoiding air bubbles. On both sides, two layers of Schleicher and Schuell GB005 filter paper (also soaked in blotting buffer) were added, and the "sandwich" was placed on a semi-dry blotting apparatus (Biorad) with the nitrocellulose versus the bottom and the gel facing the upper side. Surplus buffer and possibly remaining air bubbles were removed with a rubber roll, the apparatus assembled completely and blotting was performed at 20V for 1h.

Membranes were incubated in blocking solution 3% skim milk in TBS (20mM Tris-HCl pH 7.4, 150mM NaCl) either for 30 min at RT or over night at 4°C to block any unspecific reaction of the antibodies in the following steps. The first antibody (HD1, rabbit, prepared in Prof. Erich Wanker's lab) was diluted 1:1000 in 3% skim milk and incubated with the membrane for 45 min at RT. The membrane was then washed in the washing buffer (TTBS = 0.05 % Tween 20 + TBS) 4 times 5 to 10 min, before the second antibody (Anti-rabbit-peroxidase (POD)(Roche)) diluted 1:5000 in 3% skim milk, was added. After 1 h incubation at RT the washing steps with TTBS and TBS were repeated, and detection with Luminol (LumiLight) was performed: the gel was placed on a glass plate, and covered with the solution containing Lumi-Light substrate. After 1–3 min the excess solution was removed and the gel wrapped in a Saran-wrap carefully avoiding bubbles. Horseradish peroxidase (POD) converts Lumi-Light substrate resulting in light emission, and light is detected by exposure to X-Ray film (processed in dark room).

A.1.7 cDNA microarrays

This work has been done by the members of Dr. Ulrike Nuber lab from Max Planck Institute for Molecular Genetics, Berlin.

Generation of cDNA microarrays

Human cDNA clones were obtained from the Resource Center of the German Human Genome Project (RZPD Berlin). cDNA clones represented target genes of transcription factors implicated in HD. Additional human cDNA clones and 34 plant cDNA clones were included. Clone inserts were amplified under standard conditions using primers M13for (GTA AAA CGA CGG CCA G) and M13rev (CAG GAA ACA GCT ATG AC). Primers were obtained from MWG Biotech (Ebersberg, Germany). All PCR products were evaluated by agarose gel electrophoresis. Purified PCR products were resuspended

in 8 μl of 3x SSC and printed on Corning GAPS II slides by using a robotic spotting device (SDDC-2 MicroArrayer, ESI, Toronto, Canada ChipWriter Pro, Bio-Rad, Munich, Germany) with SMP3 pins from TeleChem International (Sunnyvale, CA).

RNA isolation and microarray hybridization

Total RNA was isolated with Trizol reagent (Invitrogen). Microarray labeling and hybridization reactions were performed using the 3DNA Array 350 Expression Array Detection kit (Genisphere, Hatfield, PA) according to the manufacturer's instructions. 6 independent samples collected at day 0 of the experiment were pooled and used as a reference. RNA was isolated from 3 samples of induced cells at day 2, and 3 samples of induced cells at day 4. 5 μg of total RNA of the reference pool (day 0) and of the single 6 samples was reverse transcribed using primers with a specific capture sequence. The reference cDNA sample was combined with one of the 6 other cDNA samples and hybridized to the microarrays in a humidified chamber at 42C for 16 hr. Dye-swap repeats were performed for each of the 6 co-hybridizations. Thus, 12 arrays were used in total. Slides were washed at room temperature in 2x SSC/0.2 percent SDS for 10 min, 2x SSC for 10 min, and 0.2x SSC for 10 min. Bound cDNA was visualized by hybridization with 3DNA (dendrimers specific for respective capture sequences conjugated to either Cy3 or Cy5) in a humidified chamber at 42C for 3 hr. Subsequently, slides were washed as before.

Image acquisition and data analysis

Fluorescence intensities of Cy3 and Cy5 were measured separately at 532 and 635 nm with a laser scanner (Affymetrix 428 Array Scanner, Affymetrix). The resulting 16-bit data files were imported into Microarray Suite image analysis software (version 2.0), which runs as an extension of IPLab Spectrum software (Scanalytics, Fairfax, VA). Raw spot intensities of Cy3 and Cy5 were locally background subtracted by the MicroArray Suite software. Empty spots and spots carrying plant gene sequences were excluded from further analysis.

A.1.8 Microarray data analysis

The statistical analysis of microarray data were analysed using software packages from Bioconductor, an open source and open development software project for the analysis and comprehension of genomic data (www.bioconductor.org). For data preprocessing, dye-swaps were combined and subsequently adjusted by lowess normalization. The statistical significance of fold changes i.e. z-scores were based on a intensity-dependent local pooled error estimate. Alternatively, a Student's t-test was applied assuming equal variances of the two samples.

A.2 Computational and mathematical tools

All numerical computations in Chapters 3–5 were done in the Matlab environment (The MathWorks, Naticks, MA). All Matlab's files and scripts are available on request.

A.2.1 Differential equations and stochastic processes

Ordinary differential equations (ODEs) were solve numerically with the medium order adaptive method `ode45`. **Stochastic differential equations** (SDE, Langevin equations) were simulated using a forward Euler method for SDE. Briefly, if the equation to solve is

$$\frac{dy(t)}{dt} = f(t, y(t)) + SL(t),$$

and y_i is the approximation of y at time $t_i = hi + t_0$. The parameter h is the fixed time step. The forward integration scheme is

$$y_{i+1} = y_i + hf(t_i, y_i) + \sqrt{h}SN,$$

where N is a random value drawn from a normal distribution with mean 0 and variance 1. For the simulations in Chapter 4, the time step was reduced until no difference between simulations were seen (h=0.02).

Stochastic clustered neuronal death process was simulated using a Gillespie algorithm. The number of cluster $N(t)$ is a stochastic process in which the probability of each cluster to die is independent of the others, and is distributed according to an exponential distribution with parameter γ. No birth is possible, so cluster death follows a kinetic similar to a first order degradation of a chemical:

$$N \xrightarrow{\gamma} \emptyset.$$

The Gillespie algorithm allows computing time trajectories of $N(t)$ that are statistically exact, i.e. the simulations have the same statistical properties as the real stochastic process. The algorithm is outlined as follows:

```
% Initialization
N(1)=N_0, t(1)=t0, i=1;
% Main loop
while N(i)>0 and t(i)<tfinal
Determine the time until the next cluster death dt.
If N(i) clusters are present, the time of the next
cluster death is exponentially distributed with
parameter N(i)*gamma.
Update N (decrease N by 1): N(i+1)=N(i-1).
Update t: t(i+1)=t(i+dt).
Update i: i=i+1;.
end
```

The age of onset is determined by the time at which $N = \rho$. The variance of AO is estimated by multiple stochastic runs. There is an analytical expression for the mean and variance of the death process but it is of limited used for large N since it involves factorials.

A.2.2 Statistical analysis

Statistical analysis was performed with the statistical package of Matlab. Parameter fitting was done with the least-square fitting algorithm `nlinfit` from Matlab. The coefficient of determination was calculated from the residuals (errors) given as an output by nonlinfit.

Appendix B

Mathematical Analysis

B.1 Stability analysis of the core model

The linearised equations around the steady state are given by the Jacobian matrix.

$$J = \begin{pmatrix} -A - k_{dh} & 0 & 0 & 0 \\ A & -k_n O_{htt} - k_{de} & -k_n M_{htt} + k_n^{-1} & 0 \\ 0 & k_n O_{htt} & k_n M_{htt} - k_a A_{htt} - (k_n^{-1} + k_{dn}) & -k_a O_{htt} + k_a^{-1} \\ 0 & 0 & k_a A_{htt} & k_a O_{htt} - (k_a^{-1} + k_{da}) \end{pmatrix}. \tag{B.1}$$

The Jacobian matrix evaluated at Steady State 1 is

$$J_1 = \begin{pmatrix} -A - k_{dh} & 0 & 0 & 0 \\ A & -k_{de} & -k_n A \dfrac{k_h}{A + k_{dh}} + k_n^{-1} & 0 \\ 0 & 0 & \dfrac{k_n A}{k_{de}} \dfrac{k_h}{A + k_{dh}} - (k_n^{-1} + k_{dn}) & k_a^{-1} \\ 0 & 0 & 0 & -(k_a^{-1} + k_{da}) \end{pmatrix}. \tag{B.2}$$

The eigenvalue equation $\det(J_1 - \lambda I) = 0$ is the 4th order polynomial

$$(-A - k_{dh} - \lambda)(-k_{de} - \lambda)\left(\frac{k_n A}{k_{de}} \frac{k_h}{A + k_{dh}} - (k_n^{-1} + k_{dn}) - \lambda\right) \Big(-(k_a^{-1} + k_{da}) - \lambda\Big) = 0. \tag{B.3}$$

The four eigenvalues of Steady State 1 are

$$\begin{aligned} \lambda_{1,1} &= -A - k_{dh}, \\ \lambda_{1,2} &= -k_{de}, \\ \lambda_{1,3} &= \frac{k_n A}{k_{de}} \frac{k_h}{A + k_{dh}} - (k_n^{-1} + k_{dn}), \\ \lambda_{1,4} &= -(k_a^{-1} + k_{da}). \end{aligned}$$

For Steady State 1 to be stable, the following condition needs to be met ($\lambda_{1,3} = 0$),

$$\frac{k_n A}{k_{de}} \frac{k_h}{A + k_{dh}} < (k_n^{-1} + k_{dn}).$$

This condition states that a bifurcation occurs at

$$A_1 = \frac{k_{dh}a}{k_n k_h - a}, \quad \text{with } a = k_{de}(k_{dn} + k_n^{-1}). \tag{Bif 1}$$

At this value, the first two steady states collide with each other, a good indication of a transcritical bifurcation. The Jacobian matrix at Steady State 2 is

$$J_2 = \begin{pmatrix} -A - k_{dh} & 0 & 0 & 0 \\ A & -k_n O_{htt}^2 - k_{de} & -k_{dn} & 0 \\ 0 & k_n O_{htt}^2 & 0 & -k_a O_{htt}^2 + k_a^{-1} \\ 0 & 0 & 0 & k_a O_{htt}^2 - (k_a^{-1} + k_{da}) \end{pmatrix}. \tag{B.4}$$

The associated characteristic equation is

$$\begin{aligned}(-A - k_{dh} - \lambda)\Big\{\Big(-k_n O_{htt}^2 - k_{de} - \lambda\Big)(-\lambda)\Big(k_a O_{htt} - (k_a^{-1} + k_{da}) - \lambda\Big) \\ + k_{dn} k_n O_{htt}^2 \Big(k_a O_{htt}^2 - (k_a^{-1} + k_{da}) - \lambda\Big)\Big\} = 0.\end{aligned} \tag{B.5}$$

The eigenvalues are

$$\begin{aligned}\lambda_{2,1} &= -A - k_{dh}, \\ \lambda_{2,2+3} &= \frac{1}{2}\left[-k_n O_{htt}^2 - k_{de} \pm \sqrt{(k_n O_{htt}^2 + k_{de})^2 - 4 k_{dn} k_n O_{htt}^2}\right], \\ \lambda_{2,4} &= k_a O_{htt}^2 - (k_a^{-1} + k_{da}).\end{aligned}$$

For $A < A_1$, $O_{htt}^2 < 0$, and $\Re(\lambda_{2,2+3}) > 0$. For $A > A_1$, $\Re(\lambda_{2,2+3}) < 0$. As long as $\lambda_{2,4} < 0$, Steady State 2 is stable, confirming the occurrence of a transcritical bifurcation between Steady State 1 and Steady State 2. For $\lambda_{2,4} = 0$, another bifurcation occurs,

$$\begin{aligned}A_2 &= \frac{k_{dh}(a+b)}{k_n k_h - (a+b)}, \\ a &= k_{de}(k_{dn} + k_n^{-1}), \\ b &= k_{dn} k_n \frac{k_a^{-1} + k_{da}}{k_a}.\end{aligned} \tag{Bif 2}$$

At this value, the second and third steady states meet (Steady State 2=Steady State 3), again pointing to a transcritical bifurcation. The Jacobian matrix evaluated at Steady State 3 is

$$J_3 = \begin{pmatrix} -A - k_{dh} & 0 & 0 & 0 \\ A & -k_n \frac{k_a^{-1} + k_{da}}{k_a} - k_{de} & -k_n M_{htt}^3 + k_n^{-1} & 0 \\ 0 & k_n \frac{k_a^{-1} + k_{da}}{k_a} & \frac{k_a^{-1}}{k_{da}}[-k_n M_{htt}^3 + k_n^{-1} + k_{dn}] & -k_{da} \\ 0 & 0 & \frac{k_a^{-1} + k_{da}}{k_{da}}[k_n M_{htt}^3 - k_n^{-1} - k_{dn}] & 0 \end{pmatrix}. \tag{B.6}$$

The associated characteristic equation is

$$(-A-k_{dh}-\lambda)\Big[-\lambda^3+\left(-k_n\frac{k_a^{-1}+k_{da}}{k_a}-k_{de}+\frac{k_a^{-1}}{k_{da}}(-k_nM_{htt}^3+k_n^{-1}+k_n)\right)\lambda^2+$$
$$\Big\{\frac{k_a^{-1}}{k_{da}}(-k_nM_{htt}^3+k_n^{-1}+k_n)\left(k_n\frac{k_a^{-1}+k_{da}}{k_a}+k_{de}\right)+(k_a^{-1}+k_{da})(-k_nM_{htt}^3+k_n^{-1}+k_n)$$
$$+(-k_nM_{htt}^3+k_n^{-1})k_n\frac{k_a^{-1}+k_{da}}{k_a}\Big\}\lambda+$$
$$\left(k_n\frac{k_a^{-1}+k_{da}}{k_a}+k_{de}\right)(k_a^{-1}+k_{da})(-k_nM_{htt}^3+k_n^{-1}+k_n)\Big]=0 \quad \text{(B.7)}$$

When $A=A_2$, Equation B.7 has a zero root, corresponding to a transcritical bifurcation. Indeed, for $A=A_2$, the constant term between the brackets in Equation B.7 vanishes,

$$\left(k_n\frac{k_a^{-1}+k_{da}}{k_a}+k_{de}\right)(k_a^{-1}+k_{da})(-k_nM_{htt}^3|_{A=A_2}+k_n^{-1}+k_n)=0 \quad \text{(B.8)}$$

For $A>A_2$, the this term is negative, providing no information on the positions of the roots, so we look with Descartes' Rule. For $A<A_2$, there is, however, at least one positive root, so Steady State 3 is unstable for $A<A_2$. Descartes' Rule provides states that the maximum number of positive real roots a polynomial has is equal to the number of sign changes in its coefficients. The third order polynomial between the brackets of Equation B.7 have the following sign pattern: (-)(-)(-)(-), for the term $-k_nM_{htt}^3|_{A>A_2}+k_n^{-1}+k_n$ is negative. This means that the characteristic equation does not have positive real roots. We can further check that if complex roots are existing, they have negative real part. The third degree polynomial can be written $-\lambda^3-c_1\lambda^2-c_2\lambda-c_3=0$ with $c_i>0$. The condition for having the real part negative is $c_1c_2>c_3$. We can verify that this is indeed the case.

The other roots have a negative real part. For $A>A_2$, Steady State 1 and Steady State 2 are unstable, as $\lambda_{2,4}>0$ and $\lambda_{2,4}<0$. A clear figure emerges from the steady state analysis.

Appendix C

List of Genes on the HD Microarray

AP1-regulated genes

Alternative AN	Unigene hs	Annotation
NM_000034	Hs.273415	aldolase A, fructose-bisphosphate
NM_000190	Hs.82609	hydroxymethylbilane synthase
NM_000399	Hs.1395	early growth response 2 (Krox-20 homolog, Drosophila)
NM_000518	Hs.155376	hemoglobin, beta
NM_000546	Hs.408312	tumor protein p53 (Li-Fraumeni syndrome)
NM_000558	Hs.449630	hemoglobin, alpha 2
NM_000586	Hs.89679	interleukin 2
NM_000586	Hs.89679	interleukin 2
NM_000588	Hs.694	interleukin 3 (colony-stimulating factor, multiple)
NM_000619	Hs.856	interferon, gamma
NM_000660	Hs.1103	transforming growth factor, beta 1 (Camurati-Engelmann disease)
NM_000758	Hs.1349	colony stimulating factor 2 (granulocyte-macrophage)
NM_000758	Hs.1349	colony stimulating factor 2 (granulocyte-macrophage)
NM_000781	Hs.76205	cytochrome P450, family 11, subfamily A, polypeptide 1
NM_000879	Hs.2247	interleukin 5 (colony-stimulating factor, eosinophil)
NM_000905	Hs.1832	neuropeptide Y
NM_000948	Hs.1905	prolactin
NM_001005	Hs.387576	ribosomal protein S3
NM_001101	Hs.426930	actin, beta
NM_001442	Hs.391561	fatty acid binding protein 4, adipocyte
NM_001955	Hs.511899	endothelin 1
NM_002055	Hs.406397	glial fibrillary acidic protein
NM_002228	Hs.78465	v-jun sarcoma virus 17 oncogene homolog (avian)
NM_002421	Hs.83169	matrix metalloproteinase 1 (interstitial collagenase)
NM_002422	Hs.375129	matrix metalloproteinase 3 (stromelysin 1, progelatinase)
NM_002467	Hs.202453	v-myc myelocytomatosis viral oncogene homolog (avian)
NM_002689	Hs.201897	polymerase (DNA-directed), alpha (70kD)
NM_002984	Hs.75703	chemokine (C-C motif) ligand 4
NM_003254	Hs.446641	tissue inhibitor of metalloproteinase 1 (erythroid potentiating activity, collagenase inhibitor)
NM_003254	Hs.446641	tissue inhibitor of metalloproteinase 1 (erythroid potentiating activity, collagenase inhibitor)
NM_003380	Hs.435800	vimentin
NM_005252	Hs.25647	v-fos FBJ murine osteosarcoma viral oncogene homolog
NM_005354	Hs.2780	jun D proto-oncogene
NM_005953	Hs.418241	metallothionein 2A
NM_006563	Hs.37860	Kruppel-like factor 1 (erythroid)
X17650	Hs.404123	myogenic factor 3

AP2-regulated genes

Alternative AN	Unigene hs	Annotation
NM_000384	Hs.280226	apolipoprotein B (including Ag(x) antigen)
NM_000515	Hs.500468	growth hormone 1
NM_000526	Hs.355214	keratin 14 (epidermolysis bullosa simplex, Dowling-Meara, Koebner)
NM_000619	Hs.856	interferon, gamma
NM_001124	Hs.441047	adrenomedullin
NM_001712	Hs.512682	carcinoembryonic antigen-related cell adhesion molecule 1 (biliary glycoprotein)
NM_001880	Hs.80285	activating transcription factor 2
NM_002026	Hs.418138	fibronectin 1

NM_002055	Hs.406397	glial fibrillary acidic protein
NM_002228	Hs.78465	v-jun sarcoma virus 17 oncogene homolog (avian)
NM_002467	Hs.202453	v-myc myelocytomatosis viral oncogene homolog (avian)
NM_002539	Hs.443409	ornithine decarboxylase 1
NM_003220	Hs.210911	transcription factor AP-2 alpha (activating enhancer binding protein 2 alpha)
NM_005953	Hs.418241	metallothionein 2A
NM_031966	Hs.23960	cyclin B1
U36308	Hs.406681	major intrinsic protein of lens fiber

AR-regulated genes

Alternative AN	Unigene hs	Annotation
AF153821	Hs.4	alcohol dehydrogenase IB (class I), beta polypeptide
M61856	Hs.511872	cytochrome P450, family 2, subfamily C, polypeptide 18
M99487	Hs.1915	folate hydrolase (prostate-specific membrane antigen) 1
NM_000348	Hs.1989	steroid-5-alpha-reductase, alpha polypeptide 2 (3-oxo-5 alpha-steroid delta 4-dehydrogenase alpha 2)
NM_000389	Hs.370771	cyclin-dependent kinase inhibitor 1A (p21, Cip1)
NM_000689	Hs.76392	aldehyde dehydrogenase 1 family, member A1
NM_001093	Hs.234898	acetyl-Coenzyme A carboxylase beta
NM_001099	Hs.388677	acid phosphatase, prostate
NM_001509	Hs.248129	glutathione peroxidase 5 (epididymal androgen-related protein)
NM_001628	Hs.75313	aldo-keto reductase family 1, member B1 (aldose reductase)
NM_003241	Hs.438265	transglutaminase 4 (prostate)
NM_003711	Hs.482121	phosphatidic acid phosphatase type 2A
NM_004104	Hs.83190	fatty acid synthase
NM_004117	Hs.7557	FK506 binding protein 5
NM_005437	Hs.422334	nuclear receptor coactivator 4
NM_005656	Hs.439309	transmembrane protease, serine 2
NM_007067	Hs.21907	MYST histone acetyltransferase 2
NM_007114	Hs.267632	TATA element modulatory factor 1
NM_014762	Hs.75616	24-dehydrocholesterol reductase
NM_016026	Hs.226007	retinol dehydrogenase 11 (all-trans and 9-cis)
NM_020168	Hs.21420	p21(CDKN1A)-activated kinase 6

Akt-regulated genes

Alternative AN	Unigene hs	Annotation
NM_000151	Hs.435783	glucose-6-phosphatase, catalytic (glycogen storage disease type I, von Gierke disease)
NM_001467	Hs.132760	solute carrier family 37 (glycerol-6-phosphate transporter), member 4
NM_004563	Hs.75812	phosphoenolpyruvate carboxykinase 2 (mitochondrial)
NM_006516	Hs.169902	solute carrier family 2 (facilitated glucose transporter), member 1

c-myc-regulated genes

Alternative AN	Unigene hs	Annotation
D13639	Hs.376071	cyclin D2
H17434	Hs.79110	nucleolin
NM_001789	Hs.1634	cell division cycle 25A
NM_001968	Hs.79306	eukaryotic translation initiation factor 4E
NM_002467	Hs.202453	v-myc myelocytomatosis viral oncogene homolog (avian)
NM_002520	Hs.411098	nucleophosmin (nucleolar phosphoprotein B23, numatrin)
NM_002539	Hs.443409	ornithine decarboxylase 1
NM_002634	Hs.75323	prohibitin
NM_003219	Hs.439911	telomerase reverse transcriptase
NM_003467	Hs.421986	chemokine (C-X-C motif) receptor 4
NM_004448	Hs.446352	v-erb-b2 erythroblastic leukemia viral oncogene homolog 2, neuro/glioblastoma derived oncogene homolog (avian)
NM_006773	Hs.363492	DEAD (Asp-Glu-Ala-Asp) box polypeptide 18
NM_006793	Hs.397062	peroxiredoxin 3
NM_016323	Hs.26663	cyclin-E binding protein 1
NM_020310	Hs.253552	MAX binding protein
NM_031966	Hs.23960	cyclin B1
R61502	Hs.183803	heat shock protein 75
T70920	Hs.848	FK506 binding protein 4, 59kDa
X16277	Hs.443409	ornithine decarboxylase 1
X54942	Hs.83758	CDC28 protein kinase regulatory subunit 2

C/EBP regulated genes

Original AN	Unigene hs	Annotation
NM_000201	Hs.386467	intercellular adhesion molecule 1 (CD54), human rhinovirus receptor
NM_000567	Hs.76452	C-reactive protein, pentraxin-related

NM_000576	Hs.126256	interleukin 1, beta
NM_000600	Hs.512234	interleukin 6 (interferon, beta 2)
NM_000613	Hs.426485	hemopexin
NM_000667	Hs.422855	alcohol dehydrogenase 1A (class I), alpha polypeptide
NM_000668	Hs.4	alcohol dehydrogenase IB (class I), beta polypeptide
NM_000669	Hs.2523	alcohol dehydrogenase 1C (class I), gamma polypeptide
NM_000882	Hs.673	interleukin 12A (natural killer cell stimulatory factor 1, cytotoxic lymphocyte maturation factor 1, p35)
NM_000887	Hs.385521	integrin, alpha X (antigen CD11C (p150), alpha polypeptide)
NM_000927	Hs.21330	ATP-binding cassette, sub-family B (MDR/TAP), member 1
NM_002187	Hs.674	interleukin 12B (natural killer cell stimulatory factor 2, cytotoxic lymphocyte maturation factor 2, p40)
NM_002569	Hs.59242	furin (paired basic amino acid cleaving enzyme)
NM_002985	Hs.489044	chemokine (C-C motif) ligand 5
NM_003286	Hs.253536	topoisomerase (DNA) I
NM_004563	Hs.75812	phosphoenolpyruvate carboxykinase 2 (mitochondrial)
NM_005252	Hs.25647	v-fos FBJ murine osteosarcoma viral oncogene homolog
NM_007115	Hs.407546	tumor necrosis factor, alpha-induced protein 6
NM_030754	Hs.1955	serum amyloid A2
NM_031226	Hs.187471	cytochrome P450, family 19, subfamily A, polypeptide 1
X01179	Hs.413083	coagulation factor VIII, procoagulant component (hemophilia A)

CREB-regulated genes

Original AN	Unigene hs	Annotation
NM_000024	Hs.2551	adrenergic, beta-2-, receptor, surface
NM_000207	Hs.89832	insulin
NM_000315	Hs.37045	parathyroid hormone
NM_000399	Hs.1395	early growth response 2 (Krox-20 homolog, Drosophila)
NM_000486	Hs.130730	aquaporin 2 (collecting duct)
NM_000492	Hs.411882	cystic fibrosis transmembrane conductance regulator, ATP-binding cassette (sub-family C, member 7)
NM_000576	Hs.126256	interleukin 1, beta
NM_000588	Hs.694	interleukin 3 (colony-stimulating factor, multiple)
NM_000596	Hs.401316	insulin-like growth factor binding protein 1
NM_000735	Hs.119689	glycoprotein hormones, alpha polypeptide
NM_000930	Hs.274404	plasminogen activator, tissue
NM_000931	Hs.274404	plasminogen activator, tissue
NM_001880	Hs.80285	activating transcription factor 2
NM_001964	Hs.326035	early growth response 1
NM_002026	Hs.418138	fibronectin 1
NM_002055	Hs.406397	glial fibrillary acidic protein
NM_002421	Hs.83169	matrix metalloproteinase 1 (interstitial collagenase)
NM_002616	Hs.445534	period homolog 1 (Drosophila)
NM_002690	Hs.180107	polymerase (DNA directed), beta
NM_003381	Hs.53973	vasoactive intestinal peptide
NM_003405	Hs.226755	tyrosine 3-monooxygenase/tryptophan 5-monooxygenase activation protein, eta polypeptide
NM_005252	Hs.25647	v-fos FBJ murine osteosarcoma viral oncogene homolog
NM_005566	Hs.2795	lactate dehydrogenase A
NM_033011	Hs.274404	plasminogen activator, tissue
U37218	Hs.401929	ribosomal protein L10
Z29078	Hs.371468	cyclin D1 (PRAD1: parathyroid adenomatosis 1)

E2F-regulated genes

Original AN	Unigene hs	Annotation
BC031061	Hs.460184	MCM4 minichromosome maintenance deficient 4 (S. cerevisiae)
NM_000321	Hs.408528	retinoblastoma 1 (including osteosarcoma)
NM_000791	Hs.83765	dihydrofolate reductase
NM_001034	Hs.226390	ribonucleotide reductase M2 polypeptide
NM_001071	Hs.87491	thymidylate synthetase
NM_001237	Hs.85137	cyclin A2
NM_001238	Hs.244723	cyclin E1
NM_001254	Hs.405958	CDC6 cell division cycle 6 homolog (S. cerevisiae)
NM_001759	Hs.376071	cyclin D2
NM_002592	Hs.78996	proliferating cell nuclear antigen
NM_002895	Hs.87	retinoblastoma-like 1 (p107)
NM_003504	Hs.114311	CDC45 cell division cycle 45-like (S. cerevisiae)
NM_003906	Hs.389037	MCM3 minichromosome maintenance deficient 3 (S. cerevisiae) associated protein
NM_003914	Hs.417050	cyclin A1
NM_004091	Hs.231444	E2F transcription factor 2
NM_004153	Hs.17908	origin recognition complex, subunit 1-like (yeast)
NM_004526	Hs.57101	MCM2 minichromosome maintenance deficient 2, mitotin (S. cerevisiae)

NM_004688	Hs.54483	N-myc (and STAT) interactor
NM_005225	Hs.96055	E2F transcription factor 1
NM_005915	Hs.444118	MCM6 minichromosome maintenance deficient 6 (MIS5 homolog, S. pombe) (S. cerevisiae)
NM_005916	Hs.438720	MCM7 minichromosome maintenance deficient 7 (S. cerevisiae)
NM_012333	Hs.78221	c-myc binding protein
NM_016937	Hs.267289	polymerase (DNA directed), alpha
NM_057182	Hs.244723	cyclin E1

Elk-1 regulated genes

Original AN	Unigene hs	Annotation
NM_000616	Hs.17483	CD4 antigen (p55)
NM_003131	Hs.444086	serum response factor (c-fos serum response element-binding transcription factor)
NM_004907	Hs.737	immediate early protein
NM_005966	Hs.107474	NGFI-A binding protein 1 (EGR1 binding protein 1)
NM_006186	Hs.82120	nuclear receptor subfamily 4, group A, member 2

Fatty acid metabolism genes

Alternative AN	Unigene hs	Annotation
NM_000016	Hs.254593	acyl-Coenzyme A dehydrogenase, C-4 to C-12 straight chain
NM_000017	Hs.348900	acyl-Coenzyme A dehydrogenase, C-2 to C-3 short chain
NM_000019	Hs.37	acetyl-Coenzyme A acetyltransferase 1 (acetoacetyl Coenzyme A thiolase)
NM_000664	Hs.449863	acetyl-Coenzyme A carboxylase alpha
NM_000786	Hs.417077	cytochrome P450, family 51, subfamily A, polypeptide 1
NM_001093	Hs.234898	acetyl-Coenzyme A carboxylase beta
NM_001607	Hs.166160	acetyl-Coenzyme A acyltransferase 1 (peroxisomal 3-oxoacyl-Coenzyme A thiolase)
NM_001608	Hs.430108	acyl-Coenzyme A dehydrogenase, long chain
NM_001875	Hs.443292	carbamoyl-phosphate synthetase 1, mitochondrial
NM_001919	Hs.403436	dodecenoyl-Coenzyme A delta isomerase (3,2 trans-enoyl-Coenzyme A isomerase)
NM_001995	Hs.511920	fatty-acid-Coenzyme A ligase, long-chain 2
NM_002004	Hs.335918	farnesyl diphosphate synthase (farnesyl pyrophosphate synthetase, dimethylallyltranstransferase, geranyltranstransferase)
NM_002107	Hs.181307	H3 histone, family 3A
NM_002130	Hs.397729	3-hydroxy-3-methylglutaryl-Coenzyme A synthase 1 (soluble)
NM_004035	Hs.379991	acyl-Coenzyme A oxidase 1, palmitoyl
NM_004104	Hs.83190	fatty acid synthase
NM_005215	Hs.172562	deleted in colorectal carcinoma
NM_014324	Hs.49598	alpha-methylacyl-CoA racemase

FOXO3 (FKHRL1)-regulated genes

Original AN	Unigene hs	Annotation
NM_000127	Hs.184161	exostoses (multiple) 1
NM_000636	Hs.384944	superoxide dismutase 2, mitochondrial
NM_000639	Hs.2007	tumor necrosis factor (ligand) superfamily, member 6
NM_001924	Hs.80409	growth arrest and DNA-damage-inducible, alpha
NM_003620	Hs.286073	protein phosphatase 1D magnesium-dependent, delta isoform
NM_004052	Hs.79428	BCL2/adenovirus E1B 19kDa interacting protein 3
NM_004064	Hs.238990	cyclin-dependent kinase inhibitor 1B (p27, Kip1)
NM_004354	Hs.13291	cyclin G2
NM_005410	Hs.275775	selenoprotein P, plasma, 1
NM_005606	Hs.18069	legumain
NM_005611	Hs.283604	retinoblastoma-like 2 (p130)
NM_006538	Hs.84063	BCL2-like 11 (apoptosis facilitator)
NM_006705	Hs.9701	growth arrest and DNA-damage-inducible, gamma
NM_014454	Hs.14125	sestrin 1
NM_138621	Hs.84063	BCL2-like 11 (apoptosis facilitator)

Genes coding heat shock proteins

Original AN	Unigene hs	Annotation
L12723	Hs.90093	heat shock 70kDa protein 4
NM_003192	Hs.75064	tubulin-specific chaperone c
NM_003193	Hs.445778	tubulin-specific chaperone e
NM_004281	Hs.15259	BCL2-associated athanogene 3
NM_004282	Hs.55220	BCL2-associated athanogene 2
NM_004607	Hs.355627	tubulin-specific chaperone a
NM_004873	Hs.5443	BCL2-associated athanogene 5

NM_004874	Hs.194726	BCL2-associated athanogene 4
NM_005125	Hs.5002	copper chaperone for superoxide dismutase
NM_005993	Hs.435541	tubulin-specific chaperone d
NM_006145	Hs.82646	DnaJ (Hsp40) homolog, subfamily B, member 1
NM_006597	Hs.180414	heat shock 70kDa protein 8
NM_006819	Hs.257827	stress-induced-phosphoprotein 1 (Hsp70/Hsp90-organizing protein)
NM_006948	Hs.352341	stress 70 protein chaperone, microsome-associated, 60kDa
NM_007355	Hs.74335	heat shock 90kDa protein 1, beta
NM_012266	Hs.237506	DnaJ (Hsp40) homolog, subfamily B, member 5
NM_012267	Hs.53066	hsp70-interacting protein
NM_016299	Hs.430666	likely ortholog of mouse heat shock protein, 70 kDa 4
NM_016306	Hs.317192	DnaJ (Hsp40) homolog, subfamily B, member 11
NM_020247	Hs.273186	chaperone, ABC1 activity of bc1 complex like (S. pombe)
NM_153201	Hs.180414	heat shock 70kDa protein 8

Irf1-regulated genes

Original AN	Unigene hs	Annotation
AF039291	Hs.102267	lysyl oxidase
BC002666	Hs.62661	guanylate binding protein 1, interferon-inducible, 67kDa
M90100	Hs.196384	prostaglandin-endoperoxide synthase 2 (prostaglandin G/H synthase and cyclooxygenase)
NM_000246	Hs.126714	MHC class II transactivator
NM_000389	Hs.370771	cyclin-dependent kinase inhibitor 1A (p21, Cip1)
NM_000585	Hs.168132	interleukin 15
NM_000593	Hs.352018	transporter 1, ATP-binding cassette, sub-family B (MDR/TAP)
NM_000639	Hs.2007	tumor necrosis factor (ligand) superfamily, member 6
NM_001223	Hs.2490	caspase 1, apoptosis-related cysteine protease (interleukin 1, beta, convertase)
NM_001227	Hs.9216	caspase 7, apoptosis-related cysteine protease
NM_001547	Hs.169274	interferon-induced protein with tetratricopeptide repeats 2
NM_002053	Hs.62661	guanylate binding protein 1, interferon-inducible, 67kDa
NM_002176	Hs.93177	interferon, beta 1, fibroblast
NM_002187	Hs.674	interleukin 12B (natural killer cell stimulatory factor 2, cytotoxic lymphocyte maturation factor 2, p40)
NM_002198	Hs.80645	interferon regulatory factor 1
NM_002534	Hs.442936	2',5'-oligoadenylate synthetase 1, 40/46kDa
NM_002535	Hs.414332	2'-5'-oligoadenylate synthetase 2, 69/71kDa
NM_003064	Hs.251754	secretory leukocyte protease inhibitor (antileukoproteinase)
NM_004705	Hs.177574	protein-kinase, interferon-inducible double stranded RNA dependent inhibitor, repressor of (P58 repressor)
NM_005101	Hs.458485	interferon, alpha-inducible protein (clone IFI-15K)
NM_006186	Hs.82120	nuclear receptor subfamily 4, group A, member 2
NM_006187	Hs.129895	2'-5'-oligoadenylate synthetase 3, 100kDa
NM_016816	Hs.442936	2',5'-oligoadenylate synthetase 1, 40/46kDa
NM_016817	Hs.414332	2'-5'-oligoadenylate synthetase 2, 69/71kDa
NM_024013	Hs.37026	interferon, alpha 1
NM_033340	Hs.9216	caspase 7, apoptosis-related cysteine protease
NM_078467	Hs.370771	cyclin-dependent kinase inhibitor 1A (p21, Cip1)
NM_139266	Hs.21486	signal transducer and activator of transcription 1, 91kDa
U04636	Hs.196384	prostaglandin-endoperoxide synthase 2 (prostaglandin G/H synthase and cyclooxygenase)

LEF1-regulated genes

Original AN	Unigene hs	Annotation
BC035872	Hs.512765	axin 1
NM_000038	Hs.75081	adenomatosis polyposis coli
NM_000165	Hs.74471	gap junction protein, alpha 1, 43kDa (connexin 43)
NM_000545	Hs.371279	transcription factor 1, hepatic; LF-B1, hepatic nuclear factor (HNF1), albumin proximal factor
NM_001426	Hs.271977	engrailed homolog 1
NM_001804	Hs.1545	caudal type homeo box transcription factor 1
NM_002026	Hs.418138	fibronectin 1
NM_002423	Hs.2256	matrix metalloproteinase 7 (matrilysin, uterine)
NM_002467	Hs.202453	v-myc myelocytomatosis viral oncogene homolog (avian)
NM_002659	Hs.179657	plasminogen activator, urokinase receptor
NM_003257	Hs.74614	tight junction protein 1 (zona occludens 1)
NM_004360	Hs.194657	cadherin 1, type 1, E-cadherin (epithelial)
NM_005438	Hs.283565	FOS-like antigen 1
NM_005992	Hs.173984	T-box 1
NM_021801	Hs.204732	matrix metalloproteinase 26

NFAT-ergulated genes

Original AN	Unigene hs	Annotation

NM_000074	Hs.652	tumor necrosis factor (ligand) superfamily, member 5 (hyper-IgM syndrome)
NM_000399	Hs.1395	early growth response 2 (Krox-20 homolog, Drosophila)
NM_000586	Hs.89679	interleukin 2
NM_000588	Hs.694	interleukin 3 (colony-stimulating factor, multiple)
NM_000589	Hs.73917	interleukin 4
NM_000619	Hs.856	interferon, gamma
NM_000639	Hs.2007	tumor necrosis factor (ligand) superfamily, member 6
NM_000879	Hs.2247	interleukin 5 (colony-stimulating factor, eosinophil)
NM_002188	Hs.845	interleukin 13
NM_002341	Hs.376208	lymphotoxin beta (TNF superfamily, member 3)
NM_004430	Hs.74088	early growth response 3
NM_004862	Hs.76507	lipopolysaccharide-induced TNF factor
NM_005593	Hs.178023	myogenic factor 5
NM_006140	Hs.520937	colony stimulating factor 2 receptor, alpha, low-affinity (granulocyte-macrophage)
NM_006264	Hs.387553	protein tyrosine phosphatase, non-receptor type 13 (APO-1/CD95 (Fas)-associated phosphatase)

NF?B-regulated genes

Original AN	Unigene hs	Annotation
BC020864	Hs.65425	calbindin 1, 28kDa
M13994	Hs.79241	B-cell CLL/lymphoma 2
M14113	Hs.413083	coagulation factor VIII, procoagulant component (hemophilia A)
NM_000029	Hs.19383	angiotensinogen (serine (or cysteine) proteinase inhibitor, clade A (alpha-1 antiproteinase, antitrypsin), member 8)
NM_000043	Hs.82359	tumor necrosis factor receptor superfamily, member 6
NM_000201	Hs.386467	intercellular adhesion molecule 1 (CD54), human rhinovirus receptor
NM_000331	Hs.332053	serum amyloid A1
NM_000417	Hs.130058	interleukin 2 receptor, alpha
NM_000450	Hs.89546	selectin E (endothelial adhesion molecule 1)
NM_000546	Hs.408312	tumor protein p53 (Li-Fraumeni syndrome)
NM_000567	Hs.76452	C-reactive protein, pentraxin-related
NM_000584	Hs.624	interleukin 8
NM_000586	Hs.89679	interleukin 2
NM_000593	Hs.352018	transporter 1, ATP-binding cassette, sub-family B (MDR/TAP)
NM_000595	Hs.36	lymphotoxin alpha (TNF superfamily, member 1)
NM_000600	Hs.512234	interleukin 6 (interferon, beta 2)
NM_001078	Hs.109225	vascular cell adhesion molecule 1
NM_001511	Hs.789	chemokine (C-X-C motif) ligand 1 (melanoma growth stimulating activity, alpha)
NM_001710	Hs.69771	B-factor, properdin
NM_002089	Hs.75765	chemokine (C-X-C motif) ligand 2
NM_002090	Hs.89690	chemokine (C-X-C motif) ligand 3
NM_002160	Hs.98998	tenascin C (hexabrachion)
NM_002176	Hs.93177	interferon, beta 1, fibroblast
NM_002229	Hs.400124	jun B proto-oncogene
NM_002522	Hs.84154	neuronal pentraxin I
NM_002658	Hs.77274	plasminogen activator, urokinase
NM_002852	Hs.2050	pentaxin-related gene, rapidly induced by IL-1 beta
NM_003152	Hs.437058	signal transducer and activator of transcription 5A
NM_003998	Hs.160557	nuclear factor of kappa light polypeptide gene enhancer in B-cells 1 (p105)
NM_004929	Hs.65425	calbindin 1, 28kDa
NM_021975	Hs.132594	v-rel reticuloendotheliosis viral oncogene homolog A, nuclear factor of kappa light polypeptide gene enhancer in B-cells 3, p65 (avian)
NM_030754	Hs.1955	serum amyloid A2
X14322	Hs.384944	superoxide dismutase 2, mitochondrial
X60459	Hs.181315	interferon (alpha, beta and omega) receptor 1
Z23115	Hs.305890	BCL2-like 1

p53-regulated genes

Original AN	Unigene hs	Annotation
AF012535	Hs.51233	tumor necrosis factor receptor superfamily, member 10b
AF019742	Hs.74034	caveolin 1, caveolae protein, 22kDa
AF029081	Hs.184510	stratifin
AK000121	Hs.6241	phosphoinositide-3-kinase, regulatory subunit, polypeptide 1 (p85 alpha)
D00618	Hs.208641	actin, alpha 2, smooth muscle, aorta
NM_000021	Hs.3260	presenilin 1 (Alzheimer disease 3)
NM_000038	Hs.75081	adenomatosis polyposis coli

NM_000043	Hs.82359	tumor necrosis factor receptor superfamily, member 6
NM_000136	Hs.253236	Fanconi anemia, complementation group C
NM_000156	Hs.81131	guanidinoacetate N-methyltransferase
NM_000208	Hs.438669	insulin receptor
NM_000321	Hs.408528	retinoblastoma 1 (including osteosarcoma)
NM_000546	Hs.408312	tumor protein p53 (Li-Fraumeni syndrome)
NM_000586	Hs.89679	interleukin 2
NM_000589	Hs.73917	interleukin 4
NM_000598	Hs.450230	insulin-like growth factor binding protein 3
NM_000600	Hs.512234	interleukin 6 (interferon, beta 2)
NM_000657	Hs.79241	B-cell CLL/lymphoma 2
NM_000927	Hs.21330	ATP-binding cassette, sub-family B (MDR/TAP), member 1
NM_001188	Hs.93213	BCL2-antagonist/killer 1
NM_001402	Hs.439552	eukaryotic translation elongation factor 1 alpha 1
NM_001702	Hs.194654	brain-specific angiogenesis inhibitor 1
NM_001909	Hs.343475	cathepsin D (lysosomal aspartyl protease)
NM_001924	Hs.80409	growth arrest and DNA-damage-inducible, alpha
NM_002066	Hs.86161	GPI anchored molecule like protein
NM_002231	Hs.323949	kangai 1 (suppression of tumorigenicity 6, prostate; CD82 antigen (R2 leukocyte antigen, antigen detected by monoclonal and antibody IA4))
NM_002307	Hs.99923	lectin, galactoside-binding, soluble, 7 (galectin 7)
NM_002375	Hs.31095	microtubule-associated protein 4
NM_002592	Hs.78996	proliferating cell nuclear antigen
NM_003236	Hs.170009	transforming growth factor, alpha
NM_003246	Hs.164226	thrombospondin 1
NM_003620	Hs.286073	protein phosphatase 1D magnesium-dependent, delta isoform
NM_003824	Hs.86131	Fas (TNFRSF6)-associated via death domain
NM_003842	Hs.51233	tumor necrosis factor receptor superfamily, member 10b
NM_004060	Hs.79101	cyclin G1
NM_004324	Hs.159428	BCL2-associated X protein
NM_004530	Hs.367877	matrix metalloproteinase 2 (gelatinase A, 72kDa gelatinase, 72kDa type IV collagenase)
NM_004879	Hs.343911	etoposide induced 2.4 mRNA
NM_004881	Hs.50649	tumor protein p53 inducible protein 3
NM_005027	Hs.211586	phosphoinositide-3-kinase, regulatory subunit, polypeptide 2 (p85 beta)
NM_005228	Hs.77432	epidermal growth factor receptor (erythroblastic leukemia viral (v-erb-b) oncogene homolog, avian)
NM_005343	Hs.37003	v-Ha-ras Harvey rat sarcoma viral oncogene homolog
NM_005978	Hs.413843	S100 calcium binding protein A2
NM_006024	Hs.5437	Tax1 (human T-cell leukemia virus type I) binding protein 1
NM_006142	Hs.184510	stratifin
NM_006497	Hs.72956	hypermethylated in cancer 1
NM_006705	Hs.9701	growth arrest and DNA-damage-inducible, gamma
NM_006819	Hs.257827	stress-induced-phosphoprotein 1 (Hsp70/Hsp90-organizing protein)
NM_006882	Hs.212217	Mdm2, transformed 3T3 cell double minute 2, p53 binding protein (mouse)
NM_007233	Hs.274329	TP53 activated protein 1
NM_013229	Hs.373575	apoptotic protease activating factor
NM_014417	Hs.87246	BCL2 binding component 3
NM_016426	Hs.122552	G-2 and S-phase expressed 1
NM_021127	Hs.96	phorbol-12-myristate-13-acetate-induced protein 1
NM_022112	Hs.160953	p53-regulated apoptosis-inducing protein 1
NM_022121	Hs.149620	PERP, TP53 apoptosis effector
NM_022470	Hs.386299	p53 target zinc finger protein
NM_030983	Hs.31095	microtubule-associated protein 4
NM_033295	Hs.2490	caspase 1, apoptosis-related cysteine protease (interleukin 1, beta, convertase)
NM_078467	Hs.370771	cyclin-dependent kinase inhibitor 1A (p21, Cip1)
NM_138924	Hs.81131	guanidinoacetate N-methyltransferase
NM_145887	Hs.438986	leucine-rich and death domain containing
NM_147184	Hs.50649	tumor protein p53 inducible protein 3
NM_147187	Hs.51233	tumor necrosis factor receptor superfamily, member 10b
NM_152240	Hs.386299	p53 target zinc finger protein

Proteasome coding genes

Original AN	Unigene hs	Annotation
NM_002786	Hs.82159	proteasome subunit, alpha type, 1
NM_002787	Hs.333786	proteasome subunit, alpha type, 2
NM_002788	Hs.246240	proteasome subunit, alpha type, 3
NM_002789	Hs.251531	proteasome subunit, alpha type, 4
NM_002790	Hs.76913	proteasome subunit, alpha type, 5
NM_002792	Hs.233952	proteasome subunit, alpha type, 7

NM_002793	Hs.352768	proteasome subunit, beta type, 1
NM_002794	Hs.432607	proteasome subunit, beta type, 2
NM_002795	Hs.82793	proteasome subunit, beta type, 3
NM_002796	Hs.89545	proteasome subunit, beta type, 4
NM_002797	Hs.422990	proteasome subunit, beta type, 5
NM_002799	Hs.197071	proteasome subunit, beta type, 7
NM_002802	Hs.356654	proteasome 26S subunit, ATPase, 1
NM_002803	Hs.61153	proteasome 26S subunit, ATPase, 2
NM_002804	Hs.250758	proteasome 26S subunit, ATPase, 3
NM_002805	Hs.79387	proteasome 26S subunit, ATPase, 5
NM_002806	Hs.156171	proteasome 26S subunit, ATPase, 6
NM_002807	Hs.3887	proteasome 26S subunit, non-ATPase, 1
NM_002808	Hs.388921	proteasome 26S subunit, non-ATPase, 2
NM_002809	Hs.9736	proteasome 26S subunit, non-ATPase, 3
NM_002810	Hs.505059	proteasome 26S subunit, non-ATPase, 4
NM_002811	Hs.440604	proteasome 26S subunit, non-ATPase, 7 (Mov34 homolog)
NM_002812	Hs.78466	proteasome 26S subunit, non-ATPase, 8
NM_002815	Hs.443379	proteasome 26S subunit, non-ATPase, 11
NM_002816	Hs.4295	proteasome 26S subunit, non-ATPase, 12
NM_002817	Hs.279554	proteasome 26S subunit, non-ATPase, 13
NM_005805	Hs.178761	proteasome 26S subunit, non-ATPase, 14
NM_006503	Hs.211594	proteasome 26S subunit, ATPase, 4
NM_014814	Hs.350939	proteasome regulatory particle subunit p44S10

RUNX-regulated genes

Original AN	Unigene hs	Annotation
NM_000250	Hs.458272	myeloperoxidase
NM_000389	Hs.370771	cyclin-dependent kinase inhibitor 1A (p21, Cip1)
NM_000588	Hs.694	interleukin 3 (colony-stimulating factor, multiple)
NM_000633	Hs.79241	B-cell CLL/lymphoma 2
NM_000757	Hs.173894	colony stimulating factor 1 (macrophage)
NM_000760	Hs.381027	colony stimulating factor 3 receptor (granulocyte)
NM_001870	Hs.646	carboxypeptidase A3 (mast cell)
NM_002965	Hs.112405	S100 calcium binding protein A9 (calgranulin B)
NM_003364	Hs.314828	uridine phosphorylase 1
NM_005311	Hs.512118	growth factor receptor-bound protein 10
NM_005356	Hs.1765	lymphocyte-specific protein tyrosine kinase
NM_006875	Hs.80205	pim-2 oncogene
NM_014793	Hs.200596	leucine carboxyl methyltransferase 2
NM_078467	Hs.370771	cyclin-dependent kinase inhibitor 1A (p21, Cip1)

Sp1-regulated genes

Original AN	Unigene hs	Annotation
AB052946	Hs.57735	scavenger receptor class F, member 1
AF004877	Hs.232115	collagen, type I, alpha 2
AF019742	Hs.74034	caveolin 1, caveolae protein, 22kDa
J00289	Hs.500457	chorionic somatomammotropin hormone 2
K02401	Hs.347963	chorionic somatomammotropin hormone 1 (placental lactogen)
M59423	Hs.376032	platelet-derived growth factor alpha polypeptide
NM_000022	Hs.407135	adenosine deaminase
NM_000034	Hs.273415	aldolase A, fructose-bisphosphate
NM_000041	Hs.110675	apolipoprotein E
NM_000043	Hs.82359	tumor necrosis factor receptor superfamily, member 6
NM_000050	Hs.160786	argininosuccinate synthetase
NM_000088	Hs.172928	collagen, type I, alpha 1
NM_000121	Hs.127826	erythropoietin receptor
NM_000190	Hs.82609	hydroxymethylbilane synthase
NM_000208	Hs.438669	insulin receptor
NM_000365	Hs.512711	triosephosphate isomerase 1
NM_000384	Hs.280226	apolipoprotein B (including Ag(x) antigen)
NM_000457	Hs.54424	hepatocyte nuclear factor 4, alpha
NM_000485	Hs.28914	adenine phosphoribosyltransferase
NM_000500	Hs.278430	cytochrome P450, family 21, subfamily A, polypeptide 2
NM_000515	Hs.500468	growth hormone 1
NM_000558	Hs.449630	hemoglobin, alpha 2
NM_000559	Hs.449631	hemoglobin, gamma A
NM_000619	Hs.856	interferon, gamma
NM_000632	Hs.172631	integrin, alpha M (complement component receptor 3, alpha; also known as CD11b (p170), macrophage antigen alpha polypeptide)
NM_000660	Hs.1103	transforming growth factor, beta 1 (Camurati-Engelmann disease)
NM_000668	Hs.4	alcohol dehydrogenase IB (class I), beta polypeptide

NM_000791	Hs.83765	dihydrofolate reductase
NM_000805	Hs.2681	gastrin
NM_000905	Hs.1832	neuropeptide Y
NM_000927	Hs.21330	ATP-binding cassette, sub-family B (MDR/TAP), member 1
NM_000930	Hs.274404	plasminogen activator, tissue
NM_001005	Hs.387576	ribosomal protein S3
NM_001020	Hs.397609	ribosomal protein S16
NM_001042	Hs.371905	solute carrier family 2 (facilitated glucose transporter), member 4
NM_001071	Hs.87491	thymidylate synthetase
NM_001511	Hs.789	chemokine (C-X-C motif) ligand 1 (melanoma growth stimulating activity, alpha)
NM_001783	Hs.79630	CD79A antigen (immunoglobulin-associated alpha)
NM_001880	Hs.80285	activating transcription factor 2
NM_002026	Hs.418138	fibronectin 1
NM_002055	Hs.406397	glial fibrillary acidic protein
NM_002100	Hs.438658	glycophorin B (includes Ss blood group)
NM_002101	Hs.81994	glycophorin C (Gerbich blood group)
NM_002228	Hs.78465	v-jun sarcoma virus 17 oncogene homolog (avian)
NM_002385	Hs.408543	myelin basic protein
NM_002467	Hs.202453	v-myc myelocytomatosis viral oncogene homolog (avian)
NM_002539	Hs.443409	ornithine decarboxylase 1
NM_002569	Hs.59242	furin (paired basic amino acid cleaving enzyme)
NM_002592	Hs.78996	proliferating cell nuclear antigen
NM_002690	Hs.180107	polymerase (DNA directed), beta
NM_002736	Hs.77439	protein kinase, cAMP-dependent, regulatory, type II, beta
NM_003122	Hs.407856	serine protease inhibitor, Kazal type 1
NM_003219	Hs.439911	telomerase reverse transcriptase
NM_003246	Hs.164226	thrombospondin 1
NM_003258	Hs.164457	thymidine kinase 1, soluble
NM_004324	Hs.159428	BCL2-associated X protein
NM_004360	Hs.194657	cadherin 1, type 1, E-cadherin (epithelial)
NM_004364	Hs.76171	CCAAT/enhancer binding protein (C/EBP), alpha
NM_004502	Hs.436181	homeo box B7
NM_005159	Hs.118127	actin, alpha, cardiac muscle
NM_005228	Hs.77432	epidermal growth factor receptor (erythroblastic leukemia viral (v-erb-b) oncogene homolog, avian)
NM_005330	Hs.117848	hemoglobin, epsilon 1
NM_005332	Hs.272003	hemoglobin, zeta
NM_005343	Hs.37003	v-Ha-ras Harvey rat sarcoma viral oncogene homolog
NM_005345	Hs.75452	heat shock 70kDa protein 1A
NM_005354	Hs.2780	jun D proto-oncogene
NM_005953	Hs.418241	metallothionein 2A
NM_006288	Hs.134643	Thy-1 cell surface antigen
NM_006398	Hs.44532	ubiquitin D
NM_017512	Hs.475848	rTS beta protein
NM_022727	Hs.63609	HpaII tiny fragments locus 9C
NM_033016	Hs.1976	platelet-derived growth factor beta polypeptide (simian sarcoma viral (v-sis) oncogene homolog)
NM_033295	Hs.2490	caspase 1, apoptosis-related cysteine protease (interleukin 1, beta, convertase)
NM_078467	Hs.370771	cyclin-dependent kinase inhibitor 1A (p21, Cip1)
NM_080649	Hs.73722	APEX nuclease (multifunctional DNA repair enzyme) 1
U36308	Hs.406681	major intrinsic protein of lens fiber
U37218	Hs.401929	ribosomal protein L10
X12784	Hs.437173	collagen, type IV, alpha 1
Z29078	Hs.371468	cyclin D1 (PRAD1: parathyroid adenomatosis 1)

Sp3-regulated genes

Original AN	Unigene hs	Annotation
M85247	Hs.2624	dopamine receptor D1
NM_001511	Hs.789	chemokine (C-X-C motif) ligand 1 (melanoma growth stimulating activity, alpha)
U36308	Hs.406681	major intrinsic protein of lens fiber

Stat1-regulated genes

Original AN	Unigene hs	Annotation
NM_000201	Hs.386467	intercellular adhesion molecule 1 (CD54), human rhinovirus receptor
NM_000246	Hs.126714	MHC class II transactivator
NM_000247	Hs.90598	MHC class I polypeptide-related sequence A
NM_000547	Hs.71304	thyroid peroxidase
NM_001085	Hs.76353	serine (or cysteine) proteinase inhibitor, clade A (alpha-1 antiproteinase, antitrypsin), member 3
NM_001223	Hs.2490	caspase 1, apoptosis-related cysteine protease (interleukin 1, beta, convertase)

NM_001224	Hs.433103	caspase 2, apoptosis-related cysteine protease (neural precursor cell expressed, developmentally down-regulated 2)
NM_001233	Hs.139851	caveolin 2
NM_001786	Hs.334562	cell division cycle 2, G1 to S and G2 to M
NM_001867	Hs.430075	cytochrome c oxidase subunit VIIc
NM_002053	Hs.62661	guanylate binding protein 1, interferon-inducible, 67kDa
NM_002162	Hs.353214	intercellular adhesion molecule 3
NM_002164	Hs.840	indoleamine-pyrrole 2,3 dioxygenase
NM_002178	Hs.274313	insulin-like growth factor binding protein 6
NM_002184	Hs.71968	interleukin 6 signal transducer (gp130, oncostatin M receptor)
NM_002198	Hs.80645	interferon regulatory factor 1
NM_002222	Hs.149900	inositol 1,4,5-triphosphate receptor, type 1
NM_002227	Hs.436004	Janus kinase 1 (a protein tyrosine kinase)
NM_002421	Hs.83169	matrix metalloproteinase 1 (interstitial collagenase)
NM_002427	Hs.2936	matrix metalloproteinase 13 (collagenase 3)
NM_003235	Hs.433680	thyroglobulin
NM_003299	Hs.192374	tumor rejection antigen (gp96) 1
NM_003373	Hs.75350	vinculin
NM_003902	Hs.118962	far upstream element (FUSE) binding protein 1
NM_003932	Hs.377199	suppression of tumorigenicity 13 (colon carcinoma) (Hsp70 interacting protein)
NM_004048	Hs.48516	beta-2-microglobulin
NM_004322	Hs.76366	BCL2-antagonist of cell death
NM_004346	Hs.141125	caspase 3, apoptosis-related cysteine protease
NM_004530	Hs.367877	matrix metalloproteinase 2 (gelatinase A, 72kDa gelatinase, 72kDa type IV collagenase)
NM_005516	Hs.381008	major histocompatibility complex, class I, E
NM_005529	Hs.211573	heparan sulfate proteoglycan 2 (perlecan)
NM_005931	Hs.211580	MHC class I polypeptide-related sequence B
NM_006472	Hs.179526	thioredoxin interacting protein
NM_006835	Hs.369110	cyclin I
NM_006889	Hs.27954	CD86 antigen (CD28 antigen ligand 2, B7-2 antigen)
NM_007111	Hs.79353	transcription factor Dp-1
NM_012333	Hs.78221	c-myc binding protein
NM_021960	Hs.86386	myeloid cell leukemia sequence 1 (BCL2-related)
NM_031966	Hs.23960	cyclin B1
NM_148954	Hs.381081	proteasome subunit, beta type, 9 (large multifunctional protease 2)

TFEB-regulated genes

Original AN	Unigene hs	Annotation
NM_000550	Hs.75219	tyrosinase-related protein 1
NM_002019	Hs.347713	fms-related tyrosine kinase 1 (vascular endothelial growth factor/vascular permeability factor receptor)
NM_003215	Hs.278005	tec protein tyrosine kinase
NM_003376	Hs.73793	vascular endothelial growth factor

Genes coding for vesicular transport proteins

Original AN	Unigene hs	Annotation
AB024494	Hs.4014	huntingtin interacting protein 14
AF049527	Hs.19121	adaptor-related protein complex 2, alpha 2 subunit
AF114488	Hs.66392	intersectin 1 (SH3 domain protein)
AF149825	Hs.334639	protein kinase C and casein kinase substrate in neurons 3
AF242529	Hs.441281	protein kinase C and casein kinase substrate in neurons 1
AF277897	Hs.77432	epidermal growth factor receptor (erythroblastic leukemia viral (v-erb-b) oncogene homolog, avian)
AF393369	Hs.387648	adaptor-related protein complex 1, sigma 3 subunit
AK055003	Hs.177193	similar to synaptotagmin V
BC034044	Hs.12436	calcium/calmodulin-dependent protein kinase (CaM kinase) II gamma
J03778	Hs.101174	microtubule-associated protein tau
L23958	Hs.7720	dynein, cytoplasmic, heavy polypeptide 1
NM_000944	Hs.272458	protein phosphatase 3 (formerly 2B), catalytic subunit, alpha isoform (calcineurin A alpha)
NM_001221	Hs.111460	calcium/calmodulin-dependent protein kinase (CaM kinase) II delta
NM_001365	Hs.23731	discs, large homolog 4 (Drosophila)
NM_001635	Hs.173034	amphiphysin (Stiff-Man syndrome with breast cancer 128kDa autoantigen)
NM_001833	Hs.207052	clathrin, light polypeptide (Lca)
NM_001834	Hs.380749	clathrin, light polypeptide (Lcb)
NM_001981	Hs.79095	epidermal growth factor receptor pathway substrate 15
NM_002628	Hs.91747	profilin 2
NM_003081	Hs.221974	synaptosomal-associated protein, 25kDa

NM_003178	Hs.445503	synapsin II
NM_003490	Hs.125878	synapsin III
NM_003941	Hs.182469	Wiskott-Aldrich syndrome-like
NM_004068	Hs.433892	adaptor-related protein complex 2, mu 1 subunit
NM_004082	Hs.74617	dynactin 1 (p150, glued homolog, Drosophila)
NM_004408	Hs.436132	dynamin 1
NM_004522	Hs.6641	kinesin family member 5C
NM_004582	Hs.78948	Rab geranylgeranyltransferase, beta subunit
NM_004712	Hs.416959	hepatocyte growth factor-regulated tyrosine kinase substrate
NM_004859	Hs.187416	clathrin, heavy polypeptide (Hc)
NM_004945	Hs.432832	dynamin 2
NM_005228	Hs.77432	epidermal growth factor receptor (erythroblastic leukemia viral (v-erb-b) oncogene homolog, avian)
NM_005550	Hs.23131	kinesin family member C3
NM_005552	Hs.512578	kinesin 2 60/70kDa
NM_005605	Hs.75206	protein phosphatase 3 (formerly 2B), catalytic subunit, gamma isoform (calcineurin A gamma)
NM_005735	Hs.2477	ARP1 actin-related protein 1 homolog B, centractin beta (yeast)
NM_005817	Hs.140452	cargo selection protein (mannose 6 phosphate receptor binding protein)
NM_006006	Hs.356349	zinc finger protein 145 (Kruppel-like, expressed in promyelocytic leukemia)
NM_006178	Hs.431279	N-ethylmaleimide-sensitive factor
NM_006277	Hs.444708	intersectin 2
NM_006400	Hs.289123	dynactin 2 (p50)
NM_006597	Hs.180414	heat shock 70kDa protein 8
NM_006888	Hs.282410	calmodulin 1 (phosphorylase kinase, delta)
NM_006950	Hs.225936	synapsin I
NM_007097	Hs.380749	clathrin, light polypeptide (Lcb)
NM_007166	Hs.39252	phosphatidylinositol binding clathrin assembly protein
NM_007229	Hs.454530	protein kinase C and casein kinase substrate in neurons 2
NM_012310	Hs.279766	kinesin family member 4A
NM_014231	Hs.20021	vesicle-associated membrane protein 1 (synaptobrevin 1)
NM_014666	Hs.132853	enthoprotin
NM_014841	Hs.304330	synaptosomal-associated protein, 91kDa homolog (mouse)
NM_014964	Hs.7407	epsin 2
NM_015074	Hs.444757	kinesin family member 1B
NM_015254	Hs.15711	kinesin family member 13B
NM_016009	Hs.136309	SH3-domain GRB2-like endophilin B1
NM_016131	Hs.236494	RAB10, member RAS oncogene family
NM_016223	Hs.334639	protein kinase C and casein kinase substrate in neurons 3
NM_016530	Hs.365655	RAB-8b protein
NM_016830	Hs.20021	vesicle-associated membrane protein 1 (synaptobrevin 1)
NM_017957	Hs.165904	epsin 3
NM_019028	Hs.163091	HIP14-related protein
NM_019595	Hs.444708	intersectin 2
NM_020145	Hs.30002	SH3-domain GRB2-like endophilin B2
NM_020804	Hs.441281	protein kinase C and casein kinase substrate in neurons 1
NM_021132	Hs.187543	protein phosphatase 3 (formerly 2B), catalytic subunit, beta isoform (calcineurin A beta)
NM_021980	Hs.390162	optineurin
NM_022113	Hs.146286	kinesin family member 13A
NM_022342	Hs.373627	kinesin family member 9
NM_022822	Hs.280792	likely ortholog of kinesin light chain 2
NM_023019	Hs.74617	dynactin 1 (p150, glued homolog, Drosophila)
NM_032559	Hs.226805	kinesin protein
NM_053024	Hs.91747	profilin 2
NM_133499	Hs.225936	synapsin I
NM_133625	Hs.445503	synapsin II
NM_133633	Hs.125878	synapsin III
NM_139316	Hs.173034	amphiphysin (Stiff-Man syndrome with breast cancer 128kDa autoantigen)
NM_147152	Hs.444708	intersectin 2
NM_147180	Hs.283852	glutamate receptor, ionotropic, N-methyl-D-aspartate 3A
NM_148921	Hs.7407	epsin 2
U01828	Hs.167	microtubule-associated protein 2
U16850	Hs.282410	calmodulin 1 (phosphorylase kinase, delta)
U53530	Hs.7720	dynein, cytoplasmic, heavy polypeptide 1

Luthi-Carter data 2000 and 2002 overlap

AF026537	Mm.6239	Hs.22584	prodynorphin
D13003	Mm.4876	Hs.167791	reticulocalbin 1, EF-hand calcium binding domain
L01695	Mm.62	Hs.512605	phosphodiesterase 1B, calmodulin-dependent

M13227	Mm.2899		Preproenkephalin 1 (Penk1)
M22326	Mm.181959	Hs.326035	early growth response 1
M69109	Mm.392	Hs.840	indoleamine-pyrrole 2,3 dioxygenase
M74149	Mm.16831	Hs.173724	creatine kinase, brain
U06483	Mm.4629	Hs.151250	intercellular adhesion molecule 5, telencephalin
U13837	Mm.217787	Hs.409131	ATPase, H+ transporting, lysosomal 70kDa, V1 subunit A
U29762	Mm.3459	Hs.414480	D site of albumin promoter (albumin D-box) binding protein
U67187	Mm.28262	Hs.78944	regulator of G-protein signalling 2, 24kDa
U93862	Mm.290786	Hs.381172	ribosomal protein L41
U96746	Mm.247542	Hs.83383	peroxiredoxin 4
W12692	Mm.180873	Hs.337766	ribosomal protein L18a
W34429	Mm.195067	Hs.83672	actinin, alpha 2
X15373	Mm.227912	Hs.149900	inositol 1,4,5-triphosphate receptor, type 1
X16995	Mm.119	Hs.1119	nuclear receptor subfamily 4, group A, member 1
X51468	Mm.2453		Somatostatin
X55674	Mm.41970	Hs.73893	dopamine receptor D2
X70398	Mm.128733	Hs.508741	chromosome 5 open reading frame 13
X80502	Mm.252110		ST8 alpha-N-acetyl-neuraminide alpha-2,8-sialyltransferase 3
X97281	Mm.1438	Hs.157818	potassium voltage-gated channel, shaker-related subfamily, beta member 1
Z31174	Mm.28896	Hs.300446	START domain containing 10
Z31235	Mm.271947	Hs.209983	stathmin 1/oncoprotein 18
Z31269	Mm.29586		Brain abundant, membrane attached signal protein 1 (Basp1)

Acknowledgement

When I decided to take the PhD position in Prof. Herzel's group, little did I know how profoundly this decision will mark my life. Personal and professional maturity came at high cost. My years in Berlin were like the city itself: enchanting and harsh. In the end, I feel nothing but love for the place and the dear people I met here.

First and foremost, I would like to thank my supervisor Prof. Hanspeter Herzel, who has always been generous with his knowledge and guidance. His enthusiasm and love for science, his fairness and kindness made me feel encouraged and secure. During the years, my husband Samuel Bernard has been untiringly resourceful and supportive, for which I am grateful. Our daughter Dora, affectionately called Terminator, is a proof that together, mathematics and biology can create a miracle. I would like to thank Prof. Michael Mackey who has been an inspiration and a guardian to me, and Prof. Erich Wanker for opening the doors of his lab in Max Delbrueck Centrum to me. I would like to thank my colleagues for careful reading of my thesis. Here, I must specially mention Dagmar, Roland and Samuel that read and reread it all. I would like to thank my parents, Vera and Stanislav Čajavec, hoping that they will brag about me disregarding their good manners. They have been part of everything in my life and each step I make is their step as well. I would like to thank my amazing friends Maja, Jelena and Boris. Their unconditional support, their humour and character gave me strength when I had none. I cherish their friendship. In Berlin, I met people that will be my friends for life: Dijana and Predrag, Antje and Roland, Nic and Ed, Ania, Dagmar, Anu, and Kiki. We share our lives and become richer for it. I would like to thank Laurenz for our wonderful escapes into the world of music. I would like to thank Maciej, Szymon and Nils, who discovered me, brought me here and safeguarded my first steps in Berlin. Last but not least, I would like to thank my many friends for encouragement and aid during my PhD.

Lebenslauf

Mein Lebenslauf wird aus Datenschutzgründen in der elektronischen Version meiner Arbeit nicht mit veröffentlicht.

Bibliography

[1] B. Aguda. Instabilities in phosphorylation-dephosphorylation cascades and cell cycle checkpoints. *Oncogene*, 18(18):2846–51, 1999.

[2] M. H. Anca, E. Gazit, R. Loewenthal, O. Ostrovsky, M. Frydman, and N. Giladi. Different phenotypic expression in monozygotic twins with Huntington disease. *Am. J. Med. Genet. A*, 124(1):89–91, 2004.

[3] S. E. Andrew, Y. P. Goldberg, B. Kremer, H. Telenius, J. Theilmann, S. Adam, E. Starr, F. Squitieri, B. Lin, M. A. Kalchman, R. K. Graham, and M. R. Hayden. The relationship between trinucleotide (CAG) repeat length and clinical features of Huntington's disease. *Nat. Genet.*, 4:398–403, 1993.

[4] S. S. Andrews and A. P. Arkin. Simulating cell biology. *Curr Biol*, 16(14):R523–R527, Jul 2006. doi: 10.1016/j.cub.2006.06.048. URL `http://dx.doi.org/10.1016/j.cub.2006.06.048`.

[5] T. C. Andrews, R. A. Weeks, N. Turjanski, R. N. Gunn, L. H. A. Watkins, B. Sahakian, J. R. Hodges, A. E. Rosser, N. W. Wood, and D. J. Brooks. Huntington's disease progression: PET and clinical observations. *Brain*, 122(12):2353–2363, 1999. URL `http://brain.oxfordjournals.org/cgi/content/abstract/122/12/2353`.

[6] A. Antonini, K. L. Leenders, R. Spiegel, D. Meier, P. Vontobel, M. Weigell-Weber, R. Sanchez-Pernaute, J. G. de Yébenez, P. Boesiger, A. Weindl, and R. P. Maguire. Striatal glucose metabolism and dopamine d2 receptor binding in asymptomatic gene carriers and patients with Huntington's disease. *Brain*, 119 (Pt 6):2085–2095, Dec 1996.

[7] B. L. Apostol, K. Illes, J. Pallos, L. Bodai, J. Wu, A. Strand, E. S. Schweitzer, J. M. Olson, A. Kazantsev, J. L. Marsh, and L. M. Thompson. Mutant huntingtin alters mapk signaling pathways in pc12 and striatal cells: Erk1/2 protects against mutant huntingtin-associated toxicity. *Hum Mol Genet*, 15(2):273–285, Jan 2006. doi: 10.1093/hmg/ddi443. URL `http://dx.doi.org/10.1093/hmg/ddi443`.

[8] L. Arning, P. H. Kraus, S. Valentin, C. Saft, J. Andrich, and J. T. Epplen. *NR2A* and *NR2B* receptor gene variations modify age at onset in Huntington disease. *Neurogenetics*, 6:25–28, 2005.

[9] M. Arrasate, S. Mitra, E. S. Schweitzer, M. R. Segal, and S. Finkbeiner. Inclusion body formation reduces levels of mutant huntingtin and the risk of neuronal death. *Nature*, 431(7010):805–810, 2004.

[10] S. J. Augood, R. L. Faull, and P. C. Emson. Dopamine D1 and D2 receptor gene expression in the striatum in Huntington's disease. *Ann. Neurol.*, 42(2):215–221, 1997.

[11] E. H. Aylward, J. Brandt, A. M. Codori, R. S. Mangus, P. E. Barta, and G. J. Harris. Reduced basal ganglia volume associated with the gene for Huntington's disease in asymptomatic at-risk persons. *Neurology*, 44(5):823–828, May 1994.

[12] E. H. Aylward, B. F. Sparks, K. M. Field, V. Yallapragada, B. D. Shpritz, A. Rosenblatt, J. Brandt, L. M. Gourley, K. Liang, H. Zhou, R. L. Margolis, and C. A. Ross. Onset and rate of striatal atrophy in preclinical Huntington disease. *Neurology*, 63 (1):66–72, 2004.

[13] A.-C. Bachoud-Lévi, V. Gaura, P. Brugières, J.-P. Lefaucheur, M.-F. Boissé, P. Maison, S. Baudic, M.-J. Ribeiro, C. Bourdet, P. Remy, P. Cesaro, P. Hantraye, and M. Peschanski. Effect of fetal neural transplants in patients with Huntington's disease 6 years after surgery: a long-term follow-up study. *Lancet Neurol*, 5(4):303–309, Apr 2006. doi: 10.1016/S1474-4422(06)70381-7. URL `http://dx.doi.org/10.1016/S1474-4422(06)70381-7`.

[14] B.-I. Bae, H. Xu, S. Igarashi, M. Fujimuro, N. Agrawal, Y. Taya, S. D. Hayward, T. H. Moran, C. Montell, C. A. Ross, S. H. Snyder, and A. Sawa. p53 mediates cellular dysfunction and behavioral abnormalities in Huntington's disease. *Neuron*, 47(1):29–41, Jul 2005. doi: 10.1016/j.neuron.2005.06.005. URL `http://dx.doi.org/10.1016/j.neuron.2005.06.005`.

[15] B. C. Baliga, S. H. Read, and S. Kumar. The biochemical mechanism of caspase-2 activation. *Cell Death Differ*, 11(11):1234–1241, Nov 2004. doi: 10.1038/sj.cdd.4401492. URL `http://dx.doi.org/10.1038/sj.cdd.4401492`.

[16] K. A. Bamford, E. D. Caine, D. K. Kido, W. M. Plassche, and I. Shoulson. Clinical-pathologic correlation in Huntington's disease: a neuropsychological and computed tomography study. *Neurology*, 39(6):796–801, Jun 1989.

[17] J. Bao, A. H. Sharp, M. V. Wagster, M. Becher, G. Schilling, C. A. Ross, V. L. Dawson, and T. M. Dawson. Expansion of polyglutamine repeat in huntingtin leads to abnormal protein interactions involving calmodulin. *Proc Natl Acad Sci U S A*, 93(10):5037–5042, May 1996.

[18] G. Bates. Huntingtin aggregation and toxicity in Huntington's disease. *The Lancet*, 361(9369):1642–1644, 2003.

[19] M. F. Beal. Mitochondrial dysfunction in neurodegenerative diseases. *Biochim Biophys Acta*, 1366(1-2):211–223, Aug 1998.

[20] M. F. Beal, N. W. Kowall, D. W. Ellison, M. F. Mazurek, K. J. Swartz, and J. B. Martin. Replication of the neurochemical characteristics of Huntington's disease by quinolinic acid. *Nature*, 321(6066):168–171, 1986. doi: 10.1038/321168a0. URL http://dx.doi.org/10.1038/321168a0.

[21] E. J. Bennett, T. A. Shaler, B. Woodman, K.-Y. Ryu, T. S. Zaitseva, C. H. Becker, G. P. Bates, H. Schulman, and R. R. Kopito. Global changes to the ubiquitin system in Huntington's disease. *Nature*, 448(7154):704–708, Aug 2007. doi: 10.1038/nature06022. URL http://dx.doi.org/10.1038/nature06022.

[22] L. Bintu, N. E. Buchler, H. G. Garcia, U. Gerland, T. Hwa, J. Kondev, T. Kuhlman, and R. Phillips. Transcriptional regulation by the numbers: applications. *Curr Opin Genet Dev*, 15(2):125–135, Apr 2005. doi: 10.1016/j.gde.2005.02.006. URL http://dx.doi.org/10.1016/j.gde.2005.02.006.

[23] L. Bintu, N. E. Buchler, H. G. Garcia, U. Gerland, T. Hwa, J. Kondev, and R. Phillips. Transcriptional regulation by the numbers: models. *Curr Opin Genet Dev*, 15(2):116–124, Apr 2005. doi: 10.1016/j.gde.2005.02.007. URL http://dx.doi.org/10.1016/j.gde.2005.02.007.

[24] N. Bluethgen, S. M. Kielbasa, B. Cajavec, and H. Herzel. HOMGL-comparing genelists across species and with different accession numbers. *Bioinformatics*, 20 (1):125–126, Jan 2004.

[25] T. Boby, A.-M. Patch, and S. J. Aves. TRbase: a database relating tandem repeats to disease genes for the human genome. *Bioinformatics*, 21(6):811–816, Mar 2005. doi: 10.1093/bioinformatics/bti059. URL http://dx.doi.org/10.1093/bioinformatics/bti059.

[26] R. A. Bodner, D. E. Housman, and A. G. Kazantsev. New directions for neurodegenerative disease therapy: using chemical compounds to boost the formation of mutant protein inclusions. *Cell Cycle*, 5(14):1477–1480, Jul 2006.

[27] R. A. Bodner, T. F. Outeiro, S. Altmann, M. M. Maxwell, S. H. Cho, B. T. Hyman, P. J. McLean, A. B. Young, D. E. Housman, and A. G. Kazantsev. Pharmacological promotion of inclusion formation: a therapeutic approach for Huntington's and parkinson's diseases. *Proc Natl Acad Sci U S A*, 103(11):4246–4251, Mar 2006. doi: 10.1073/pnas.0511256103. URL http://dx.doi.org/10.1073/pnas.0511256103.

[28] B. Bohrmann, M. Adrian, J. Dubochet, P. Kuner, F. Mueller, W. Huber, C. Nordstedt, and H. Döbeli. Self-assembly of beta-amyloid 42 is retarded by small molecular ligands at the stage of structural intermediates. *J Struct Biol*, 130(2-3):232–246, Jun 2000. doi: 10.1006/jsbi.2000.4241. URL http://dx.doi.org/10.1006/jsbi.2000.4241.

[29] R. M. Bonelli and G. K. Wenning. Pharmacological management of Huntington's disease: an evidence-based review. *Curr Pharm Des*, 12(21):2701–2720, 2006.

[30] N. M. Bonini. Chaperoning brain degeneration. *Proc Natl Acad Sci U S A*, 99 Suppl 4:16407–16411, Dec 2002. doi: 10.1073/pnas.152330499. URL `http://dx.doi.org/10.1073/pnas.152330499`.

[31] F. Borovecki, L. Lovrecic, J. Zhou, H. Jeong, F. Then, H. D. Rosas, S. M. Hersch, P. Hogarth, B. Bouzou, R. V. Jensen, and D. Krainc. Genome-wide expression profiling of human blood reveals biomarkers for Huntington's disease. *Proc Natl Acad Sci U S A*, 102(31):11023–11028, Aug 2005. doi: 10.1073/pnas.0504921102. URL `http://dx.doi.org/10.1073/pnas.0504921102`.

[32] E. Brouillet, P. Hantraye, R. J. Ferrante, R. Dolan, A. Leroy-Willig, N. W. Kowall, and M. F. Beal. Chronic mitochondrial energy impairment produces selective striatal degeneration and abnormal choreiform movements in primates. *Proc Natl Acad Sci U S A*, 92(15):7105–7109, Jul 1995.

[33] J. Carmichael, J. Chatellier, A. Woolfson, C. Milstein, A. R. Fersht, and D. C. Rubinsztein. Bacterial and yeast chaperones reduce both aggregate formation and cell death in mammalian cell models of Huntington's disease. *Proc. Natl. Acad. Sci. USA*, 97(17):9701–9705, 2000.

[34] E. Cattaneo, D. Rigamonti, D. Goffredo, C. Zuccato, F. Squitieri, and S. Sipione. Loss of normal huntingtin function: new developments in Huntington's disease research. *Trends Neurosci*, 24(3):182–188, Mar 2001.

[35] E. Cattaneo, C. Zuccato, and M. Tartari. Normal huntingtin function: an alternative approach to Huntington's disease. *Nat Rev Neurosci*, 6(12):919–930, Dec 2005. doi: 10.1038/nrn1806. URL `http://dx.doi.org/10.1038/nrn1806`.

[36] J. H. Cha. Transcriptional dysregulation in Huntington's disease. *Trends Neurosci*, 23(9):387–392, Sep 2000.

[37] J. H. Cha, C. M. Kosinski, J. A. Kerner, S. A. Alsdorf, L. Mangiarini, S. W. Davies, J. B. Penney, G. P. Bates, and A. B. Young. Altered brain neurotransmitter receptors in transgenic mice expressing a portion of an abnormal human Huntington disease gene. *Proc Natl Acad Sci U S A*, 95(11):6480–6485, May 1998.

[38] E. Y. W. Chan, R. Luthi-Carter, A. Strand, S. M. Solano, S. A. Hanson, M. M. DeJohn, C. Kooperberg, K. O. Chase, M. DiFiglia, A. B. Young, B. R. Leavitt, J.-H. J. Cha, N. Aronin, M. R. Hayden, and J. M. Olson. Increased huntingtin protein length reduces the number of polyglutamine-induced gene expression changes in mouse models of Huntington's disease. *Hum Mol Genet*, 11(17):1939–1951, Aug 2002.

[39] B. Chattopadhyay, K. Baksi, S. Mukhopadhyay, and N. P. Bhattacharyya. Modulation of age at onset of Huntington disease patients by variations in tp53 and human caspase activated dnase (hcad) genes. *Neurosci Lett*, 374(2):81–86, Feb 2005. doi: 10.1016/j.neulet.2004.10.018. URL `http://dx.doi.org/10.1016/j.neulet.2004.10.018`.

[40] C. Cheadle, Y. S. Cho-Chung, K. G. Becker, and M. P. Vawter. Application of z-score transformation to affymetrix data. *Appl Bioinformatics*, 2(4):209–217, 2003.

[41] Y. S. Choo, G. V. W. Johnson, M. MacDonald, P. J. Detloff, and M. Lesort. Mutant huntingtin directly increases susceptibility of mitochondria to the calcium-induced permeability transition and cytochrome c release. *Hum Mol Genet*, 13(14):1407–1420, Jul 2004. doi: 10.1093/hmg/ddh162. URL `http://dx.doi.org/10.1093/hmg/ddh162`.

[42] V. Chopra, J. H. Fox, G. Lieberman, K. Dorsey, W. Matson, P. Waldmeier, D. E. Housman, A. Kazantsev, A. B. Young, and S. Hersch. A small-molecule therapeutic lead for Huntington's disease: preclinical pharmacology and efficacy of C2-8 in the R6/2 transgenic mouse. *Proc Natl Acad Sci U S A*, 104(42):16685–16689, Oct 2007. doi: 10.1073/pnas.0707842104. URL `http://dx.doi.org/10.1073/pnas.0707842104`.

[43] G. Clarke, R. A. Collins, B. R. Leavitt, D. F. Andrews, M. R. Hayden, C. J. Lumsden, and R. R. McInnes. A one-hit model of cell death in inherited neuronal degenerations. *Nature*, 406(6792):195–199, 2000.

[44] R. Coles, R. Caswell, and D. C. Rubinsztein. Functional analysis of the Huntington's disease (hd) gene promoter. *Hum Mol Genet*, 7(5):791–800, May 1998.

[45] J. T. Coyle and P. Puttfarcken. Oxidative stress, glutamate, and neurodegenerative disorders. *Science*, 262(5134):689–695, Oct 1993.

[46] L. Cui, H. Jeong, F. Borovecki, C. N. Parkhurst, N. Tanese, and D. Krainc. Transcriptional repression of pgc-1alpha by mutant huntingtin leads to mitochondrial dysfunction and neurodegeneration. *Cell*, 127(1):59–69, Oct 2006. doi: 10.1016/j.cell.2006.09.015. URL `http://dx.doi.org/10.1016/j.cell.2006.09.015`.

[47] S. W. Davies, M. Turmaine, C. B. A., M. DiFiglia, A. H. Sharp, C. A. Ross, E. Scherzinger, E. E. Wanker, L. Mangiarini, and G. P. Bates. Formation of neuronal intranuclear inclusions underlies the neurological dysfunction in mice transgenic for the hd mutation. *Cell*, 90(3):537–548, Aug 1997.

[48] A. Doble. The role of excitotoxicity in neurodegenerative disease: implications for therapy. *Pharmacol Ther*, 81(3):163–221, Mar 1999.

[49] A. W. Dunah, H. Jeong, A. Griffin, Y.-M. Kim, D. G. Standaert, S. M. Hersch, M. M. Mouradian, A. B. Young, N. Tanese, and D. Krainc. Sp1 and TAFII130 transcriptional activity disrupted in early Huntington's disease. *Science*, 296(5576):2238–2243, Jun 2002. doi: 10.1126/science.1072613. URL `http://dx.doi.org/10.1126/science.1072613`.

[50] M. Duyao, C. Ambrose, R. Myers, A. Novelletto, F. Persichetti, M. Frontali, S. Folstein, C. Ross, M. Franz, M. Abbott, J. Gray, P. Conneally, A. Young, J. Penney, Z. Hollingsworth, I. Shoulson, A. Lazzarini, A. Falek, W. Koroshetz, D. Sax, E. Bird, J. Vonsattel, E. Bonilla, J. Alvir, J. B. Conde, J.-H. Cha,

L. Dure, F. Gomez, M. Ramos, J. Sanchez-Ramos, S. Snodgrass, M. de Young, N. Wexler, C. Moscowitz, G. Penchaszadeh, H. MacFarlane, M. Anderson, B. Jenkins, J. Srinidhi, G. Barnes, J. Gusella, and M. MacDonald. Trinucleotide repeat length instability and age of onset in Huntington's disease. *Nat. Genet.*, 4:387–392, 1993.

[51] D. E. Ehrnhoefer, M. Duennwald, P. Markovic, J. L. Wacker, S. Engemann, M. Roark, J. Legleiter, J. L. Marsh, L. M. Thompson, S. Lindquist, P. J. Muchowski, and E. E. Wanker. Green tea (-)-epigallocatechin-gallate modulates early events in huntingtin misfolding and reduces toxicity in Huntington's disease models. *Hum Mol Genet*, 15(18):2743–2751, Sep 2006. doi: 10.1093/hmg/ddl210. URL `http://dx.doi.org/10.1093/hmg/ddl210`.

[52] L. A. Farrer. Suicide and attempted suicide in Huntington disease: implications for preclinical testing of persons at risk. *Am J Med Genet*, 24(2):305–311, Jun 1986. doi: 10.1002/ajmg.1320240211. URL `http://dx.doi.org/10.1002/ajmg.1320240211`.

[53] R. J. Ferrante, N. W. Kowall, M. F. Beal, E. P. Richardson, E. D. Bird, and J. B. Martin. Selective sparing of a class of striatal neurons in Huntington's disease. *Science*, 230(4725):561–563, Nov 1985.

[54] J. Ferrell. Tripping the switch fantastic: how a protein kinase cascade can convert graded inputs into switch-like outputs. *Trends in Biochemical Sciences*, 21(12): 460–466, 1996.

[55] J. Gafni and L. M. Ellerby. Calpain activation in Huntington's disease. *J Neurosci*, 22(12):4842–4849, Jun 2002.

[56] J. Gafni, E. Hermel, J. E. Young, C. L. Wellington, M. R. Hayden, and L. M. Ellerby. Inhibition of calpain cleavage of huntingtin reduces toxicity: accumulation of calpain/caspase fragments in the nucleus. *J Biol Chem*, 279(19):20211–20220, May 2004. doi: 10.1074/jbc.M401267200. URL `http://dx.doi.org/10.1074/jbc.M401267200`.

[57] L. R. Gauthier, B. C. Charrin, M. Borrell-Pages, J. P. Dompierre, H. Rangone, F. P. Cordelieres, J. De Mey, M. E. MacDonald, V. Lessmann, S. Humbert, and F. Saudou. Huntingtin controls neurotrophic support and survival of neurons by enhancing bdnf vesicular transport along microtubules. *Cell*, 118(1):127–138, 2004.

[58] H. P. Gerber, K. Seipel, O. Georgiev, M. Haefferer, M. Hug, S. Rusconi, and W. Schaffner. Transcriptional activation modulated by homopolymeric glutamine and proline stretches. *Science*, 263(5148):808–811, Feb 1994.

[59] F. G. Gervais, R. Singaraja, S. Xanthoudakis, C. A. Gutekunst, B. R. Leavitt, M. Metzler, A. S. Hackam, J. Tam, J. P. Vaillancourt, V. Houtzager, D. M. Rasper, S. Roy, M. R. Hayden, and D. W. Nicholson. Recruitment and activation of caspase-8 by the huntingtin-interacting protein hip-1 and a novel partner hippi. *Nat. Cell Biol*, 4(2):95–105, 2002.

[60] S. Gines, E. Ivanova, I.-S. Seong, C. A. Saura, and M. E. MacDonald. Enhanced akt signaling is an early pro-survival response that reflects n-methyl-d-aspartate receptor activation in Huntington's disease knock-in striatal cells. *J Biol Chem*, 278(50):50514–50522, Dec 2003. doi: 10.1074/jbc.M309348200. URL http://dx.doi.org/10.1074/jbc.M309348200.

[61] H. Goehler, M. Lalowski, U. Stelzl, S. Waelter, M. Stroedicke, U. Worm, A. Droege, K. S. Lindenberg, M. Knoblich, C. Haenig, M. Herbst, J. Suopanki, E. Scherzinger, C. Abraham, B. Bauer, R. Hasenbank, A. Fritzsche, A. H. Ludewig, K. Buessow, S. H. Coleman, C.-A. Gutekunst, B. G. Landwehrmeyer, H. Lehrach, and E. E. Wanker. A protein interaction network links git1, an enhancer of huntingtin aggregation, to Huntington's disease. *Mol Cell*, 15(6):853–865, Sep 2004. doi: 10.1016/j.molcel.2004.09.016. URL http://dx.doi.org/10.1016/j.molcel.2004.09.016.

[62] Y. P. Goldberg, D. W. Nicholson, D. M. Rasper, M. A. Kalchman, H. B. Koide, R. K. Graham, M. Bromm, P. Kazemi-Esfarjani, N. A. Thornberry, J. P. Vaillancourt, and M. R. Hayden. Cleavage of huntingtin by apopain, a proapoptotic cysteine protease, is modulated by the polyglutamine tract. *Nat Genet*, 13(4):442–449, Aug 1996. doi: 10.1038/ng0896-442. URL http://dx.doi.org/10.1038/ng0896-442.

[63] M. Gu, M. T. Gash, V. M. Mann, F. Javoy-Agid, J. M. Cooper, and A. H. Schapira. Mitochondrial defect in Huntington's disease caudate nucleus. *Ann Neurol*, 39(3):385–389, Mar 1996. doi: 10.1002/ana.410390317. URL http://dx.doi.org/10.1002/ana.410390317.

[64] F. X. Guix, I. Uribesalgo, M. Coma, and F. J. Munoz. The physiology and pathophysiology of nitric oxide in the brain. *Prog Neurobiol*, 76(2):126–152, Jun 2005. doi: 10.1016/j.pneurobio.2005.06.001. URL http://dx.doi.org/10.1016/j.pneurobio.2005.06.001.

[65] S. Gunawardena, L.-S. Her, R. G. Brusch, R. A. Laymon, I. R. Niesman, B. Gordesky-Gold, L. Sintasath, N. M. Bonini, and L. S. B. Goldstein. Disruption of axonal transport by loss of huntingtin or expression of pathogenic polyq proteins in drosophila. *Neuron*, 40(1):25–40, Sep 2003.

[66] C. Gutekunst, F. Norflus, and S. Hersch. *Huntington's disease*, chapter The neuropathology of Huntington's disease, pages 251–275. Oxford University Press, 2001.

[67] A. J. Hannan. Novel therapeutic targets for Huntington's disease. *Expert Opin Ther Targets*, 9(4):639–650, Aug 2005. doi: 10.1517/14728222.9.4.639. URL http://dx.doi.org/10.1517/14728222.9.4.639.

[68] D. G. Hay, K. Sathasivam, S. Tobaben, B. Stahl, M. Marber, R. Mestril, A. Mahal, D. L. Smith, B. Woodman, and G. P. Bates. Progressive decrease in chaperone protein levels in a mouse model of Huntington's disease and induction of stress proteins as a therapeutic approach. *Hum Mol Genet*, 13(13):1389–1405, Jul 2004. doi: 10.1093/hmg/ddh144. URL http://dx.doi.org/10.1093/hmg/ddh144.

[69] J. C. Hedreen and S. E. Folstein. Early loss of neostriatal striosome neurons in Huntington's disease. *J. Neuropathol. Exp. Neurol*, 54:105–120, 1995.

[70] H. Heinsen, M. Strik, M. Bauer, K. Luther, G. Ulmar, D. Gangnus, G. Jungkunz, W. Eisenmenger, and M. Gotz. Cortical and striatal neurone number in Huntington's disease. *Acta Neuropathol. (Berl)*, 88(4):320–333, 1994.

[71] E. Hermel, J. Gafni, S. S. Propp, B. R. Leavitt, C. L. Wellington, J. E. Young, A. S. Hackam, A. V. Logvinova, A. L. Peel, S. F. Chen, V. Hook, R. Singaraja, S. Krajewski, P. C. Goldsmith, H. M. Ellerby, M. R. Hayden, D. E. Bredesen, and L. M. Ellerby. Specific caspase interactions and amplification are involved in selective neuronal vulnerability in Huntington's disease. *Cell Death Differ*, 11(4): 424–438, 2004.

[72] E. Hockly, V. M. Richon, B. Woodman, D. L. Smith, X. Zhou, E. Rosa, K. Sathasivam, S. Ghazi-Noori, A. Mahal, P. A. S. Lowden, J. S. Steffan, J. L. Marsh, L. M. Thompson, C. M. Lewis, P. A. Marks, and G. P. Bates. Suberoylanilide hydroxamic acid, a histone deacetylase inhibitor, ameliorates motor deficits in a mouse model of Huntington's disease. *Proc Natl Acad Sci U S A*, 100(4):2041–2046, Feb 2003. doi: 10.1073/pnas.0437870100. URL `http://dx.doi.org/10.1073/pnas.0437870100`.

[73] C. C. Huang, P. W. Faber, F. Persichetti, V. Mittal, J. P. Vonsattel, M. E. MacDonald, and J. F. Gusella. Amyloid formation by mutant huntingtin: threshold, progressivity and recruitment of normal polyglutamine proteins. *Somat Cell Mol Genet*, 24(4):217–233, Jul 1998.

[74] S. Humbert, E. A. Bryson, F. P. Cordelières, N. C. Connors, S. R. Datta, S. Finkbeiner, M. E. Greenberg, and F. Saudou. The IGF-1/Akt pathway is neuroprotective in Huntington's disease and involves huntingtin phosphorylation by Akt. *Dev Cell*, 2(6):831–837, Jun 2002.

[75] G. Huntington. On chorea. *The Medical and Surgical Reporter: A Weekly Journal*, 26(1):317–321, 1872.

[76] N. R. Jana, M. Tanaka, G. Wang, and N. Nukina. Polyglutamine length-dependent interaction of Hsp40 and Hsp70 family chaperones with truncated N-terminal huntingtin: their role in suppression of aggregation and cellular toxicity. *Hum. Mol. Genet.*, 9(13):2009–2018, 2000.

[77] B. G. Jenkins, W. J. Koroshetz, M. F. Beal, and B. R. Rosen. Evidence for impairment of energy metabolism in vivo in Huntington's disease using localized 1h nmr spectroscopy. *Neurology*, 43(12):2689–2695, Dec 1993.

[78] M. Johannessen, M. P. Delghandi, and U. Moens. What turns CREB on? *Cell Signal*, 16(11):1211–1227, Nov 2004. doi: 10.1016/j.cellsig.2004.05.001. URL `http://dx.doi.org/10.1016/j.cellsig.2004.05.001`.

[79] L. S. Kaltenbach, E. Romero, R. R. Becklin, R. Chettier, R. Bell, A. Phansalkar, A. Strand, C. Torcassi, J. Savage, A. Hurlburt, G.-H. Cha, L. Ukani, C. L.

Chepanoske, Y. Zhen, S. Sahasrabudhe, J. Olson, C. Kurschner, L. M. Ellerby, J. M. Peltier, J. Botas, and R. E. Hughes. Huntingtin interacting proteins are genetic modifiers of neurodegeneration. *PLoS Genet*, 3(5):e82, May 2007. doi: 10.1371/journal.pgen.0030082. URL `http://dx.doi.org/10.1371/journal.pgen.0030082`.

[80] D. Kaplan and L. Glass. *Understanding Nonlinear Dynamics*. Springer, 1995.

[81] A. G. Kazantsev and S. M. Hersch. Drug targeting of dysregulated transcription in Huntington's disease. *Prog Neurobiol*, 83(4):249–259, Nov 2007. doi: 10.1016/j.pneurobio.2007.02.005. URL `http://dx.doi.org/10.1016/j.pneurobio.2007.02.005`.

[82] K. B. Kegel, M. Kim, E. Sapp, C. McIntyre, J. G. Castano, N. Aronin, and M. DiFiglia. Huntingtin expression stimulates endosomal-lysosomal activity, endosome tubulation, and autophagy. *J Neurosci*, 20(19):7268–7278, Oct 2000.

[83] K. Kieburtz, M. MacDonald, C. Shih, A. Feigin, K. Steinberg, K. Bordwell, C. Zimmerman, J. Srinidhi, J. Sotack, and J. Gusella. Trinucleotide repeat length and progression of illness in Huntington's disease. *J Med Genet*, 31(11):872–874, Nov 1994.

[84] S. Kim, T. Koga, M. Isobe, B. E. Kern, T. Yokochi, Y. E. Chin, G. Karsenty, T. Taniguchi, and H. Takayanagi. Stat1 functions as a cytoplasmic attenuator of Runx2 in the transcriptional program of osteoblast differentiation. *Genes Dev*, 17(16):1979–1991, Aug 2003. doi: 10.1101/gad.1119303. URL `http://dx.doi.org/10.1101/gad.1119303`.

[85] H. Kita, J. Carmichael, J. Swartz, S. Muro, A. Wyttenbach, K. Matsubara, D. C. Rubinsztein, and K. Kato. Modulation of polyglutamine-induced cell death by genes identified by expression profiling. *Hum Mol Genet*, 11(19):2279–2287, Sep 2002.

[86] A. Kitamura, H. Kubota, C.-G. Pack, G. Matsumoto, S. Hirayama, Y. Takahashi, H. Kimura, M. Kinjo, R. I. Morimoto, and K. Nagata. Cytosolic chaperonin prevents polyglutamine toxicity with altering the aggregation state. *Nat Cell Biol*, 8(10):1163–1170, Oct 2006. doi: 10.1038/ncb1478. URL `http://dx.doi.org/10.1038/ncb1478`.

[87] W. Kolch. Defining systems biology: through the eyes of a biochemist. *IET Syst Biol*, 2(1):5, Jan 2008. doi: 10.1049/iet-syb:20070060. URL `http://dx.doi.org/10.1049/iet-syb:20070060`.

[88] S. Kuemmerle, C. A. Gutekunst, A. M. Klein, X. J. Li, S. H. Li, M. F. Beal, S. M. Hersch, and R. J. Ferrante. Huntington aggregates may not predict neuronal death in Huntington's disease. *Ann Neurol*, 46(6):842–849, Dec 1999.

[89] A. Kuhn, D. R. Goldstein, A. Hodges, A. D. Strand, T. Sengstag, C. Kooperberg, K. Becanovic, M. A. Pouladi, K. Sathasivam, J.-H. J. Cha, A. J. Hannan, M. R.

Hayden, B. R. Leavitt, S. B. Dunnett, R. J. Ferrante, R. Albin, P. Shelbourne, M. Delorenzi, S. J. Augood, R. L. M. Faull, J. M. Olson, G. P. Bates, L. Jones, and R. Luthi-Carter. Mutant huntingtin's effects on striatal gene expression in mice recapitulate changes observed in human Huntington's disease brain and do not differ with mutant huntingtin length or wild-type huntingtin dosage. *Hum Mol Genet*, 16(15):1845–1861, Aug 2007. doi: 10.1093/hmg/ddm133. URL `http://dx.doi.org/10.1093/hmg/ddm133`.

[90] C. Landles and G. P. Bates. Huntingtin and the molecular pathogenesis of Huntington's disease. Fourth in molecular medicine review series. *EMBO Rep*, 5(10): 958–963, Oct 2004. doi: 10.1038/sj.embor.7400250. URL `http://dx.doi.org/10.1038/sj.embor.7400250`.

[91] D. R. Langbehn, R. R. Brinkman, D. Falush, J. S. Paulsen, M. R. Hayden, and International Huntington's Disease Collaborative Group. A new model for prediction of the age of onset and penetrance for Huntington's disease based on CAG length. *Clin. Genet*, 65:267–277, 2004.

[92] E.-N. Lee, H.-J. Cho, C.-H. Lee, D. Lee, K. C. Chung, and S. R. Paik. Phthalocyanine tetrasulfonates affect the amyloid formation and cytotoxicity of alpha-synuclein. *Biochemistry*, 43(12):3704–3715, Mar 2004. doi: 10.1021/bi0356707. URL `http://dx.doi.org/10.1021/bi0356707`.

[93] S.-T. Lee and M. Kim. Aging and neurodegeneration. molecular mechanisms of neuronal loss in Huntington's disease. *Mech Ageing Dev*, 127(5):432–435, May 2006. doi: 10.1016/j.mad.2006.01.022. URL `http://dx.doi.org/10.1016/j.mad.2006.01.022`.

[94] S. H. Li, S. Lam, A. L. Cheng, and X. J. Li. Intranuclear huntingtin increases the expression of caspase-1 and induces apoptosis. *Hum Mol Genet*, 9(19):2859–2867, Nov 2000.

[95] S.-H. Li, A. L. Cheng, H. Zhou, S. Lam, M. Rao, H. Li, and X.-J. Li. Interaction of Huntington disease protein with transcriptional activator Sp1. *Mol Cell Biol*, 22 (5):1277–1287, Mar 2002.

[96] R. Lodi, A. H. Schapira, D. Manners, P. Styles, N. W. Wood, D. J. Taylor, and T. T. Warner. Abnormal in vivo skeletal muscle energy metabolism in Huntington's disease and dentatorubropallidoluysian atrophy. *Ann Neurol*, 48(1):72–76, Jul 2000.

[97] A. Lunkes, K. S. Lindenberg, L. Ben-Haiem, C. Weber, D. Devys, G. B. Landwehrmeyer, J. L. Mandel, and Y. Trottier. Proteases acting on mutant huntingtin generate cleaved products that differentially build up cytoplasmic and nuclear inclusions. *Mol Cell*, 10(2):224–225, 2002.

[98] R. Luthi-Carter, A. Strand, N. L. Peters, S. M. Solano, Z. R. Hollingsworth, A. S. Menon, A. S. Frey, B. S. Spektor, E. B. Penney, G. Schilling, C. A. Ross, D. R. Borchelt, S. J. Tapscott, A. B. Young, J. H. Cha, and J. M. Olson. Decreased expression of striatal signaling genes in a mouse model of Huntington's disease. *Hum Mol Genet*, 9(9):1259–1271, May 2000.

[99] R. Luthi-Carter, S. A. Hanson, A. D. Strand, D. A. Bergstrom, W. Chun, N. L. Peters, A. M. Woods, E. Y. Chan, C. Kooperberg, D. Krainc, A. B. Young, S. J. Tapscott, and J. M. Olson. Dysregulation of gene expression in the R6/2 model of polyglutamine disease: parallel changes in muscle and brain. *Hum Mol Genet*, 11 (17):1911–1926, Aug 2002.

[100] R. Luthi-Carter, A. D. Strand, S. A. Hanson, C. Kooperberg, G. Schilling, A. R. L. Spada, D. E. Merry, A. B. Young, C. A. Ross, D. R. Borchelt, and J. M. Olson. Polyglutamine and transcription: gene expression changes shared by DRPLA and Huntington's disease mouse models reveal context-independent effects. *Hum Mol Genet*, 11(17):1927–1937, Aug 2002.

[101] M. E. MacDonald. Huntingtin: alive and well and working in middle management. *Sci STKE*, 2003(207):pe48, Nov 2003. doi: 10.1126/stke.2003.207.pe48. URL `http://dx.doi.org/10.1126/stke.2003.207.pe48`.

[102] R. L. Margolis and C. A. Ross. Diagnosis of Huntington disease. *Clin Chem*, 49 (10):1726–1732, Oct 2003.

[103] D. Martindale, A. Hackam, A. Wieczorek, L. Ellerby, C. Wellington, K. McCutcheon, R. Singaraja, P. Kazemi-Esfarjani, R. Devon, S. U. Kim, D. E. Bredesen, F. Tufaro, and M. R. Hayden. Length of huntingtin and its polyglutamine tract influences localization and frequency of intracellular aggregates. *Nat Genet*, 18(2): 150–154, Feb 1998. doi: 10.1038/ng0298-150. URL `http://dx.doi.org/10.1038/ng0298-150`.

[104] M. P. Mattson. Neuroprotective signaling and the aging brain: take away my food and let me run. *Brain Res*, 886(1-2):47–53, Dec 2000.

[105] L. B. Menalled and M.-F. Chesselet. Mouse models of Huntington's disease. *Trends Pharmacol Sci*, 23(1):32–39, Jan 2002.

[106] T. W. Miller, T. L. Shirley, W. J. Wolfgang, X. Kang, and A. Messer. DNA vaccination against mutant huntingtin ameliorates the HDR6/2 diabetic phenotype. *Mol Ther*, 7(5 Pt 1):572–579, May 2003.

[107] D. M. Mutch, A. Berger, R. Mansourian, A. Rytz, and M.-A. Roberts. The limit fold change model: a practical approach for selecting differentially expressed genes from microarray data. *BMC Bioinformatics*, 3:17, Jun 2002.

[108] R. H. Myers, D. S. Sax, M. Schoenfeld, E. D. Bird, P. A. Wolf, J. P. Vonsattel, R. F. White, and J. B. Martin. Late onset of Huntington's disease. *J Neurol Neurosurg Psychiatry*, 48(6):530–534, Jun 1985.

[109] P. Naarding, H. P. Kremer, and F. G. Zitman. Huntington's disease: a review of the literature on prevalence and treatment of neuropsychiatric phenomena. *Eur Psychiatry*, 16(8):439–445, Dec 2001.

[110] N. Nakao, P. Brundin, K. Funa, O. Lindvall, and P. Odin. Trophic and protective actions of brain-derived neurotrophic factor on striatal DARPP-32-containing neurons in vitro. *Brain Res Dev Brain Res*, 90(1-2):92–101, Dec 1995.

[111] J. Nasir, S. B. Floresco, J. R. O'Kusky, V. M. Diewert, J. M. Richman, J. Zeisler, A. Borowski, J. D. Marth, A. G. Phillips, and M. R. Hayden. Targeted disruption of the Huntington's disease gene results in embryonic lethality and behavioral and morphological changes in heterozygotes. *Cell*, 81(5):811–823, Jun 1995.

[112] F. C. Nucifora, M. Sasaki, M. F. Peters, H. Huang, J. K. Cooper, M. Yamada, H. Takahashi, S. Tsuji, J. Troncoso, V. L. Dawson, T. M. Dawson, and C. A. Ross. Interference by huntingtin and atrophin-1 with CBP-mediated transcription leading to cellular toxicity. *Science*, 291(5512):2423–2428, Mar 2001. doi: 10.1126/science.1056784. URL `http://dx.doi.org/10.1126/science.1056784`.

[113] K. Obrietan and K. R. Hoyt. CRE-mediated transcription is increased in Huntington's disease transgenic mice. *J Neurosci*, 24(4):791–796, Jan 2004. doi: 10.1523/JNEUROSCI.3493-03.2004. URL `http://dx.doi.org/10.1523/JNEUROSCI.3493-03.2004`.

[114] G. Orphanides and D. Reinberg. A unified theory of gene expression. *Cell*, 108(4):439–451, Feb 2002.

[115] M. Pallitto and R. Murphy. A mathematical model of the kinetics of β-amyloid fibril growth from the denatured state. *Biophys J*, 81(3):1805–1822, 2001.

[116] U. B. Pandey, Z. Nie, Y. Batlevi, B. A. McCray, G. P. Ritson, N. B. Nedelsky, S. L. Schwartz, N. A. DiProspero, M. A. Knight, O. Schuldiner, R. Padmanabhan, M. Hild, D. L. Berry, D. Garza, C. C. Hubbert, T.-P. Yao, E. H. Baehrecke, and J. P. Taylor. Hdac6 rescues neurodegeneration and provides an essential link between autophagy and the ups. *Nature*, 447(7146):859–863, Jun 2007. doi: 10.1038/nature05853. URL `http://dx.doi.org/10.1038/nature05853`.

[117] A. V. Panov, C. A. Gutekunst, B. R. Leavitt, M. R. Hayden, J. R. Burke, W. J. Strittmatter, and J. T. Greenamyre. Early mitochondrial calcium defects in Huntington's disease are a direct effect of polyglutamines. *Nat Neurosci*, 5(8):731–736, 2002.

[118] J. A. Parker, J. B. Connolly, C. Wellington, M. Hayden, J. Dausset, and C. Neri. Expanded polyglutamines in caenorhabditis elegans cause axonal abnormalities and severe dysfunction of plm mechanosensory neurons without cell death. *Proc Natl Acad Sci U S A*, 98(23):13318–13323, Nov 2001. doi: 10.1073/pnas.231476398. URL `http://dx.doi.org/10.1073/pnas.231476398`.

[119] M. F. Perutz and A. H. Windle. Cause of neural death in neurodegenerative diseases attributable to expansion of glutamine repeats. *Nature*, 412(6843):143–144, 2001.

[120] M. F. Perutz, T. Johnson, M. Suzuki, and J. T. Finch. Glutamine repeats as polar zippers: their possible role in inherited neurodegenerative diseases. *Proc Natl Acad Sci U S A*, 91(12):5355–5358, Jun 1994.

[121] M. F. Perutz, B. J. Pope, D. Owen, E. E. Wanker, and E. Scherzinger. Aggregation of proteins with expanded glutamine and alanine repeats of the glutamine-rich and asparagine-rich domains of Sup35 and of the amyloid beta-peptide of amyloid plaques. *Proc Natl Acad Sci U S A*, 99(8):5596–5600, Apr 2002. doi: 10.1073/pnas.042681599. URL http://dx.doi.org/10.1073/pnas.042681599.

[122] Z. H. Qin, R. W. Chen, Y. Wang, M. Nakai, D. M. Chuang, and T. N. Chase. Nuclear factor kappab nuclear translocation upregulates c-myc and p53 expression during nmda receptor-mediated apoptosis in rat striatum. *J Neurosci*, 19(10):4023–4033, May 1999.

[123] A. Rao, C. Luo, and P. G. Hogan. Transcription factors of the nfat family: regulation and function. *Annu Rev Immunol*, 15:707–747, 1997. doi: 10.1146/annurev.immunol.15.1.707. URL http://dx.doi.org/10.1146/annurev.immunol.15.1.707.

[124] T. R. Rieger, R. I. Morimoto, and V. Hatzimanikatis. Bistability explains threshold phenomena in protein aggregation both in vitro and in vivo. *Biophys J*, 90(3):886–895, Feb 2006. doi: 10.1529/biophysj.105.066662. URL http://dx.doi.org/10.1529/biophysj.105.066662.

[125] D. Rigamonti, J. H. Bauer, C. De-Fraja, L. Conti, S. Sipione, C. Sciorati, E. Clementi, A. Hackam, M. R. Hayden, Y. Li, J. K. Cooper, C. A. Ross, S. Govoni, C. Vincenz, and E. Cattaneo. Wild-type huntingtin protects from apoptosis upstream of caspase-3. *J Neurosci*, 20(10):3705–3713, 2000.

[126] B. E. Riley and H. T. Orr. Polyglutamine neurodegenerative diseases and regulation of transcription: assembling the puzzle. *Genes Dev*, 20(16):2183–2192, Aug 2006. doi: 10.1101/gad.1436506. URL http://dx.doi.org/10.1101/gad.1436506.

[127] J. D. Robertson, M. Enoksson, M. Suomela, B. Zhivotovsky, and S. Orrenius. Caspase-2 acts upstream of mitochondria to promote cytochrome c release during etoposide-induced apoptosis. *J Biol Chem*, 277(33):29803–29803, 2002.

[128] J.-C. Rochet. Novel therapeutic strategies for the treatment of protein-misfolding diseases. *Expert Rev Mol Med*, 9(17):1–34, 2007. doi: 10.1017/S1462399407000385. URL http://dx.doi.org/10.1017/S1462399407000385.

[129] H. D. Rosas, J. Goodman, Y. I. Chen, B. G. Jenkins, D. N. Kennedy, N. Makris, M. Patti, L. J. Seidman, M. F. Beal, and W. J. Koroshetz. Striatal volume loss in HD as measured by MRI and the influence of CAG repeat. *Neurology*, 57(6):1025–1028, 2001. URL http://www.neurology.org/cgi/content/abstract/57/6/1025.

[130] A. Rosenblatt, R. R. Brinkman, K. Y. Liang, E. W. Almqvist, R. L. Margolis, C. Y. Huang, M. Sherr, M. L. Franz, M. H. Abbott, M. R. Hayden, and C. A. Ross. Familial influence on age of onset among siblings with Huntington disease. *Am. J. Med. Genet*, 105(5):399–403, 2001.

[131] C. A. Ross. Polyglutamine pathogenesis: emergence of unifying mechanisms for Huntington's disease and related disorders. *Neuron*, 35(5):819–822, Aug 2002.

[132] C. A. Ross and M. A. Poirier. Protein aggregation and neurodegenerative disease. *Nat Med*, 10 Suppl:S10–S17, Jul 2004. doi: 10.1038/nm1066. URL `http://dx.doi.org/10.1038/nm1066`.

[133] D. C. Rubinsztein, J. Leggo, M. Chiano, A. Dodge, G. Norbury, E. Rosser, and D. Craufurd. Genotypes at the GluR6 kainate receptor locus are associated with variation in the age of onset of Huntington's disease. *Proc. Natl. Acad. Sci. USA*, 94(8):3872–3876, 1997. URL `http://www.pnas.org/cgi/content/abstract/94/8/3872`.

[134] H. Ryu, J. Lee, K. Zaman, J. Kubilis, R. J. Ferrante, B. D. Ross, R. Neve, and R. R. Ratan. Sp1 and Sp3 are oxidative stress-inducible, antideath transcription factors in cortical neurons. *J Neurosci*, 23(9):3597–3606, May 2003.

[135] S. Sachdev, L. Bruhn, H. Sieber, A. Pichler, F. Melchior, and R. Grosschedl. PIASy, a nuclear matrix-associated SUMO E3 ligase, represses LEF1 activity by sequestration into nuclear bodies. *Genes Dev*, 15(23):3088–3103, Dec 2001.

[136] I. Sanchez, C. J. Xu, P. Juo, A. Kakizaka, J. Blenis, and J. Yuan. Caspase-8 is required for cell death induced by expanded polyglutamine repeats. *Neuron*, 22(3):623–633, Mar 1999.

[137] I. Sanchez, C. Mahlke, and J. Yuan. Pivotal role of oligomerization in expanded polyglutamine neurodegenerative disorders. *Nature*, 421(6921):373–379, 2003.

[138] M. Sandri, J. Lin, C. Handschin, W. Yang, Z. P. Arany, S. H. Lecker, A. L. Goldberg, and B. M. Spiegelman. PGC-1alpha protects skeletal muscle from atrophy by suppressing FoxO3 action and atrophy-specific gene transcription. *Proc Natl Acad Sci U S A*, 103(44):16260–16265, Oct 2006. doi: 10.1073/pnas.0607795103. URL `http://dx.doi.org/10.1073/pnas.0607795103`.

[139] F. Saudou, S. Finkbeiner, D. Devys, and M. E. Greenberg. Huntingtin acts in the nucleus to induce apoptosis but death does not correlate with the formation of intranuclear inclusions. *Cell*, 95(1):55–66, Oct 1998.

[140] E. Scherzinger, R. Lurz, M. Turmaine, L. Mangiarini, B. Hollenbach, R. Hasenbank, G. P. Bates, S. W. Davies, H. Lehrach, and E. E. Wanker. Huntingtin-encoded polyglutamine expansions form amyloid-like protein aggregates in vitro and in vivo. *Cell*, 90(3):549–558, 1997.

[141] E. Scherzinger, A. Sittler, K. Schweiger, V. Heiser, R. Lurz, R. Hasenbank, G. P. Bates, H. Lehrach, and E. E. Wanker. Self-assembly of polyglutamine-containing huntingtin fragments into amyloid-like fibrils: implications for Huntington's disease pathology. *Proc Natl Acad Sci USA*, 96(8):4604–4609, 1999.

[142] N. W. Schiffer, S. A. Broadley, T. Hirschberger, P. Tavan, H. A. Kretzschmar, A. Giese, C. Haass, F. U. Hartl, and B. Schmid. Identification of anti-prion compounds as efficient inhibitors of polyglutamine protein aggregation in a zebrafish model. *J Biol Chem*, 282(12):9195–9203, Mar 2007. doi: 10.1074/jbc.M607865200. URL `http://dx.doi.org/10.1074/jbc.M607865200`.

[143] B. Schilling, J. Gafni, C. Torcassi, X. Cong, R. H. Row, M. A. LaFevre-Bernt, M. P. Cusack, T. Ratovitski, R. Hirschhorn, C. A. Ross, B. W. Gibson, and L. M. Ellerby. Huntingtin phosphorylation sites mapped by mass spectrometry. modulation of cleavage and toxicity. *J Biol Chem*, 281(33):23686–23697, Aug 2006. doi: 10.1074/jbc.M513507200. URL `http://dx.doi.org/10.1074/jbc.M513507200`.

[144] M. A. Schwarzschild, R. L. Cole, and S. E. Hyman. Glutamate, but not dopamine, stimulates stress-activated protein kinase and AP-1-mediated transcription in striatal neurons. *J Neurosci*, 17(10):3455–3466, May 1997.

[145] J. G. Seidman and C. Seidman. Transcription factor haploinsufficiency: when half a loaf is not enough. *J Clin Invest*, 109(4):451–455, Feb 2002.

[146] H. Seo, K.-C. Sonntag, and O. Isacson. Generalized brain and skin proteasome inhibition in Huntington's disease. *Ann Neurol*, 56(3):319–328, Sep 2004. doi: 10.1002/ana.20207. URL `http://dx.doi.org/10.1002/ana.20207`.

[147] A. H. Sharp, S. J. Loev, G. Schilling, S. H. Li, X. J. Li, J. Bao, M. V. Wagster, J. A. Kotzuk, J. P. Steiner, A. Lo, and et al. Widespread expression of Huntington's disease gene (IT15) protein product. *Neuron*, 14(5):1065–1074, 1995.

[148] S. Sipione, D. Rigamonti, M. Valenza, C. Zuccato, L. Conti, J. Pritchard, C. Kooperberg, J. M. Olson, and E. Cattaneo. Early transcriptional profiles in huntingtin-inducible striatal cells by microarray analyses. *Hum Mol Genet*, 11(17):1953–1965, Aug 2002.

[149] A. Sittler, R. Lurz, G. Lueder, J. Priller, H. Lehrach, M. K. Hayer-Hartl, F. U. Hartl, and E. E. Wanker. Geldanamycin activates a heat shock response and inhibits huntingtin aggregation in a cell culture model of Huntington's disease. *Hum Mol Genet*, 10(12):1307–1315, Jun 2001.

[150] M. Sjoeborg, K. Pietz, A. Ahgren, N. Yamada, O. Lindvall, K. Funa, and P. Odin. Expression of platelet-derived growth factor after intrastriatal ibotenic acid injury. *Exp Brain Res*, 119(2):245–250, Mar 1998.

[151] J. R. Slaughter, M. P. Martens, and K. A. Slaughter. Depression and Huntington's disease: prevalence, clinical manifestations, etiology, and treatment. *CNS Spectr*, 6(4):306–326, Apr 2001.

[152] R. Smith, P. Brundin, and J.-Y. Li. Synaptic dysfunction in Huntington's disease: a new perspective. *Cell Mol Life Sci*, 62(17):1901–1912, Sep 2005. doi: 10.1007/s00018-005-5084-5. URL `http://dx.doi.org/10.1007/s00018-005-5084-5`.

[153] R. G. Snell, J. C. MacMillan, J. P. Cheadle, I. Fenton, L. P. Lazarou, P. Davies, M. E. MacDonald, J. F. Gusella, P. S. Harper, and D. J. Shaw. Relationship between trinucleotide repeat expansion and phenotypic variation in Huntington's disease. *Nat. Genet.*, 4:393–397, 1993.

[154] S. A. Sorensen and K. Fenger. Causes of death in patients with Huntington's disease and in unaffected first degree relatives. *J Med Genet*, 29(12):911–914, Dec 1992.

[155] F. Squitieri, G. Sabbadini, P. Mandich, C. Gellera, E. Di Maria, E. Bellone, B. Castellotti, E. Nargi, U. de Grazia, M. Frontali, and A. Novelletto. Family and molecular data for a fine analysis of age at onset in Huntington disease. *Am. J. Med. Genet*, 95:366–373, 2000.

[156] J. S. Steffan, A. Kazantsev, O. Spasic-Boskovic, M. Greenwald, Y. Z. Zhu, H. Gohler, E. E. Wanker, G. P. Bates, D. E. Housman, and L. M. Thompson. The Huntington's disease protein interacts with p53 and CREB-binding protein and represses transcription. *Proc Natl Acad Sci U S A*, 97(12):6763–6768, Jun 2000. doi: 10.1073/pnas.100110097. URL `http://dx.doi.org/10.1073/pnas.100110097`.

[157] J. S. Steffan, L. Bodai, J. Pallos, M. Poelman, A. McCampbell, B. L. Apostol, A. Kazantsev, E. Schmidt, Y. Z. Zhu, M. Greenwald, R. Kurokawa, D. E. Housman, G. R. Jackson, J. L. Marsh, and L. M. Thompson. Histone deacetylase inhibitors arrest polyglutamine-dependent neurodegeneration in Drosophila. *Nature*, 413(6857):739–743, 2001.

[158] J. S. Steffan, N. Agrawal, J. Pallos, E. Rockabrand, L. C. Trotman, N. Slepko, K. Illes, T. Lukacsovich, Y. Z. Zhu, E. Cattaneo, P. P. Pandolfi, L. M. Thompson, and J. L. Marsh. Sumo modification of huntingtin and Huntington's disease pathology. *Science*, 304(5667):100–104, 2004.

[159] H. R. Stennicke and G. S. Salvesen. Catalytic properties of the caspases. *Cell Death Differ*, 6(11):1054–1059, Nov 1999. doi: 10.1038/sj.cdd.4400599. URL `http://dx.doi.org/10.1038/sj.cdd.4400599`.

[160] M. Stork, A. Giese, H. A. Kretzschmar, and P. Tavan. Molecular dynamics simulations indicate a possible role of parallel beta-helices in seeded aggregation of polyGln. *Biophys J*, 88(4):2442–2451, Apr 2005. doi: 10.1529/biophysj.104.052415. URL `http://dx.doi.org/10.1529/biophysj.104.052415`.

[161] K. L. Sugars and D. C. Rubinsztein. Transcriptional abnormalities in Huntington disease. *Trends Genet*, 19(5):233–238, May 2003.

[162] M. Swat, A. Kel, and H. Herzel. Bifurcation analysis of the regulatory modules of the mammalian G1/S transition. *Bioinformatics*, 20(10):1506–1511, 2004.

[163] S. Tahk, B. Liu, V. Chernishof, K. A. Wong, H. Wu, and K. Shuai. Control of specificity and magnitude of NF-kappa B and STAT1-mediated gene activation through PIASy and PIAS1 cooperation. *Proc Natl Acad Sci U S A*, 104(28):11643–11648, Jul 2007. doi: 10.1073/pnas.0701877104. URL `http://dx.doi.org/10.1073/pnas.0701877104`.

[164] H. Takano and J. F. Gusella. The predominantly HEAT-like motif structure of huntingtin and its association and coincident nuclear entry with dorsal, an NF-kB/Rel/dorsal family transcription factor. *BMC Neurosci*, 3:15, Oct 2002.

[165] N. Tanese and R. Tjian. Coactivators and TAFs: a new class of eukaryotic transcription factors that connect activators to the basal machinery. *Cold Spring Harb Symp Quant Biol*, 58:179–185, 1993.

[166] The Huntington's Disease Collaborative Research Group. A novel gene containing a trinucleotide repeat that is expanded and unstable on Huntington's disease chromosomes. *Cell*, 72(6):971–983, 1993.

[167] M. J. Thieben, A. J. Duggins, C. D. Good, L. Gomes, N. Mahant, F. Richards, E. McCusker, and R. S. Frackowiak. The distribution of structural neuropathology in pre-clinical Huntington's disease. *Brain*, 125:1815–1828, 2002.

[168] F. Trettel, D. Rigamonti, P. Hilditch-Maguire, V. C. Wheeler, A. H. Sharp, F. Persichetti, E. Cattaneo, and M. E. MacDonald. Dominant phenotypes produced by the HD mutation in STHdh(Q111) striatal cells. *Hum Mol Genet*, 9(19):2799–2809, Nov 2000.

[169] Y. Trottier, D. Devys, G. Imbert, F. Saudou, I. An, Y. Lutz, C. Weber, Y. Agid, E. C. Hirsch, and J. L. Mandel. Cellular localization of the Huntington's disease protein and discrimination of the normal and mutated form. *Nat Genet*, 10(1):104–110, May 1995. doi: 10.1038/ng0595-104. URL `http://dx.doi.org/10.1038/ng0595-104`.

[170] C. M. Troy, L. A. Stefanis, L. Greene, and M. L. Shelanski. Nedd2 is required for apoptosis after trophic factor withdrawal, but not superoxide dismutase (SOD1) downregulation, in sympathetic neurons and PC12 cells. *J Neurosci*, 17(6):1911–1918, 1997.

[171] C. Vacher, L. Garcia-Oroz, and D. C. Rubinsztein. Overexpression of yeast hsp104 reduces polyglutamine aggregation and prolongs survival of a transgenic mouse model of Huntington's disease. *Hum Mol Genet*, 14(22):3425–3433, Nov 2005. doi: 10.1093/hmg/ddi372. URL `http://dx.doi.org/10.1093/hmg/ddi372`.

[172] N. Van Kampen. *Stochastic Processes in Physics and Chemistry*. North Holland, 2007.

[173] W. M. C. van Roon-Mom, S. J. Reid, A. L. Jones, M. E. MacDonald, R. L. M. Faull, and R. G. Snell. Insoluble TATA-binding protein accumulation in Huntington's disease cortex. *Brain Res Mol Brain Res*, 109(1-2):1–10, Dec 2002.

[174] P. Vanhoutte, J. V. Barnier, B. Guibert, C. Pagès, M. J. Besson, R. A. Hipskind, and J. Caboche. Glutamate induces phosphorylation of Elk-1 and CREB, along with c-fos activation, via an extracellular signal-regulated kinase-dependent pathway in brain slices. *Mol Cell Biol*, 19(1):136–146, Jan 1999.

[175] J. P. Vonsattel, R. H. Myers, T. J. Stevens, R. J. Ferrante, E. D. Bird, and E. P. Richardson. Neuropathological classification of Huntington's disease. *J Neuropathol Exp Neurol*, 44(6):559–577, Nov 1985.

[176] S. Waelter, A. Boeddrich, R. Lurz, E. Scherzinger, G. Lueder, H. Lehrach, and E. E. Wanker. Accumulation of mutant huntingtin fragments in aggresome-like inclusion bodies as a result of insufficient protein degradation. *Mol Biol Cell*, 12 (5):1393–1407, 2001.

[177] C. L. Wellington, L. M. Ellerby, A. S. Hackam, R. L. Margolis, M. A. Trifiro, R. Singaraja, K. McCutcheon, G. S. Salvesen, S. S. Propp, M. Bromm, K. J. Rowland, T. Zhang, D. Rasper, S. Roy, N. Thornberry, L. Pinsky, A. Kakizuka, C. A. Ross, D. W. Nicholson, D. E. Bredesen, and M. R. Hayden. Caspase cleavage of gene products associated with triplet expansion disorders generates truncated fragments containing the polyglutamine tract. *J Biol Chem*, 273(15):9158–9167, 1998.

[178] C. L. Wellington, R. Singaraja, L. Ellerby, J. Savill, S. Roy, B. Leavitt, E. Cattaneo, A. Hackam, A. Sharp, N. Thornberry, D. W. Nicholson, D. E. Bredesen, and M. R. Hayden. Inhibiting caspase cleavage of huntingtin reduces toxicity and aggregate formation in neuronal and nonneuronal cells. *J. Biol. Chem.*, 275(26):19831–19838, 2000.

[179] C. L. Wellington, L. M. Ellerby, C. A. Gutekunst, D. Rogers, S. Warby, R. K. Graham, O. Loubser, J. van Raamsdonk, R. Singaraja, Y. Z. Yang, J. Gafni, D. Bredesen, S. M. Hersch, B. R. Leavitt, S. Roy, D. W. Nicholson, and M. R. Hayden. Caspase cleavage of mutant huntingtin precedes neurodegeneration in Huntington's disease. *J Neurosci*, 15(22):7862–7872, 2002.

[180] A. Williams, L. Jahreiss, S. Sarkar, S. Saiki, F. M. Menzies, B. Ravikumar, and D. C. Rubinsztein. Aggregate-prone proteins are cleared from the cytosol by autophagy: therapeutic implications. *Curr Top Dev Biol*, 76:89–101, 2006. doi: 10.1016/S0070-2153(06)76003-3. URL `http://dx.doi.org/10.1016/S0070-2153(06)76003-3`.

[181] E. Wingender, X. Chen, R. Hehl, H. Karas, I. Liebich, V. Matys, T. Meinhardt, M. Pruess, I. Reuter, and F. Schacherer. TRANSFAC: an integrated system for gene expression regulation. *Nucleic Acids Res*, 28(1):316–319, Jan 2000.

[182] A. Wyttenbach, J. Swartz, H. Kita, T. Thykjaer, J. Carmichael, J. Bradley, R. Brown, M. Maxwell, A. Schapira, T. F. Orntoft, K. Kato, and D. C. Rubinsztein. Polyglutamine expansions cause decreased CRE-mediated transcription and early gene expression changes prior to cell death in an inducible cell model of Huntington's disease. *Hum. Mol. Genet.*, 10(17):1829–1845, 2001.

[183] A. Yanai, K. Huang, R. Kang, R. R. Singaraja, P. Arstikaitis, L. Gan, P. C. Orban, A. Mullard, C. M. Cowan, L. A. Raymond, R. C. Drisdel, W. N. Green, B. Ravikumar, D. C. Rubinsztein, A. El-Husseini, and M. R. Hayden. Palmitoylation of huntingtin by HIP14 is essential for its trafficking and function. *Nat Neurosci*, 9(6):824–831, Jun 2006. doi: 10.1038/nn1702. URL `http://dx.doi.org/10.1038/nn1702`.

[184] W. Yang, J. R. Dunlap, R. B. Andrews, and R. Wetzel. Aggregated polyglutamine peptides delivered to nuclei are toxic to mammalian cells. *Hum Mol Genet*, 11(23): 2905–2917, Nov 2002.

[185] W. Zhai, H. Jeong, L. Cui, D. Krainc, and R. Tjian. In vitro analysis of huntingtin-mediated transcriptional repression reveals multiple transcription factor targets. *Cell*, 123(7):1241–1253, Dec 2005. doi: 10.1016/j.cell.2005.10.030. URL `http://dx.doi.org/10.1016/j.cell.2005.10.030`.

[186] C. Zuccato, A. Ciammola, D. Rigamonti, B. R. Leavitt, D. Goffredo, L. Conti, M. E. MacDonald, R. M. Friedlander, V. Silani, M. R. Hayden, T. Timmusk, S. Sipione, and E. Cattaneo. Loss of huntingtin-mediated BDNF gene transcription in Huntington's disease. *Science*, 293(5529):493–498, Jul 2001. doi: 10.1126/science.1059581. URL `http://dx.doi.org/10.1126/science.1059581`.

[187] C. Zuccato, M. Tartari, A. Crotti, D. Goffredo, M. Valenza, L. Conti, T. Cataudella, B. Leavitt, M. R. Hayden, T. Timmusk, D. Rigamonti, and E. Cattaneo. Huntingtin interacts with REST/NRSF to modulate the transcription of NRSE-controlled neuronal genes. *Nat. Genet.*, 35(1):76–83, 2003.

List of Figures

List of Tables

Selbständigkeitserklärung

Hiermit erkläre ich, die vorliegende Arbeit selbständig ohne fremde Hilfe verfaßt und nur die angegebene Literatur und Hilfsmittel verwendet zu haben.